Probing functional (re)organization in photosynthesis by time-resolved fluorescence spectroscopy

CANER ÜNLÜ

Thesis committee

Promotor

Prof. Dr H. van Amerongen

Professor of Biophysics

Wageningen University

Other members

Prof. Dr J.T. Zuilhof, Wageningen University

Dr J.W. Borst, Wageningen University

Prof. Dr C. Büchel, Institut für Molekulare Biowissenschaften, Universität Frankfurt, Germany

Dr G. Garab, Institute of Plant Biology Biological Research Centre, Szeged, Hungary

This research was conducted under the auspices of the Graduate School of Experimental Plant Sciences

Probing functional (re)organization in photosynthesis by time-resolved fluorescence spectroscopy

Caner Ünlü

Thesis

submitted in fulfillment of the requirements
for the degree of doctor
at Wageningen University
by the authority of the Rector Magnificus
Prof. Dr M.J. Kropff,
in the presence of the
Thesis Committee appointed by the Academic Board
to be defended in public
on Wednesday 20 May 2015
at 4 p.m. in the Aula.

Caner Ünlü
Probing functional (re)organization in photosynthesis by time-resolved fluorescence spectroscopy,
119 pages.

PhD thesis, Wageningen University, Wageningen, NL (2015)

With references, with summaries in Dutch and English

ISBN 978-94-6257-282-9

The research described in this thesis was financially supported by Netherlands Organization for Scientific Research (NWO) *via* the Council for Chemical Sciences (Project number: 700.59.016).

Table of Contents

Abbreviations

α-DM	n-dodecyl α D maltoside
β-DM	n-dodecyl β D maltoside
λ_{det}	Determination wavelength
λ_{exc}	Excitation wavelength
ATP	adenosine triphosphate
ATPase	adenosine triphosphate synthase
ADP	adenosine diphosphate
Car	carotenoid
Chl	chorophyll
CP24/26/29/43/47	chlorophyll binding protein with apparent molecular mass 24/26/29/43/47 kDa
Cyt *b6f*	Cytochrome *b6f*
DAS	decay associated spectrum/spectra
DMBQ	dimethyl-benzoquinone
EET	excitation energy transfer
ET	Electron transport
ERPE	Exciton/radical pair equilibrium
TEM	transmission electron microscopy
Fd	ferrodoxin
fwhm	full width at half maximum
FLIM	fluorescence lifetime imaging microscopy
FRET	Förster resonance energy transfer
HPLC	High Performance liquid chromatography
IRF	instrument response function
KO	knock-out
LED	Light emitting diode
LHC	Light Harvesting Complex
LHCI	Light Harvesting Complex I
LHCII	Light Harvesting Complex II
LHCB	light-harvesting proteins
LT	Low temperature
$NADP^+$	nicotinamide adenine dinucleotide phosphate (oxidized form)
NADPH	nicotinamide adenine dinucleotide phosphate (reduced form)
NoM	No minor Antenna
NPQ	nonphotochemical quenching
P680	Primary electron donor absorbing at 680 nm
P700	Primary electron donor absorbing at 700 nm
PQ	plastoquinone
PQH2	plastoquinol
PC	plastocyanin
PS	Photosystem
PSI	Photosystem I
PSI-LHCI	Photosystem I - Light Harvesting Complex I supercomplex
PSII	Photosystem II
PSII-LHCII	Photosystem II - Light Harvesting Complex II complex

qE	energy dependent quenching
Q_A	plastoquinone A
Q_B	plastoquinone B
RC	Reaction Center
RNA	Ribonucleic acid
SDS-PAGE	Sodium dodecyl sulfate polyacrylamide gel electrophoresis
SI	Supporting information
TAP	Tris acetate-phophate
TCSPC	time-correlated single photon counting
$TMPDH_2$	N,N,N,N-tetramethyl-p-phenylene-diamine, reduced form
OD	Optical density
WT	wild type

Chapter 1

General Introduction

CHAPTER 1

1.1 General Introduction

Photosynthesis is the conversion of sunlight energy into chemical energy by many living organisms such as plants, green algae and cyanobacteria [1, 2]. During photosynthesis, carbohydrates (glucose, fructose, starch…) and oxygen (as a by-product) are synthesized by using carbon dioxide and water [3]. Carbohydrates and oxygen are very important compounds for aerobic organisms because they are the main substrates for respiration, which is the energy-producing process for all aerobic living organisms [4]. At the end of the respiration, carbon dioxide and water are released and together with respiration, photosynthesis acts as part of a cycle and serves as a vital connection between the energy from the sun and all living organisms [4].

In plants and green algae, photosynthesis takes place in organelles named chloroplasts. Chloroplasts are ellipsoidal organelles with a diameter of 5-10 μm and thickness of 3-4 μm and contain a thylakoid membrane, which is a matrix of interconnected photosynthetic membranes [5]. Thylakoid membranes consist of highly organised pigment-protein complexes and electron carriers; Photosystem II (PSII), Cytochrome b6f (cyfb_6f), Photosystem I (PSI) and ATP synthase [5], embedded in a lipid bilayer. Photosynthesis proceeds in two main steps, the light reactions and the dark reactions [1, 6, 7]. The photosynthesis process starts in the thylakoid membranes with the light reactions, and at the end of the light reactions ATP, NADPH and oxygen are synthesized [1, 7]. Then the ATP and NADPH are used in the dark reactions to synthesize carbohydrates, which form one of the most important energy sources on Earth [6].

1.2 Electron flow in light reactions

During the light reactions, the light absorbed by the photosystems induces electronic excitations, which lead to charge separation in the reaction centres of PSI and PSII located in the cores of the photosystems [8-14]. These photosystems are essential for photosynthetic electron transport, which operates in two different modes, cyclic electron flow and linear electron flow, to provide ATP and NADPH for the Calvin-Benson cycle in dark reactions (Figure 1). [15, 16].

1.2.1 Linear Electron Flow

The linear electron flow starts with the absorption of light by PSII. Part of the captured light energy by PSII-LHCII complex is transferred to PSII core – P680 (Primary electron donor absorbing at 680 nm) and then the P680 is photo-oxidized and donates an electron to the primary electron acceptor of PSII (pheophytin) [1, 13, 15, 17]. The electrons released from P680 are replenished by electrons which become available during the process of splitting water into hydrogen ions and oxygen [18]. After photo-excitation of PSII, electrons are transferred to PSI via a number of electron carriers and cofactors (plastoquinone, plastoquinol, cyt b_6f and plastocyanin) [18]. The electrons are transferred to cytb_6f by plastoquinol. Then, the electrons follow two separate paths. A part of electrons goes to

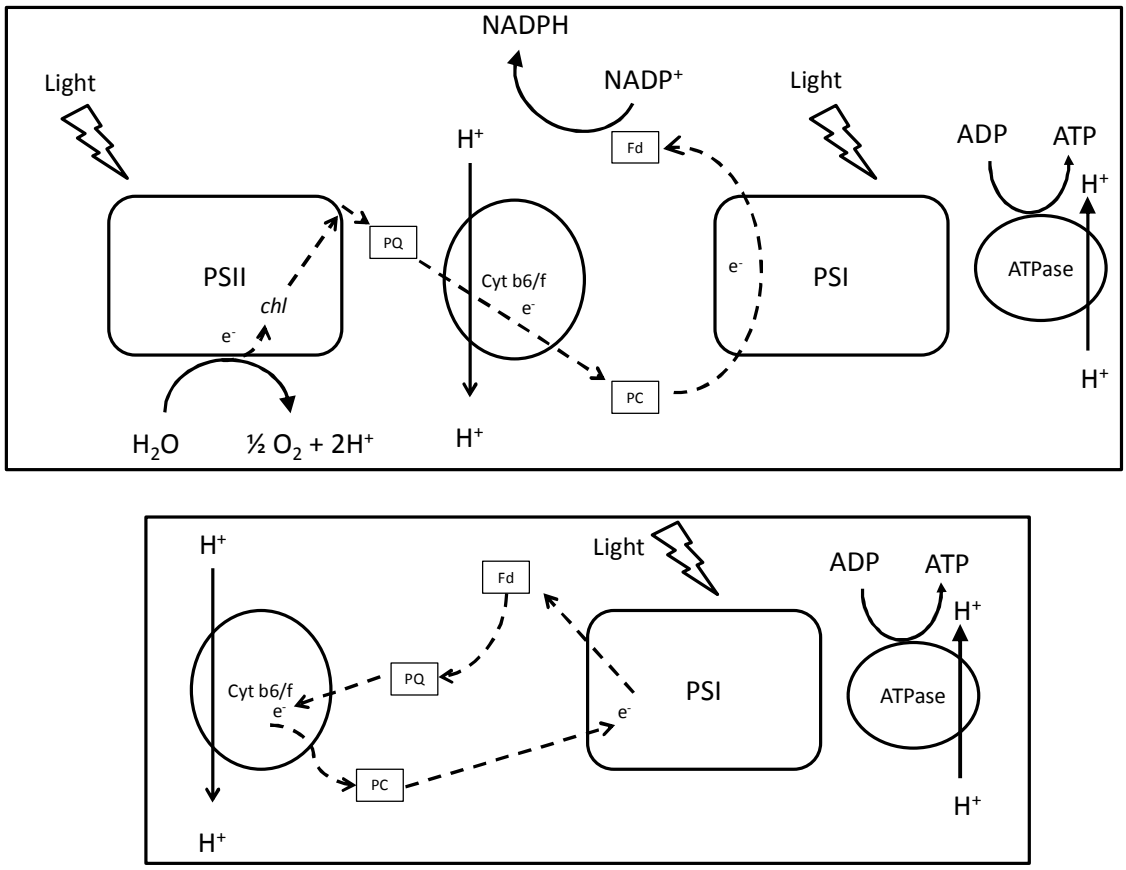

Figure 1. Schematic model of electron transport chain (dashed arrows) of oxygenic photosynthetic organism; the upper part represents linear electron transport and the lower part represents cyclic electron transport, Abbreviations: PSI, Photosystem I; PSII, Photosystem II; PQ, plastoquinone; PC, plastocyanin; Cyt b_6f, cytochrome b6f complex; ATPase, ATP synthase.

plastocyanin and arrives at PSI-LHCI complex afterwards. The other part of electrons are transferred to plastoquinone (PQ) pool in stroma side (Q-cycle) and protons are released from stroma to lumen to create a proton gradient across the thylakoid membrane along with hydrogen ions which are extracted from water. This proton gradient drives synthesis of ATP via ATP synthase. At the same time, PSI-LHCI complex absorbs light and transfers it to the PSI core-P700 (Primary electron donor absorbing at 700 nm) [13]. Then, P700 is photo-oxidized and donates an electron to the primary electron acceptor of PSI[3]. The electrons released from P700 are replenished by the electrons which come from PSII. The photo-excited electrons are transferred through ferrodoxin via a second electron transport chain [3]. Finally, $NADP^+$ reductase catalyses the electron transfer from ferrodoxin to $NADP^+$ and NADPH is synthesized [3].

1.2.2 Cyclic Electron Flow

Cyclic electron flow takes place around PSI and during the process, electrons from PSI core are transferred to an electron carrier, ferrodoxin [19]. Then, a second electron carrier, plastoquinone,

transports electrons to cyt b_6f. During the process, energy is provided to create a proton gradient across the membrane which is used to synthesize ATP [19]. Finally, the electrons transferred to P700 by plastocyanin and the electron flow is completed [19, 20].

1.3 Photosystems in plants and green algae

As mentioned above, light capture and subsequent charge separation processes occur in photosystems I and II (PSI and PSII) [13, 14, 21]. In plants and green algae both photosystems consist of a pigment-protein core complex surrounded by outer light-harvesting complexes (LHCs) [13, 14]. Both photosystems contain light-harvesting pigments (chlorophylls and carotenoids) and proteins; however, the composition and organization of pigments and proteins differ for each photosystem as well as for each organism [13, 14].

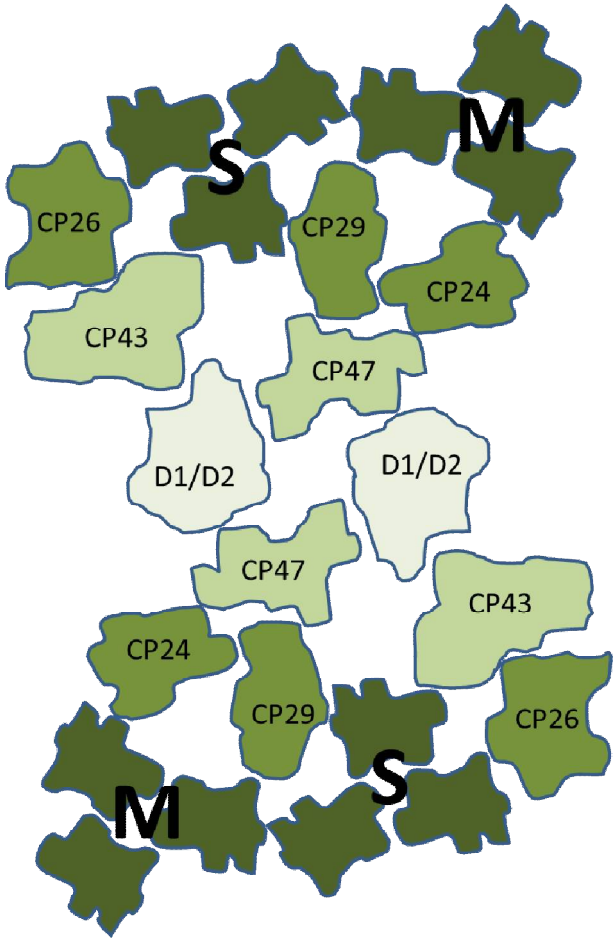

Figure 2 ***Membrane organization of PSII in Arabidopsis thaliana****. The core of PSII consists of reaction center (D1/D2) together with CP47 and CP43. Minor antenna complexes (CP24, CP26 and CP29) with the major antenna complexes LHCII (dark green) form peripheral antenna that surrounds the core. The binding strength of trimeric LHCII at different locations is strong (S) or moderate (M) PSII structure is based on the study of Caffari et al* [22, 23].

1.3.1 PSII-LHCII complex

PSII-LHCII is a large supramolecular pigment-protein complex located in the thylakoid membranes of plants and green algae. Its reaction center (RC) consists of several subunits carrying the cofactors for electron transport and forms, together with the proteins CP43 and CP47 a so-called core complex (Figure 2.) [24, 25]. Besides carotenoids, each PSII core monomer contains 35 chlorophylls *a*. Core complexes usually form dimers (C_2), which usually bind a variety of nuclear-encoded light-harvesting proteins (Lhcbs) : These outer Lhcbs consist of various components : The major light-harvesting complex LHCII (a trimer) harbours 12 carotenoids (Cars) and 42 chlorophylls (Chls), 24 of which are Chls *a* and the rest is Chls *b* [26]. Amongst all, the chl *a* pigments are largely responsible for excitation energy transfer (EET) to the PSII RC. The minor monomeric antennae, CP29 and CP26 are located in close connection to the core, and seem to mediate the binding of an LHCII trimer (strongly bound), thus forming the basic PSII-LHCII structure C_2S_2 [27]. In *C. reinhardtii,* it was recently shown that the PSII-LHCII complex contains three LHCII trimers per monomeric core [28]. In addition there are usually 3-4 extra LHCII trimers present per monomeric core [29]. Moreover, in higher plants another monomeric subunit (CP24) binds the PSII core and the amount of LHCII in the plant membranes is variable and usually ranges from ~2 to ~4 trimers per PSII core, most of which are functionally connected to PSII, although part is also associated with PSI [30] . Besides light harvesting, the outer antenna of PSII plays a crucial role in photoprotective and regulatory mechanisms such as limiting the level of Chl triplet states [31-33], scavenging of reactive oxygen species [34] and activating non-radiative de-excitation pathways [35].

1.3.2 PSI-LHCI complex

PSI-LHCI is a large pigment-protein complex which is located in thylakoid membranes like PSII-LHCII [36]. PSI-LHCI is organized differently in plants and green algae [36-39]. The green alga *C. reinhardtii* contains monomeric PSI core complexes which consist of two large protein subunits (PSAa and PSAb) that bind around 100 Chls *a* and surrounded by 14 protein subunits [40]. PSI core in plants binds 4 LHCs (Lhca1-4) [36]. However, In *C. reinhardtii* PSI antenna size differs and there are 9 Lhca's per PSI thereby extending its light harvesting capacity [40]. Despite the fact that LHCI and LHCII show high genetic sequence homology, there is an important difference between them. LHCI contains low-energy chlorophylls, so called "red chlorophylls" [10, 41-43]. These red chlorophylls absorbs light above 700 nm and are responsible for uphill energy transfer to P700 in the PSI reaction center [42-44].

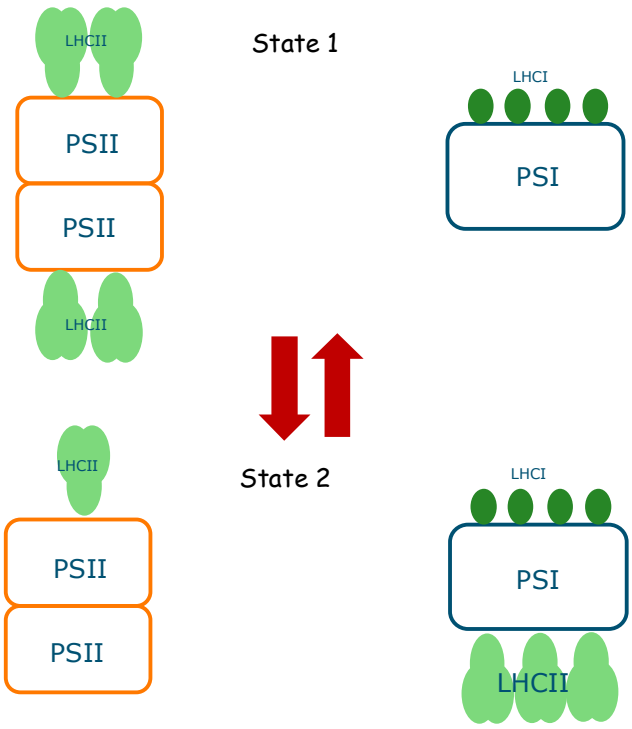

Figure 3. A simplified cartoon of the model for state transitions in C. reinhardtii as proposed by Delosme et al.[45] This model is disputed in this thesis. For schematic representation of our model, please see general discussion (chapter 6)

1.4 State transitions

For optimal linear electron transport from water to $NADP^+$ a balance is needed for the amount of light absorbed by the pigments in the two photosystems. Although both PSI and PSII contain Chls and Cars, their absorption spectra differ, with PSII being more effective in absorbing blue light and PSI in absorbing far-red light [46-48]. Because the intensity and spectral composition of light can vary, organisms need to rapidly adjust the relative absorption cross sections of both PSs. This regulation occurs via so-called state transitions, and it involves the relocation of Lhcs between PSII and PSI [49]. In higher plants, it is generally accepted that most of the LHCII is bound to PSII in state 1, while in state 2, which can be induced by overexciting PSII, part of LHCII (around 15%) moves to PSI [49, 50]. However, it should be noted recently that this dogma was disputed by Wientjes et al. who showed that in most conditions one LHCII trimer is attached to PSI and only under stress conditions it moves to PSII [30]. State transitions are regulated by the redox state of the PQ pool via the reversible phosphorylation of LHCII [49, 51-54]. On the other hand, the green alga *C. reinhardtii* is thought to exhibit state transitions to a far larger extent than higher plants. The widely accepted view is that during the transition from state 1 to state 2, 80% of the major antenna complexes dissociates from PSII and attaches to PSI (Figure 3) [45].

The possible mechanisms for reorganisation of LHCII upon state transitions in *Chlamydomonas reinhardtii* have been discussed for several decades [45, 55-66]. For a long time people adhered to the opinion that upon the transition from state 1 to state 2, 80% of LHCII detaches from PSII and attaches

completely to PSI in *Chlamydomonas reinhardtii* [45, 57]. However, our recent work based on *in vivo* time-resolved fluorescence kinetics for state-locked cells disputed this view [65]. In our study, it was concluded that the changes in the PSI structure upon state transitions are minor, whereas LHCII is most likely partly detaching from PSII and becoming [65] although also those changes are not very large quenched (will be discussed in detail in Chapter 2). Even more recently, Nagy et al. confirmed this conclusion [66]. Also, in an early fluorescence kinetics study on the green alga *Scenedesmus obliquus*, it was shown that the changes in the PSI structure are minor upon state transitions [67]. Altogether, these studies do not support the view that the detached LHCII completely attaches to PSI [45] but they support an early view of Allen, who suggested that the detached LHCII goes into a thermal energy dissipative mode upon state transitions [49].

1.5 Quantum Dots: possible antenna systems for Artificial Photosynthesis

The foreseen "energy crisis" related to complete consumption of fossil-derived fuels on Earth is getting closer; however, most of our industry and economy still depends on fossil-derived fuels [68-71]. To overcome the energy problem, alternative energy sources are set to be used, such as nuclear energy, wind energy, solar energy, etc [71]. Amongst the alternative energy sources, the "clean energy" sources are of most interest in order to preserve nature and the Earth ecosystem [72]. Photosynthesis is one the cleanest energy sources on Earth and there are series of on-going studies about understanding and benefiting more from photosynthesis [73, 74]. Moreover, nowadays "artificial photosynthesis" is becoming a more and more popular research [75-81]. Artificial photosynthesis is a photocatalytic water splitting process which splits water into hydrogen ions and oxygen by using sunlight [75-81]. Since the discovery of water splitting using titanium dioxide in the 1970s [82], numerous studies have been performed to develop systems for photocatalysis and artificial photosynthesis [75-81, 83]. To design a system that performs artificial photosynthesis, it might for instance be possible to mimick the structural and functional organisation of natural photosynthesis [75-81]. In natural photosynthesis, chlorophylls and carotenoids are used as light absorbing pigments [1, 2]. For artificial photosynthesis, chlorophylls and carotenoids are replaced with several different synthetic materials which can act as light absorbing materials such as ruthenium complexes, rhodium complexes, iridium complexes, platinum complexes, porphyrin complexes and quantum dots [75-81]. Amongst all others, quantum dots have a great advantage with their ability to collect light over a wide spectral window and being very efficient in excitation energy transfer [84, 85].

Quantum dots are defined as semiconductor nanocrystals comprised of groups II–VI or III–V elements, and are described as particles with physical dimensions smaller than the exciton Bohr radius (Figure 4.)

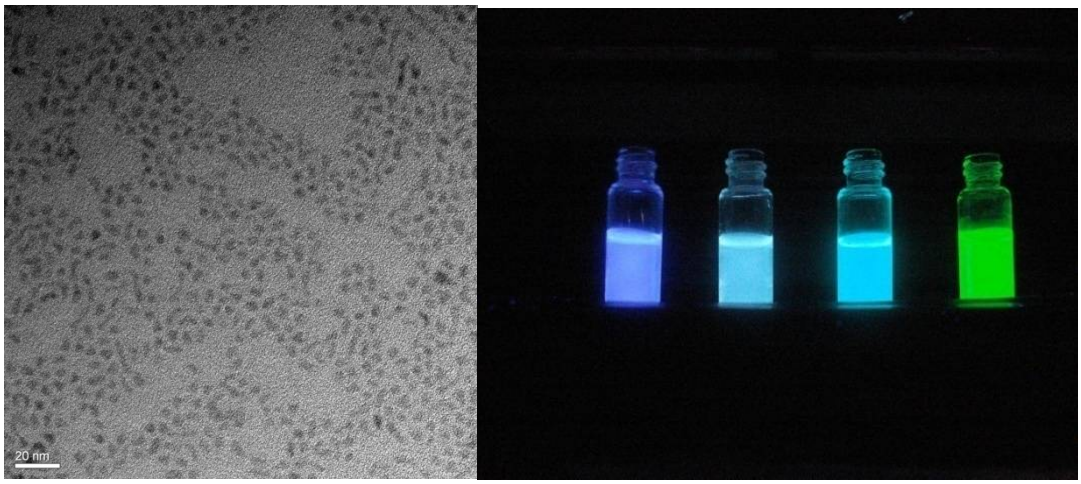

Figure 4. Transmission electron microscopy (TEM) image (left) and fluorescence under UV light (right) of CdSSe quantum dots. The diameter of quantum dot is around 4 nm. The fluorescence of CdSSe quantum dot changes from violet to green depending on the size of quantum dot [86]

[87-90]. They possess unique photophysical properties such as high quantum yields (varies from 20% to 90% depending on size and structure), enhanced photostability compared to organic dyes, size and composition dependent emission and absorption spectra [84-86, 91, 92]. Quantum dots are of interest because they are used in many different application areas such as solar cells, cancer research, LED (Light emitting diodes), lasers, artificial photosynthesis [84-86, 91-93]. Recent studies showed that quantum dots can indeed be a good alternative as a light harvesting molecule in artificial photosynthesis systems [85, 94, 95]. Moreover, surface properties of quantum dots can be modified [96] and quantum dots can be attached to complex biological photosynthetic systems, such as reaction centers, which can allow to tune or enhance light-harvesting properties of natural photosynthesis [85] .

1.6 Experimental Techniques

Chlorophyll fluorescence is often used to investigate the photosynthetic performance *in vivo* and *in vitro* [1, 2, 97], making use of the fact that each complex has its own characteristic emission behaviour [1, 2, 97]. However, the charge separation in photosystems and the energy transfer between photosystems occur extremely fast (ranging from picoseconds to nanoseconds) and steady-state fluorescence techniques are not enough to study energy transfer in photosynthesis. Therefore, to provide both quantitative and functional information about the fast processes of the photosystems, time-resolved fluorescence spectroscopy can be used [22, 30, 98-100]. In time-resolved (picosecond) fluorescence spectroscopy, the fluorescence intensity is recorded as a function of time after excitation by short laser pulses and energy transfer between chlorophyll molecules can be tracked [1].

In this thesis, fluorescence kinetics of photosystems are detected by time-correlated single-photon counting (TCSPC) and streak camera. In chapter 2 and chapter 4, TCSPC is used and in chapter 3 and

5, a streak camera is used to detect the fluorescence kinetics. Both TCSPC and streak camera have their own advantages. With a streak camera, it is possible to record the temporal evolution of the entire emission spectrum within a single measurement. In addition, the time resolution of streak camera is around 2-10 ps[101]. On the other hand, TCSPC can record a fluorescence trace only for a single wavelength and the instrument response function can be 30 ps at best [102] . However, the sensitivity of the TCSPC setup is far higher than for the streak camera which allows us to use very low laser powers to excite the samples [103]. Also, the time window of TCSPC (12 ns) is longer as compared to that of the streak camera (2 ns) which allows detection of longer lifetimes more accurately.

Also, in chapter 2, fluorescence lifetime imaging microscopy (FLIM) is used to monitor the *C. reinhardtii* cells. FLIM is a combination of two techniques; TCSPC and microscopy. In a FLIM image, each pixel contains two different types of information; a fluorescence decay curve detected with the use of TCSPC and the fluorescence intensity [104, 105]. FLIM is a powerful technique to distinguish inhomogeneities of the fluorescence kinetics in a cell or a cell culture [65].

1.7 This Thesis

To optimize their photosynthetic performance most oxygen-evolving organisms are able to shuttle light-harvesting pigment-protein complexes between photosystems I and II. These photosystems work in series to transform light energy into chemical energy. It is generally accepted that 80% of the light-harvesting complexes is participating in the reorganization in the green alga *Chlamydomonas reinhardtii,* a model organism for photosynthesis research. However, in this thesis we demonstrate that such a large remodeling does not occur. Light-harvesting complexes can indeed detach from photosystem II but only a small fraction subsequently attaches to photosystem I. This phenomenon has significant implications for our way of thinking about the efficiency of regulation in photosynthesis. Besides reorganization of light-harvesting complexes between photosystems in *Chlamydomonas reinhardtii*, the role of minor harvesting complexes in excitation energy transfer to reaction centers in photosystem II and multiexciton dynamics of quantum dots, which can be used as replacement of light-harvesting complexes in artificial photosynthesis systems, are discussed.

In chapter 2, time-resolved fluorescence spectroscopy is applied to study changes in PSI and PSII antenna size in response to state transitions for wild-type (WT) *C. reinhardtii in vivo*. The cells were locked in different states, using the same method as used for previous photoacoustic measurements [45, 57], and fluorescence decay curves were recorded at room temperature. The results led us to challenge some of the generally accepted views, especially concerning the structure of the PSI supercomplex in state 2 and the fate of the detached LHCII. The main changes during state transitions occur in PSII whereas changes in the PSI supercomplex turn out to be less pronounced. In addition, it appears that both in state 1 and 2 a pool of LHCII exists that is neither connected to PSI nor to PSII while its size is larger in state 2.

In chapter 3, we have performed picosecond fluorescence measurements on state–locked WT *Chlamydomonas reinhardtii* cells at 77 K by using a streak-camera setup in order to investigate in detail the changes in fluorescence kinetics for different states. Our data show that the changes in 77 K fluorescence upon state transitions are mostly related to the changes in PSII and LHCII fluorescence, whereas PSI fluorescence hardly changes. These results support on the one hand our recent conclusion that LHCII detaches from PSII in state 2 conditions but only a fraction attaches to PSI while the detached antenna becomes quenched [65, 66], and on the other hand reveals the origin of the characteristic change in the ratio of the fluorescence intensity at 680 nm and 720 nm at 77 K, thereby resolving the apparent discrepancy between room temperature and 77K results

In chapter 4, thylakoid membranes of *A. thaliana* have been studied with time-resolved fluorescence spectroscopy using different combinations of excitation and detection wavelengths, in order to (partly) separate PSI and PSII-LHCII contributions. In particular, PSII-LHCII fluorescence decay kinetics have been measured on thylakoids isolated from wild-type Arabidopsis, from the double knock-out mutants koCP26/24 and koCP29/24, and from a mutant depleted of all minor antennae (NoM). The main goal of this study was to investigate how the depletion of specific Lhcs affects the excitation- and electron-transfer parameters of PSII. In the absence of all minor Lhcs of PSII, the functional connection between LHCII from the PSII cores appears to be strongly impaired and LHCII is substantially quenched, which is probably related to the fact that the NoM plants are strongly hampered in their growth as compared to WT plants. For double knock-out mutants, the outer antenna is better connected to the PSII core and the corresponding plants also grow significantly better than the NoM plants.

In chapter 5, we have performed picosecond fluorescence measurements on ZnCdTe ternary quantum dots at room temperature by using a streak-camera setup in order to investigate in detail the fluorescence kinetics for ZnCdTe quantum dots with different size and structure by using different excitation laser intensities. Our data show that the changes in fluorescence kinetics are mostly related to the changes in structure and excitation laser intensities. In heterogeneous structured ZnCdTe quantum dots, the fluorescence kinetics become faster. Also, in both homogeneous and heterogeneous ZnCdTe quantum dots, a new peak is observed in high energy region of emission spectrum when using high excitation intensities, which shows that the radiative processes that occur from higher energy states become more favoured as the excitation intensity increases.

1.8 References

[1] H. Van Amerongen, L. Valkunas, R. Van Grondelle, Photosynthetic Excitons, 2000, World Scientific, Singapore, 2000.
[2] R.E. Blankenship, Molecular mechanisms of photosynthesis, Blackwell Science Ltd, 2002.
[3] N. Nelson, A. Ben-Shem, The complex architecture of oxygenic photosynthesis, Nature Reviews Molecular Cell Biology, 5 (2004) 971-982.
[4] B. Ke, Photosynthesis photobiochemistry and photobiophysics, Springer, 2001.
[5] R.R. Wise, The chloroplast. Basics and applications, Annals of Botany, 112 (2013) vii.
[6] E.J. Badin, M. Calvin, The Path of Carbon in Photosynthesis .9. Photosynthesis, Photoreduction and the Hydrogen Oxygen Carbon Dioxide Dark Reaction, Journal of the American Chemical Society, 72 (1950) 5266-5270.
[7] D.I. Arnon, Light Reactions of Photosynthesis, Proceedings of the National Academy of Sciences of the United States of America, 68 (1971) 2883-&.
[8] G.H. Schatz, H. Brock, A.R. Holzwarth, Kinetic and Energetic Model for the Primary Processes in Photosystem-Ii, Biophysical Journal, 54 (1988) 397-405.
[9] A.N. Melkozernov, S. Lin, R.E. Blankenship, Excitation dynamics and heterogeneity of energy equilibration in the core antenna of photosystem I from the cyanobacterium Synechocystis sp. PCC 6803, Biochemistry, 39 (2000) 1489-1498.
[10] B. Gobets, R. van Grondelle, Energy transfer and trapping in photosystem I, Biochimica Et Biophysica Acta-Bioenergetics, 1507 (2001) 80-99.
[11] N. Nelson, C.F. Yocum, Structure and function of photosystems I and II, Annual Review of Plant Biology, 57 (2006) 521-565.
[12] A. Busch, M. Hippler, The structure and function of eukaryotic photosystem I, Biochimica Et Biophysica Acta-Bioenergetics, 1807 (2011) 864-877.
[13] R. Croce, H. van Amerongen, Light-harvesting in photosystem I, Photosynthesis Research, 116 (2013) 153-166.
[14] H. van Amerongen, R. Croce, Light harvesting in photosystem II, Photosynthesis Research, 116 (2013) 251-263.
[15] R. Croce, H. van Amerongen, Natural strategies for photosynthetic light harvesting, Nature Chemical Biology, 10 (2014) 492-501.
[16] H. Takahashi, S. Clowez, F.A. Wollman, O. Vallon, F. Rappaport, Cyclic electron flow is redox-controlled but independent of state transition, Nature Communications, 4 (2013).
[17] H. van Amerongen, R. van Grondelle, Understanding the energy transfer function of LHCII, the major light-harvesting complex of green plants, Journal of Physical Chemistry B, 105 (2001) 604-617.
[18] J.F. Allen, W.B.M. de Paula, S. Puthiyaveetil, J. Nield, A structural phylogenetic map for chloroplast photosynthesis, Trends in Plant Science, 16 (2011) 645-655.
[19] J. Alric, Cyclic electron flow around photosystem I in unicellular green algae, Photosynthesis Research, 106 (2010) 47-56.
[20] Y. Munekaga, M. Hashimoto, C. Miyaka, K.I. Tomizawa, T. Endo, M. Tasaka, T. Shikanai, Cyclic electron flow around photosystem I is essential for photosynthesis, Nature, 429 (2004) 579-582.
[21] H. van Amerongen, J.P. Dekker, Light harvesting in photosystem II, in: Light-Harvesting Antennas in Photosynthesis, Kluwer Academic Publishers, 2003, pp. 219-251.
[22] S. Caffarri, R. Kouril, S. Kereiche, E.J. Boekema, R. Croce, Functional architecture of higher plant photosystem II supercomplexes, Embo Journal, 28 (2009) 3052-3063.
[23] S. Caffarri, K. Broess, R. Croce, H. van Amerongen, Excitation Energy Transfer and Trapping in Higher Plant Photosystem II Complexes with Different Antenna Sizes, Biophysical Journal, 100 (2011) 2094-2103.
[24] K.N. Ferreira, T.M. Iverson, K. Maghlaoui, J. Barber, S. Iwata, Architecture of the photosynthetic oxygen-evolving center, Science, 303 (2004) 1831-1838.
[25] Y. Umena, K. Kawakami, J.R. Shen, N. Kamiya, Crystal structure of oxygen-evolving photosystem II at a resolution of 1.9 angstrom, Nature, 473 (2011) 55-U65.

[26] Z.F. Liu, H.C. Yan, K.B. Wang, T.Y. Kuang, J.P. Zhang, L.L. Gui, X.M. An, W.R. Chang, Crystal structure of spinach major light-harvesting complex at 2.72 angstrom resolution, Nature, 428 (2004) 287-292.
[27] E.J. Boekema, H. van Roon, J.F.L. van Breemen, J.P. Dekker, Supramolecular organization of photosystem II and its light-harvesting antenna in partially solubilized photosystem II membranes, European Journal of Biochemistry, 266 (1999) 444-452.
[28] R. Tokutsu, N. Kato, K.H. Bui, T. Ishikawa, J. Minagawa, Revisiting the Supramolecular Organization of Photosystem II in Chlamydomonas reinhardtii, Journal of Biological Chemistry, 287 (2012) 31574-31581.
[29] B. Drop, M. Webber-Birungi, S.K.N. Yadav, A. Filipowicz-Szymanska, F. Fusetti, E.J. Boekema, R. Croce, Light-harvesting complex II (LHCII) and its supramolecular organization in Chlamydomonas reinhardtii, Biochimica Et Biophysica Acta-Bioenergetics, 1837 (2014) 63-72.
[30] E. Wientjes, H. van Amerongen, R. Croce, LHCII is an antenna of both photosystems after long-term acclimation, Biochimica et biophysica acta, 1827 (2013) 420-426.
[31] S.S. Lampoura, V. Barzda, G.M. Owen, A.J. Hoff, H. van Amerongen, Aggregation of LHCII leads to a redistribution of the triplets over the central xanthophylls in LHCII, Biochemistry, 41 (2002) 9139-9144.
[32] M. Mozzo, L. Dall'Osto, R. Hienerwadel, R. Bassi, R. Croce, Photoprotection in the antenna complexes of photosystem II - Role of individual xanthophylls in chlorophyll triplet quenching, Journal of Biological Chemistry, 283 (2008) 6184-6192.
[33] V. Barzda, E.J.G. Peterman, R. van Grondelle, H. van Amerongen, The influence of aggregation on triplet formation in light-harvesting chlorophyll a/b pigment-protein complex II of green plants, Biochemistry-Us, 37 (1998) 546-551.
[34] N. Betterle, M. Ballottari, S. Zorzan, S. de Bianchi, S. Cazzaniga, L. Dall'Osto, T. Morosinotto, R. Bassi, Light-induced Dissociation of an Antenna Hetero-oligomer Is Needed for Non-photochemical Quenching Induction, Journal of Biological Chemistry, 284 (2009) 15255-15266.
[35] P. Horton, A.V. Ruban, R.G. Walters, Regulation of light harvesting in green plants, Annual Review of Plant Physiology and Plant Molecular Biology, 47 (1996) 655-684.
[36] A. Ben-Shem, F. Frolow, N. Nelson, Crystal structure of plant photosystem I, Nature, 426 (2003) 630-635.
[37] P. Fromme, P. Jordan, N. Krauss, Structure of photosystem I, Biochimica Et Biophysica Acta-Bioenergetics, 1507 (2001) 5-31.
[38] A. Ben-Shem, F. Frolow, N. Nelson, Evolution of photosystem I - from symmetry through pseudosymmetry to asymmetry, Febs Letters, 564 (2004) 274-280.
[39] E.J. Boekema, J.P. Dekker, M.G. Vanheel, M. Rogner, W. Saenger, I. Witt, H.T. Witt, Evidence for a Trimeric Organization of the Photosystem-I Complex from the Thermophilic Cyanobacterium Synechococcus Sp, Febs Letters, 217 (1987) 283-286.
[40] B. Drop, M. Webber-Birungi, F. Fusetti, R. Kouril, K.E. Redding, E.J. Boekema, R. Croce, Photosystem I of Chlamydomonas reinhardtii Contains Nine Light-harvesting Complexes (Lhca) Located on One Side of the Core, Journal of Biological Chemistry, 286 (2011) 44878-44887.
[41] R.E. Blankenship, Energy transfer and trapping in photosystem I and a bacterial model, Abstracts of Papers of the American Chemical Society, 212 (1996) 120-PHYS.
[42] E. Wientjes, I.H.M. van Stokkum, H. van Amerongen, R. Croce, The Role of the Individual Lhcas in Photosystem I Excitation Energy Trapping, Biophysical Journal, 101 (2011) 745-754.
[43] E. Wientjes, R. Croce, The light-harvesting complexes of higher-plant Photosystem I: Lhca1/4 and Lhca2/3 form two red-emitting heterodimers, Biochemical Journal, 433 (2011) 477-485.
[44] E. Wientjes, I.H.M. van Stokkum, H. van Amerongen, R. Croce, Excitation-Energy Transfer Dynamics of Higher Plant Photosystem I Light-Harvesting Complexes, Biophysical Journal, 100 (2011) 1372-1380.
[45] R. Delosme, J. Olive, F.A. Wollman, Changes in light energy distribution upon state transitions: An in vivo photoacoustic study of the wild type and photosynthesis mutants from Chlamydomonas reinhardtii, Biochimica Et Biophysica Acta-Bioenergetics, 1273 (1996) 150-158.
[46] N. Murata, Control of Excitation Transfer in Photosynthesis .I. Light-Induced Change of Chlorophyll a Fluorescence in Porphyridium Cruentum, Biochimica Et Biophysica Acta, 172 (1969) 242-&.

[47] Bonavent.C, J. Myers, Fluorescence and Oxygen Evolution from Chlorella Pyrenoidosa, Biochimica Et Biophysica Acta, 189 (1969) 366-+.
[48] J.F. Allen, J. Bennett, K.E. Steinback, C.J. Arntzen, Chloroplast Protein-Phosphorylation Couples Plastoquinone Redox State to Distribution of Excitation-Energy between Photosystems, Nature, 291 (1981) 25-29.
[49] J.F. Allen, Protein-Phosphorylation in Regulation of Photosynthesis, Biochimica Et Biophysica Acta, 1098 (1992) 275-335.
[50] R. Kouril, A. Zygadlo, A.A. Arteni, C.D. de Wit, J.P. Dekker, P.E. Jensen, H.V. Scheller, E.J. Boekema, Structural characterization of a complex of photosystem I and light-harvesting complex II of Arabidopsis thaliana, Biochemistry, 44 (2005) 10935-10940.
[51] S. Bellafiore, F. Barneche, G. Peltier, J.D. Rochaix, State transitions and light adaptation require chloroplast thylakoid protein kinase STN7, Nature, 433 (2005) 892-895.
[52] N. Depege, S. Bellafiore, J.D. Rochaix, Role of chloroplast protein kinase Stt7 in LHCII phosphorylation and state transition in Chlamydomonas, Science, 299 (2003) 1572-1575.
[53] V. Bonardi, P. Pesaresi, T. Becker, E. Schleiff, R. Wagner, T. Pfannschmidt, P. Jahns, D. Leister, Photosystem II core phosphorylation and photosynthetic acclimation require two different protein kinases, Nature, 437 (2005) 1179-1182.
[54] A. Shapiguzov, B. Ingelsson, I. Samol, C. Andres, F. Kessler, J.D. Rochaix, A.V. Vener, M. Goldschmidt-Clermont, The PPH1 phosphatase is specifically involved in LHCII dephosphorylation and state transitions in Arabidopsis, Proceedings of the National Academy of Sciences of the United States of America, 107 (2010) 4782-4787.
[55] F.A. Wollman, P. Delepelaire, Correlation between Changes in Light Energy-Distribution and Changes in Thylakoid Membrane Polypeptide Phosphorylation in Chlamydomonas-Reinhardtii, Journal of Cell Biology, 98 (1984) 1-7.
[56] W.P. Williams, J.F. Allen, State-1/State-2 Changes in Higher-Plants and Algae, Photosynthesis Research, 13 (1987) 19-45.
[57] M.M. Fleischmann, S. Ravanel, R. Delosme, J. Olive, F. Zito, F.A. Wollman, J.D. Rochaix, Isolation and characterization of photoautotrophic mutants of Chlamydomonas reinhardtii deficient in state transition, Journal of Biological Chemistry, 274 (1999) 30987-30994.
[58] G. Finazzi, R.P. Barbagallo, E. Bergo, R. Barbato, G. Forti, Photoinhibition of Chlamydomonas reinhardtii in State 1 and State 2 - Damages to the photosynthetic apparatus under linear and cyclic electron flow, Journal of Biological Chemistry, 276 (2001) 22251-22257.
[59] G. Forti, G. Caldiroli, State transitions in Chlamydomonas reinhardtii. The role of the Mehler reaction in state 2-to-state 1 transition, Plant Physiology, 137 (2005) 492-499.
[60] J. Kargul, M.V. Turkina, J. Nield, S. Benson, A.V. Vener, J. Barber, Light-harvesting complex II protein CP29 binds to photosystem I of Chlamydomonas reinhardtii under State 2 conditions, Febs Journal, 272 (2005) 4797-4806.
[61] H. Takahashi, M. Iwai, Y. Takahashi, J. Minagawa, Identification of the mobile light-harvesting complex II polypeptides for state transitions, Plant and Cell Physiology, 47 (2006) S105-S105.
[62] M. Iwai, M. Yokono, N. Inada, J. Minagawa, Live-cell imaging of photosystem II antenna dissociation during state transitions, Proceedings of the National Academy of Sciences of the United States of America, 107 (2010) 2337-2342.
[63] J. Minagawa, State transitions-The molecular remodeling of photosynthetic supercomplexes that controls energy flow in the chloroplast, Biochimica Et Biophysica Acta-Bioenergetics, 1807 (2011) 897-905.
[64] B. Drop, K.N.S. Yadav, E.J. Boekema, R. Croce, Consequences of state transitions on the structural and functional organization of Photosystem I in the green alga Chlamydomonas reinhardtii, Plant Journal, 78 (2014) 181-191.
[65] C. Unlu, B. Drop, R. Croce, H. van Amerongen, State transitions in Chlamydomonas reinhardtii strongly modulate the functional size of photosystem II but not of photosystem I, Proceedings of the National Academy of Sciences of the United States of America, 111 (2014) 3460-3465.
[66] G. Nagy, R. Unnep, O. Zsiros, R. Tokutsu, K. Takizawa, L. Porcar, L. Moyet, D. Petroutsos, G. Garab, G. Finazzi, J. Minagawa, Chloroplast remodeling during state transitions in Chlamydomonas reinhardtii as revealed by noninvasive techniques in vivo, Proceedings of the National Academy of Sciences of the United States of America, 111 (2014) 5042-5047.

[67] J. Wendler, A.R. Holzwarth, State Transitions in the green-alga Scenedesmus-obliquus probed by time-resolved chlorophyll fluorescence spectroscopy and global data-analysis, Biophysical Journal, 52 (1987) 717-728.
[68] P.B. Weisz, Basic choices and constraints on long-term energy supplies, Physics Today, 57 (2004) 47-52.
[69] A.A. Bartlett, Sustained Availability - a Management Program for Nonrenewable Resources, American Journal of Physics, 54 (1986) 398-402.
[70] C.J. Campbell, Industry urged to watch for regular oil production peaks, depletion signals, Oil & Gas Journal, 101 (2003) 38-45.
[71] P.V. Kamat, Meeting the Clean Energy Demand: Nanostructure Architectures for Solar Energy Conversion, The Journal of Physical Chemistry C, 111 (2007) 2834-2860.
[72] N. Myers, J. Kent, New consumers: The influence of affluence on the environment, Proceedings of the National Academy of Sciences of the United States of America, 100 (2003) 4963-4968.
[73] A. Melis, Photosynthesis-to-fuels: from sunlight to hydrogen, isoprene, and botryococcene production, Energy & Environmental Science, 5 (2012) 5531-5539.
[74] A.J. Nozik, J. Miller, Introduction to Solar Photon Conversion, Chemical Reviews, 110 (2010) 6443-6445.
[75] D. Gust, T.A. Moore, A.L. Moore, Solar Fuels via Artificial Photosynthesis, Accounts of Chemical Research, 42 (2009) 1890-1898.
[76] L. Hammarstrom, S. Hammes-Schiffer, Artificial Photosynthesis and Solar Fuels, Accounts of Chemical Research, 42 (2009) 1859-1860.
[77] W.J. Song, Z.F. Chen, M.K. Brennaman, J.J. Concepcion, A.O.T. Patrocinio, N.Y.M. Iha, T.J. Meyer, Making solar fuels by artificial photosynthesis, Pure and Applied Chemistry, 83 (2011) 749-768.
[78] S.W. Hogewoning, E. Wientjes, P. Douwstra, G. Trouwborst, W. van Ieperen, R. Croce, J. Harbinson, Photosynthetic Quantum Yield Dynamics: From Photosystems to Leaves, Plant Cell, 24 (2012) 1921-1935.
[79] S. Styring, Artificial photosynthesis for solar fuels, Faraday Discussions, 155 (2012) 357-376.
[80] S. Styring, Fuels from solar energy and water-from natural to artificial photosynthesis, Journal of Biological Inorganic Chemistry, 19 (2014) S721-S721.
[81] Y. Tachibana, L. Vayssieres, J.R. Durrant, Artificial photosynthesis for solar water-splitting, 6 (2012) 511-518.
[82] A. Fujishima, K. Honda, Electrochemical Photolysis of Water at a Semiconductor Electrode, Nature, 238 (1972) 37-+.
[83] S.C. Warren, K. Voitchovsky, H. Dotan, C.M. Leroy, M. Cornuz, F. Stellacci, C. Hebert, A. Rothschild, M. Gratzel, Identifying champion nanostructures for solar water-splitting, Nature Materials, 12 (2013) 842-849.
[84] I. Nabiev, A. Sukhanova, M. Artemyev, V. Oleinikov, Fluorescent colloidal particles as a detection tools in biotechnology systems, Colloidal Nanoparticles in Biotechnology, (2008) 133-168.
[85] I. Nabiev, A. Rakovich, A. Sukhanova, E. Lukashev, V. Zagidullin, V. Pachenko, Y.P. Rakovich, J.F. Donegan, A.B. Rubin, A.O. Govorov, Fluorescent Quantum Dots as Artificial Antennas for Enhanced Light Harvesting and Energy Transfer to Photosynthetic Reaction Centers, Angewandte Chemie International Edition, 49 (2010) 7217-7221.
[86] C. Unlu, G.U. Tosun, S. Sevim, S. Ozcelik, Developing a facile method for highly luminescent colloidal CdSxSe1-x ternary nanoalloys, Journal of Materials Chemistry C, 1 (2013) 3026-3034.
[87] M.G. Bawendi, Synthesis and spectroscopy of II-VI quantum dots: An overview, in: E. Burstein, C. Weisbuch (Eds.) NATO Advanced Study Institute on Confined Electrons and Photons - New Physics and Applications, Erice, Italy, 1993, pp. 339-356.
[88] M.G. Bawendi, P.J. Carroll, W.L. Wilson, L.E. Brus, LUMINESCENCE PROPERTIES OF CDSE QUANTUM CRYSTALLITES - RESONANCE BETWEEN INTERIOR AND SURFACE LOCALIZED STATES, Journal of Chemical Physics, 96 (1992) 946-954.
[89] P.M. Allen, M.G. Bawendi, Ternary I-III-VI quantum dots luminescent in the red to near-infrared, Journal of the American Chemical Society, 130 (2008) 9240-+.
[90] T. Jamieson, R. Bakhshi, D. Petrova, R. Pocock, M. Imani, A.M. Seifalian, Biological applications of quantum dots, Biomaterials, 28 (2007) 4717-4732.

[91] T. Nann, W.M. Skinner, Quantum Dots for Electro-Optic Devices, Acs Nano, 5 (2011) 5291-5295.
[92] N. Hildebrandt, Biofunctional Quantum Dots: Controlled Conjugation for Multiplexed Biosensors, Acs Nano, 5 (2011) 5286-5290.
[93] D.V. Talapin, J.S. Lee, M.V. Kovalenko, E.V. Shevchenko, Prospects of Colloidal Nanocrystals for Electronic and Optoelectronic Applications, Chemical Reviews, 110 (2010) 389-458.
[94] H.M. Chen, C.K. Chen, Y.C. Chang, C.W. Tsai, R.S. Liu, S.F. Hu, W.S. Chang, K.H. Chen, Quantum Dot Monolayer Sensitized ZnO Nanowire-Array Photoelectrodes: True Efficiency for Water Splitting, Angewandte Chemie-International Edition, 49 (2010) 5966-5969.
[95] H.M. Chen, C.K. Chen, R.S. Liu, C.C. Wu, W.S. Chang, K.H. Chen, T.S. Chan, J.F. Lee, D.P. Tsai, A New Approach to Solar Hydrogen Production: a ZnO-ZnS Solid Solution Nanowire Array Photoanode, Advanced Energy Materials, 1 (2011) 742-747.
[96] A. Hoshino, K. Fujioka, T. Oku, M. Suga, Y.F. Sasaki, T. Ohta, M. Yasuhara, K. Suzuki, K. Yamamoto, Physicochemical properties and cellular toxicity of nanocrystal quantum dots depend on their surface modification, Nano Letters, 4 (2004) 2163-2169.
[97] K. Maxwell, G.N. Johnson, Chlorophyll fluorescence - a practical guide, Journal of Experimental Botany, 51 (2000) 659-668.
[98] K. Broess, G. Trinkunas, A. van Hoek, R. Croce, H. van Amerongen, Determination of the excitation migration time in Photosystem II - Consequences for the membrane organization and charge separation parameters, Biochimica Et Biophysica Acta-Bioenergetics, 1777 (2008) 404-409.
[99] B. van Oort, M. Alberts, S. de Bianchi, L. Dall'Osto, R. Bassi, G. Trinkunas, R. Croce, H. van Amerongen, Effect of Antenna-Depletion in Photosystern II on Excitation Energy Transfer in Arabidopsis thaliana, Biophysical Journal, 98 (2010) 922-931.
[100] L.J. Tian, S. Farooq, H. van Amerongen, Probing the picosecond kinetics of the photosystem II core complex in vivo, Physical Chemistry Chemical Physics, 15 (2013) 3146-3154.
[101] I.H. Van Stokkum, B. Van Oort, F. Van Mourik, B. Gobets, H. Van Amerongen, (Sub)-picosecond spectral evolution of fluorescence studied with a synchroscan streak-camera system and target analysis, in: Biophysical techniques in photosynthesis, Springer, 2008, pp. 223-240.
[102] O.J.G. Somsen, L.B. Keukens, M.N. de Keijzer, A. van Hoek, H. van Amerongen, Structural heterogeneity in DNA: Temperature dependence of 2-aminopurine fluorescence in dinucleotides, Chemphyschem, 6 (2005) 1622-1627.
[103] B. van Oort, Ultrafast fluorescence of photosynthetic crystals and light-harvesting complexes, in, s.n.], [S.l., 2008.
[104] E. Russinova, J.W. Borst, M. Kwaaitaal, A. Cano-Delgado, Y.H. Yin, J. Chory, S.C. de Vries, Heterodimerization and endocytosis of Arabidopsis brassinosteroid receptors BRI1 and AtSERK3 (BAK1), Plant Cell, 16 (2004) 3216-3229.
[105] B. van Oort, A. Amunts, J.W. Borst, A. van Hoek, N. Nelson, H. van Amerongen, R. Croce, Picosecond Fluorescence of Intact and Dissolved PSI-LHCI Crystals, Biophysical Journal, 95 (2008) 5851-5861.

CHAPTER 1

Chapter 2

State transitions in *Chlamydomonas reinhardtii* strongly modulate the functional size of Photosystem II but not of Photosystem I

Caner Ünlü[a], Bartlomiej Drop[b], Roberta Croce[b], Herbert van Amerongen[a,c]

[a]Laboratory of Biophysics, Wageningen University, 6703 HA Wageningen, The Netherlands, [b]Department of Physics and Astronomy, Faculty of Sciences, VU University Amsterdam, 1081 HV Amsterdam, The Netherlands, [c]MicroSpectroscopy Centre, Wageningen University, 6703 HA Wageningen, The Netherlands.

Based on:

Ünlü, C., Drop, B., Croce, R., & van Amerongen, H. (2014). State transitions in Chlamydomonas reinhardtii strongly modulate the functional size of photosystem II but not of photosystem I. *Proceedings of the National Academy of Sciences of the USA*, *111*(9), 3460-3465

CHAPTER 2

2.1 ABSTRACT

Plants and green algae optimize photosynthesis in changing light conditions by balancing the amount of light absorbed by photosystems I and II. These photosystems work in series to extract electrons from water and reduce $NADP^+$ to NADPH. Light-harvesting complexes (LHCs) are held responsible for maintaining the balance by moving from one photosystem to the other in a process called state transitions. In the green alga *Chlamydomonas reinhardtii*, a photosynthetic model organism, state transitions are thought to involve 80% of the LHCs. Here we demonstrate with picosecond-fluorescence spectroscopy on *C. reinhardtii* cells that although LHCs indeed detach from Photosystem II in state-2 conditions only a fraction attaches to Photosystem I. The detached antenna complexes become protected against photodamage via shortening of the excited-state lifetime. It is discussed how the transition from state 1 to state 2 can protect *C. reinhardtii* in high-light conditions and how this differs from the situation in plants.

2.2 INTRODUCTION

Oxygenic photosynthesis is the most important process for fuelling life on earth. Light capture and subsequent charge separation processes occur in the photosystems I and II (PSI and PSII). In plants and green algae both PSs consist of a pigment-protein core complex surrounded by outer LHCs. Electronic excitations induced by the absorption of sunlight lead to charge separation in the reaction centres (RCs) of PSI and PSII, located in the cores of the PSs. These PSs work in series to extract electrons from water and reduce $NADP^+$ to NADPH. For optimal linear electron transport from water to $NADP^+$ a balance is needed for the amount of light absorbed by the pigments in the two PSs.

Besides carotenoids, the PSII core contains 35 chlorophylls *a* (Chls *a*) whereas this number is close to 100 for PSI [1]. The outer LHCs consist of various components: The major light-harvesting complex LHCII (a trimer) harbours 12 carotenoids (Cars) and 42 chlorophylls (Chls), 24 of which are Chls *a* [2], the pigments that are largely responsible for excitation energy transfer (EET) to the PSII RC. In higher plants there are also three monomeric minor LHCs per core, called CP24, CP26, and CP29, which show high sequence homology with LHCII (see e.g. [3]). In non-stressed conditions between 85 and 90% of the excitations in PSII lead to charge separation in the RC [4]. PSI in plants binds 4 LHCs (Lhca1-4) [5]. The amount of LHCII in the plant membranes is variable and usually ranges from ~2 to ~4 trimers per PSII core, most of which are functionally connected to PSII, although part is also associated with PSI [6]. In *C. reinhardtii* PSI antenna size differs and there are 9 Lhca's per PSI [7]. Nine LhcbM genes, plus CP29 and CP26 codify for the antenna complexes of PSII [8] and it was recently shown that in addition to CP26 and CP29 the PSII supercomplex contains three LHCII trimers per monomeric core [9]. In addition there are usually 3-4 extra LHCII trimers present per monomeric core (Drop et al. 2014) (see also below).

Although both PSI and PSII contain Chls and Cars, their absorption spectra differ, with PSII being more effective in absorbing blue light and PSI in absorbing far-red light [10-12]. Because intensity and spectral composition can vary, organisms need to rapidly adjust the relative absorption cross sections of both PSs. This regulation occurs via so-called state transitions, and it involves the relocation of Lhcs between PSII and PSI [13].

In higher plants all LHCII is bound to PSII in state 1, while in state 2, which can be induced by overexciting PSII, part of LHCII (around 15%) moves to PSI [13, 14]. State transitions are regulated by the redox state of the plastoquinone (PQ) pool via the reversible phosphorylation of LHCII [13, 15-18]. The green alga *C. reinhardtii*, that has widely been used as a model system in photosynthesis research and that might also become important for the production of food and feed ingredients and future biofuels [19], is thought to exhibit state transitions to a far larger extent than higher plants. The widely accepted view is that during the transition from state 1 to state 2, 80% of the major antenna complexes dissociates from PSII and attaches to PSI [20]. This picture is based on results that were obtained with photoacoustic measurements, which were used to determine the quantum yield of both PSs in different states. This view has been supported by the finding that the PSII supercomplex is largely disassembled in state 2 [21]. However, although a PSI-LHCII supercomplex from *C. reinhardtii* has been isolated [22], the amount of LHCII associated with it has not been quantified and it has also not been shown that the additional LHCII is capable of transferring energy to the PSI core. More recently, it was argued based on biochemical analysis that also CP26 and CP29 are participating in state transitions in *C. reinhardtii* [21-24], but again a quantitative analysis is missing.

Besides biochemical techniques, time-resolved fluorescence spectroscopy can be helpful to study state transitions and to enlighten the EET processes. The main advantage of this technique is that it can provide both quantitative and functional information for the different states *in vivo* [6]. However, the number of time-resolved fluorescence studies on green algae and especially their state transitions is limited [25-28]. Wendler and Holzwarth studied state transitions in the green alga *Scenedesmus obliquus* using time-resolved fluorescence spectroscopy [26]. They interpreted their data at that time in terms of reversible migration of LHCs between PSII α- and β-centres during state transitions, whereas it was concluded that the size of PSI was not measurably changing [26]. Another study was performed by Iwai et al. [27], who used fluorescence lifetime imaging microscopy (FLIM) to visualize state transitions in *C. reinhardtii*. The authors reported the dissociation of LHCII from PSII during the first part of the transition from state 1 to state 2, but they did not investigate what was happening during the later phase [27]. Recently, Wientjes et al. [6] performed a study on light acclimation and state transitions in the plant *Arabidopsis thaliana* and amongst others it was demonstrated quantitatively how time-resolved fluorescence properties of thylakoid membranes change when the relative amount of LHCII attached to PSI and PSII changes [6]: When LHCII attaches to PSI, the amplitude of a

component with fluorescence lifetime below 100 ps increases significantly whereas the contribution of the components with lifetimes of several hundreds of ps concomitantly decreases, and the corresponding lifetimes become shorter [6]. The former component is mainly due to PSI (with or without LHCII connected) and the latter are due to PSII (with varying amounts of LHCII connected). It is important to point out that the amplitudes of the decay components are directly proportional to the number of pigments that correspond to these decay components, [6, 29]. Therefore, if during state transitions LHCs are moving from PSII to PSI then the amplitude(s) of the PSI decay components will increase, whereas those of PSII will decrease. In general, such a reorganization will also lead to some changes in the fluorescence lifetimes. If in addition also quenching processes are introduced, this will lead to an additional change in the lifetime but not in the amplitude [30]

Here we applied time-resolved fluorescence spectroscopy to study changes in PSI and PSII antenna size in response to state transitions for wild-type (WT) *C. reinhardtii in vivo*. The cells were locked in different states, using the same method as used for previous photoacoustic measurements [20, 31], and fluorescence decay curves were recorded at room temperature. The results led us to challenge some of the generally accepted views, especially concerning the structure of the PSI supercomplex in state 2 and the fate of the detached LHCII. The main changes during state transitions occur in PSII whereas changes in the PSI supercomplex turn out to be less pronounced. In addition, it appears that both in state 1 and 2 a pool of LHCII exists that is neither connected to PSI nor to PSII while its size is larger in state 2.

2.3 METHODS

Strains and Growth Conditions. WT *C. reinhardtii* cells were grown under continuous white light illumination in TAP (Tris-acetate-phosphate) medium [32]. Cells were shaken in a rotary shaker (100 rpm) at 30^0C and illuminated by a white lamp at 10 μmol photons.m^2.s^{-1}. All cells were grown in 250 ml flasks with a growing volume of 50 ml, and maintained in the logarithmic growth phase. Also a higher light intensity (100 μmol.photons m^2.s^{-1}) was used to grow cells and the results are shown in SI.

State Locking. Cells were locked in state 1 or 2 in the following ways commonly used for state transitions studies on *C. reinhardtii* [20, 24, 31, 33, 34]: State 1 was obtained by incubating the cells in the dark while vigorously shaking for 2 hours (to oxidize the PQ pool with oxygen present) and state 2 was obtained by dark incubation in anaerobic conditions achieved by nitrogen bubbling for 25 min. (to over-reduce the PQ pool in the absence of oxygen) starting from cells in state 1, a method that was also applied by Delosme et al. [20, 31, 34]. Cells were directly used for time-resolved fluorescence measurements without further treatment.

Fluorescence Measurements

1. Steady-state fluorescence.

77K steady-state fluorescence spectra were recorded with a Jobin Yvon Fluorolog FL3 – 22 spectrofluorimeter using liquid nitrogen and corrected for wavelength-dependent detection sensitivity and fluctuations in lamp output. The λ_{exc} was 440 nm; a bandwidth of 2 nm was used for excitation and emission.

2. Time-resolved fluorescence

Time-correlated single photon counting (TCSPC) measurements were performed with a home-built setup [35]. Samples were excited with 400 nm and 465 nm pulses of 0.2 ps at repetition rate 3.8 MHz. To avoid closure of RCs and induction of unwanted state transitions the excitation intensity was kept low (0.5 – 1.5 μW) with a count rate of 3000 photons per second or lower. The size of the excitation spot was 2 mm. The instrument response function or IRF (40 – 50 ps FWHM) was obtained with pinacyanol iodide in methanol with 6 ps fluorescence lifetime [36, 37]. Measurements were done for 5 minutes. Fluorescence was detected at 679 nm, 701 nm and 720 nm using interference filters (15 nm width). Data were collected using a multichannel analyser with a maximum time window of 4096 channels at 5 or 2 ps/channel. One complete experiment consisted of recording data sets of reference compound, state locked cells and again reference compound, which was repeated at least twice with a fresh sample for each condition to check reproducibility.

Two-photon excitation (860 nm) FLIM was also performed *in vivo*; cells were placed on a cover glass and pressed between microscope and cover glasses. The setup was described previously [36, 38]. Fluorescence of *C. reinhardtii* was detected via nondescanned single-photon counting detection, through two bandpass filters of 700 nm (75 nm width). The average lifetimes per pixel were analysed with the SCP image software. All measurements were done at 22 ^{0}C.

3. Data Analysis.

Data obtained with the TCSPC setup were globally analysed using the "TRFA Data Processing Package" of the Scientific Software Technologies Center (Belarusian State University, Minsk, Belarus). Fluorescence decay curves were fitted to multi–exponential decay functions ($\sum_i p_i e^{-t/\tau_i}$) with relative amplitudes (p) and corresponding lifetimes (τ) that was convoluted with the IRF. The quality of a fit was judged from the χ^2 value and by visual inspection of residuals and autocorrelation thereof. The number of exponentials was 5 in all cases, whereas one of these components was an artefact with lifetime between 0.1 ps and 1 ps which was mainly used to improve the fit quality at early times. These artefacts are not further considered. The fit results were interpreted

in terms of the average fluorescence lifetime (τ_{avg}) for τ_2, τ_3 and τ_4 according to $\tau_{avg} = \sum_{i=2}^{4} p_i \tau_i$ where $\sum_{i=1}^{4} p_i = 1$

Acknowledgements: This work was supported financially by the Netherlands Organization for Scientific Research (NWO) via the Council for Chemical Sciences (HvA) and by an ERC Consolidator grant 281341 (RC).

2.4 RESULTS

Low-temperature (LT) steady-state fluorescence. 77K steady-state fluorescence spectra of state-1- and state-2-locked cells of WT *C. reinhardtii* were recorded upon 440 nm excitation (Figure 1). The spectra show the changing ratio of the intensity at 688 nm and 710 nm, which is characteristic for state transitions. The difference in ratio is thought to indicate that more LHC's are associated with PSII (fluorescence around 688 nm) in state 1 than in state 2 when LHCs largely associate with PSI (fluorescence around 710 nm). To study the underlying processes in more detail, we performed time-resolved fluorescence measurements *in vivo* at room temperature.

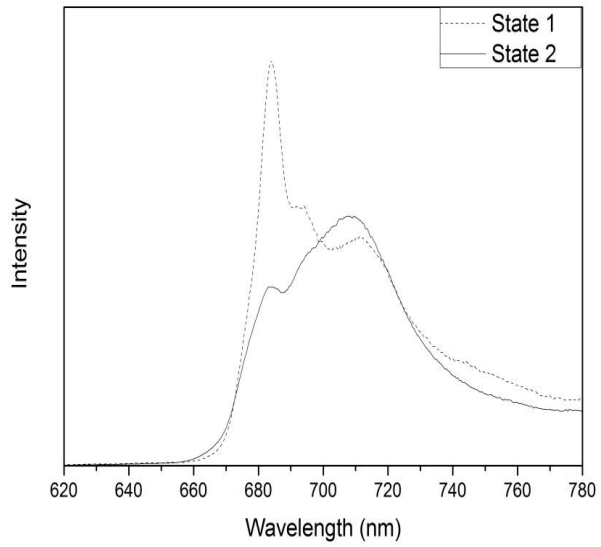

***Figure 1**. 77K fluorescence spectra of state-1-locked (dash) and state-2-locked (line) C. reinhardtii cells. The λ_{exc} was 440 nm. Note that the concentrations of the cells were identical for both states and the same was true for all the settings of the fluorimeter. Therefore, the intensities of the spectra can be directly compared to each other in an absolute sense. The fluorescence quantum yield of PSI in state 2 is only slightly higher than in state 1.*

Room-temperature time-resolved fluorescence

Time-resolved fluorescence measurements of *C. reinhardtii* cells in state 1 and 2 were performed with a TCSPC setup. Subpicosecond laser pulses of 400 nm, exciting relatively more Chls *a*, and pulses of 465 nm, exciting relatively more Chls *b* (and thus more antenna complexes) were used [39, 40]. For detection use was made of 679 nm, 701 nm and 720 nm interference band filters. Figure 2 shows that the fluorescence decay kinetics of state-1-locked cells are somewhat slower than those of

cells in state 2 for every excitation (λ_{exc}) and detection wavelength (λ_{det}) and the exact difference depends on the combination of wavelengths.

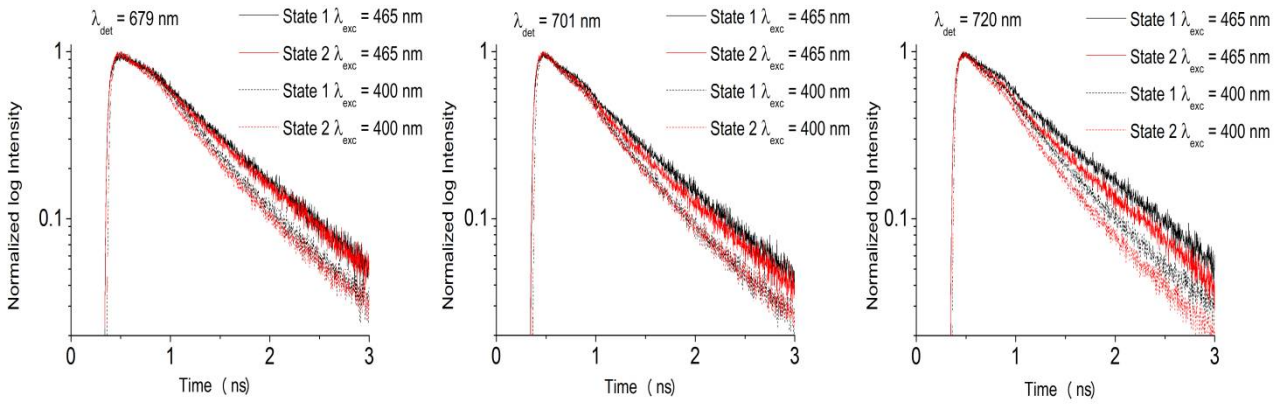

Figure 2. *Fluorescence decay curves for state-1- (black) and state-2-locked (red) C. reinhardtii cells at λ_{det} 679, 701 and 720 nm and excited at 465 nm and 400 nm. These data were globally analysed by TRFA software*

To obtain quantitative information from these decay curves, global analysis was performed and for all excitation and detection wavelengths the curves were fitted with the same lifetimes, at least for a specific state [6], even though individual lifetimes don't necessarily correspond one-to-one to specific physical processes. Global analysis of fluorescence decay curves of state-locked *C. reinhardtii* cells requires 5 decay components but the very fast one (~1 ps) has no real physical meaning since it is far shorter than the IRF and it does not have to be considered further (see *Methods*). The residual plots for all different state-locked cells in the SI demonstrate that 5 exponentials are sufficient. Fitting results are given in Tables 1 and 2.

Table 1. *Global analysis results for TCSPC data obtained by excitation at 400 nm at RT for state-locked C. reinhardtii.*

	State 1				State 2		
λ_{det} (nm)	**679**	**701**	**720**	**λ_{det} (nm)**	**679**	**701**	**720**
τ (ps)	*p*	*p*	*p*	τ (ps)	*p*	*p*	*p*
67(τ_1)	0.36	0.55	0.56	66(τ_1)	0.38	0.54	0.55
266(τ_2)	0.28	0.23	0.20	216(τ_2)	0.25	0.21	0.20
663(τ_3)	0.33	0.21	0.23	551(τ_3)	0.29	0.22	0.22
1902(τ_4)	0.03	0.01	0.01	1285(τ_4)	0.08	0.03	0.03

Confidence intervals of fluorescence lifetimes (τ) as calculated by exhaustive search were <5%, lifetimes were calculated from 2–4 repeats; p indicates relative amplitudes

Table 2. *Global analysis results for TCSPC data obtained by excitation at 465 nm at RT for state-locked C. reinhardtii.*

	State 1				State 2		
λ_{det} (nm)	**679**	**701**	**720**	**λ_{det} (nm)**	**679**	**701**	**720**
τ (ps)	*p*	*p*	*p*	τ (ps)	*p*	*p*	*p*
68(τ_1)	0.39	0.54	0.54	74(τ_1)	0.43	0.58	0.57
254(τ_2)	0.24	0.20	0.19	259(τ_2)	0.24	0.20	0.20
837(τ_3)	0.34	0.23	0.24	715(τ_3)	0.20	0.15	0.14
1909(τ_4)	0.03	0.03	0.03	1222(τ_4)	0.13	0.08	0.09

Confidence intervals of fluorescence lifetimes (τ) as calculated by exhaustive search were <5%, lifetimes were calculated from 2–4 repeats; p indicates relative amplitudes

The lifetime τ_1 in Tables 1 and 2, which is in the range 65–75 ps, is mainly due to PSI [26, 29]. Because PSI fluorescence is red-shifted as compared to PSII fluorescence, the relative amplitude of this component increases upon going from λ_{det}=679 to 720 nm. Only small changes occur in both the value of τ_1 and the corresponding amplitude due to the state change in *C. reinhardtii*. For λ_{exc}=400 nm, τ_1 is identical for state 1 and 2, and the corresponding amplitude is also the same. For λ_{exc}=465 nm, τ_1 is 6 ps shorter for state 1 than for state 2, whereas the corresponding amplitude is ~4% higher in state 2. Therefore, although some increase of both amplitude and lifetime of the PSI component can be observed, this increase is far smaller than one might expect based on literature [20]. The small increase in lifetime and amplitude lead to a small increase of the amount of PSI steady-state fluorescence, which becomes more pronounced at 77K and is (largely) responsible for the change in the ratio of fluorescence at 688 and 720 nm (Figure 1).

The lifetimes τ_2 and τ_3 in Tables 1 and 2 are mainly due to PSII with the highest amplitude at λ_{det}=679 nm, as expected for PSII [26], there is also some contribution from disconnected LHCs (discussed below). Lifetime τ_2 becomes shorter in state 2, 216 ps instead of 266 ps for λ_{exc}=400 nm but for λ_{exc}=465 nm, τ_2 remains more or less unchanged, 259 ps for state 2 vs. 254 ps for state 1. The amplitude remains the same for both excitation wavelengths. The shortening of τ_3 upon going to state 2 is more pronounced: for λ_{exc}=400 nm τ_3 goes down from 663 to 551 ps whereas the amplitude remains more or less constant, and for λ_{exc}=465 nm from 837 to 715 ps whereas the amplitude drops by 12%. In general, the average lifetime for PSII is shorter in state 2 (for both excitation wavelengths), while the total amplitude remains more or less constant for λ_{exc}=400 nm. Finally, the small contribution (at most 3%) of the longest component (τ_4) in state-1-locked cells is ascribed to some free chl but mainly to disconnected LHCs (note that the contribution of τ_4 to the average lifetime was even smaller when cells were grown in higher light conditions (See SI)). However, it should be noted that the amplitude of τ_4 increases for state-2-locked cells (5% at λ_{exc}=400 nm, 10 % at λ_{exc}=465 nm when detecting at 679 nm), which may be due to an increase of the amount of disconnected LHCs [25].

Comparing different excitation wavelengths

The main purpose of the present study is to understand the functional/organizational differences for PSI, PSII and dissociated LHCII in state 1 and 2. Whereas PSI has its own characteristic red-shifted fluorescence, the spectra of PSII and LHCII at room temperature largely overlap. In order to at least qualitatively distinguish between PSII and LHCII, the fluorescence decay kinetics were measured for state-1- and state-2-locked cells using different excitation wavelengths: 400 nm (excites relatively more the PSII core complexes) and 465 nm (excites relatively more the outer antenna complexes) [40]. Comparison of the decay curves for both excitation wavelengths shows that the decay is significantly slower for λ_{exc}=465 nm, both in state 1 and 2. Whereas τ_1 predominantly reflects the PSI decay time τ_2 -τ_4 correspond to PSII and LHCII and because it is *a priori* difficult to discriminate between PSII and LHCII we start by considering these lifetimes together. For state 1, the amplitude-weighted average lifetime τ_{avg} of τ_2 -τ_4 is 547 ps for λ_{exc}=400 nm (relatively more core excitation), whereas it is 660 ps for λ_{exc}=465 nm (λ_{det}=679 nm in both cases). The substantial difference (113 ps) indicates that either part of the antenna complexes is very badly connected to PSII core or not connected at all [29]. The same conclusion can be drawn from the data on state-2-locked cells, where τ_{avg} is 510 ps for λ_{exc}=400 nm, and it is 638 ps for λ_{exc}=465 nm (λ_{det}=679 nm in both cases). In conclusion, both for state-1- and state-2-locked cells we find a substantial fraction of badly connected or even fully detached LHCII. In order to confirm that this is an intrinsic property of individual cells and it is not due to a fraction of damaged or dead cells we also performed 2-photon FLIM experiments to monitor the variation between cells and a typical picture with densely packed cells is given in Figure 3, demonstrating that the fluorescence lifetime of all cells are very similar (on average around 400 ps, see SI, Figure S4) and thus that these long lifetime components are indeed an intrinsic property of individual *C. reinhardtii* cells. It is worth mentioning that the FLIM lifetimes that were previously determined by Minagawa and coworkers [27] were far shorter (around 200 ps), possibly because of the high excitation densities in their 1-photon FLIM experiments which can lead to singlet-singlet annihilation [41]. In contrast, it is possible with the 2-photon FLIM setup used here to record images with lifetimes that are very similar to lifetimes that are obtained with "macroscopic" TCSPC and streak-camera picosecond fluorescence setups [36, 42].

2.5 DISCUSSION

Energy partitioning between PSI and PSII has already been the subject of intense research for many years [12, 43]. Genetic approaches have led to the discovery of key proteins involved, such as kinases and phosphatases, regulating the phosphorylation state of LHCII and its relocation between PSII and PSI [15, 44, 45]. Biochemical and physiological studies have provided information about the mechanism and importance of state transitions in plants [46, 47] and the green alga *C. reinhardtii* [21,

22]. Important differences seem to exist between state transitions in *C. reinhardtii* and plants, such as the participation of the monomeric antennae CP26 and CP29 only in *C. reinhardtii* [21, 22] and the percentage of LHCII that participates (80% for *C. reinhardtii* vs. 15% for higher plants) [13, 20].

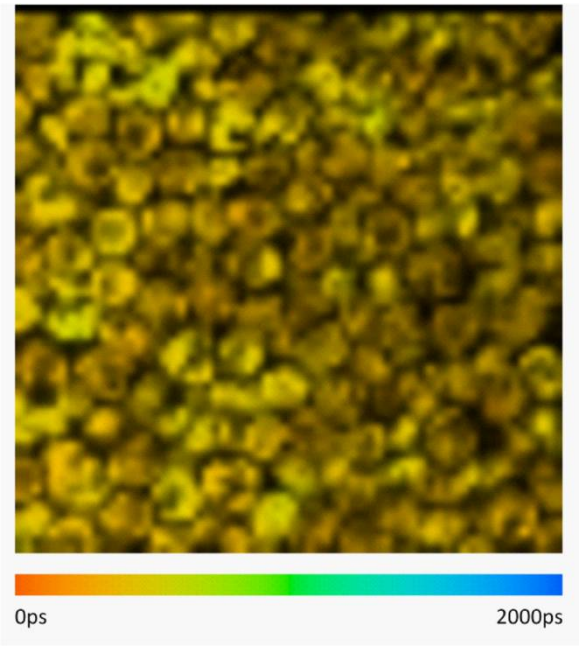

Figure 3. *Two-photon FLIM image of C. reinhardtii with the average lifetimes per pixel plotted using a colour scale. The fluorescence decay in each pixel was analysed by SPC image software, and the colour scale is between 0-2000 ps. (The average lifetime distribution is also given in a histogram in SI, Figure S4).*

Recently, long term acclimation and state transitions in *A. thaliana* were studied in detail, using amongst others time-resolved fluorescence techniques [6]. It was shown that the amplitude of the fluorescence lifetime that is due to PSI increases significantly when LHCII becomes attached to it [20]. It is thus remarkable that in *C. reinhardtii* only relatively minor differences can be observed between the PSI fluorescence kinetics for state 1 and 2 whereas the percentage of moving antenna is thought to be much higher (80 vs. 15%). If indeed 80% of the LHCII would move from PSII to PSI upon going from state 1 to state 2, this should lead to an increase of the relative amplitude of the PSI component by almost 40% (see SI) but the observed increase is at most 4% . Even if on average only one LHCII trimer would move from PSII to PSI this should still already lead to an increase of PSI amplitude by 6% (see SI). Therefore it should be concluded that the change in the average size of PSI is clearly smaller than one might have expected. This is further supported by the fact that also the corresponding lifetime hardly increases (only by 6 ps, at most).

In order to confirm in an independent way the fact that the amount of LHCII moving to PSI is substantially lower than what is generally believed, we also recorded 77K fluorescence excitation spectra in state 1 and 2, while monitoring the fluorescence of PSI at 712 nm and of PSII/LHCII at 680 nm (see SI, Figure S2). When comparing the excitation spectra of PSI and PSII it is clear that the spectral contributions around 475 and 650 nm are much smaller for PSI. These contributions are arising from Chl *b* and thus from the connected LHCs. Upon going from state 1 to state 2, there is a

minor increase of this contribution for PSI (in particular around 650 nm) whereas a small decrease can be observed for PSII (especially around 475 nm). So the LT fluorescence excitation spectra confirm the fact that little LHC is moving to PSI. A similar conclusion can be drawn from the 77K emission spectra recorded for different excitation wavelengths (see SI, Figure S3).

Although the changes in amplitude and lifetime of PSI are relatively minor, there is on the other hand a significant decrease of the average lifetime (not amplitude) of the slower decay components which are usually thought to originate from PSII. Our data imply that there must be a substantial change in PSII organization in agreement with earlier biochemical data [21]. The decrease of the average "PSII" lifetime can in principle be explained by a mechanism that is partly similar to the one that was recently proposed by Minagawa and coworkers [27]. According to this mechanism, a dynamic equilibrium exists between LHCII associated to PSII, LHCII associated to PSI, and LHCII dissociated from both PS's, being self-aggregated in a separate LHCII pool, where the fluorescence (excited state) of LHCII is quenched. In state 1 the majority of LHCII is bound to PSII whereas for state 2 the equilibrium shifts direction LHCII bound to PSI via aggregated LHCII. Our data do not confirm the association of a large amount of LHCII to PSI (at most a small fraction of LHCII becomes associated to PSI), but the fact that the "PSII lifetimes" become faster in state 2 while the total amplitude remains similar, can be explained by the detachment of LHCII from PSII while at the same time LHCII becomes quenched, otherwise one would expect the appearance of long-lived fluorescence component of around 4 ns [37]. A simple explanation for such quenching can indeed be aggregation of LHCII: Compared to monomeric and trimeric LHCII, aggregated LHCII is heavily quenched and the corresponding lifetimes can even be as short as 30 ps although a typical average lifetime is several hundreds of ps [37]. For a complete understanding of the phenomenon of state transitions it is important to sort out whether LHCII really dissociates and aggregates upon going from state 1 to state 2 and in order to do so we compared the kinetics for excitation at different wavelengths.

In a previous picosecond fluorescence study on thylakoid membranes from *A. thaliana*, van Oort et al. used two excitation wavelengths in order to maximally vary the relative number of excitations in the core and outer antenna of PSII [29]. The main purpose of that work was to determine the migration time of excitations to the RCs and to separate the PSI and PSII fluorescence kinetics from each other. It was however also found that in a CP24-less mutant, part of the outer antenna is detached from the PSII core, leading to a substantial increase of the fluorescence lifetime when relatively more outer antenna is excited. At the same time it could be concluded that this detached antenna was quenched because the fraction of pigments with a long fluorescence lifetime (several ns) was very small. Also in the present study a substantial difference in the average lifetime is observed for the two excitation wavelengths: It becomes much longer when relatively more outer antenna is excited at 465 nm as opposed to 400 nm. This means that a pool of LHCII is rather badly connected to the PSII cores

(leading to long migration times and thus long fluorescence lifetimes) or even completely disconnected, which from a functional point of view is nearly the same. Concurrently, this badly connected pool of LHCII is substantially quenched, considering the relatively short excited-state lifetimes. Remarkably, a large difference in excited-state lifetime for the two excitation wavelengths is observed both for state 1 and 2, meaning that in both states part of the antenna is disconnected from PSII. The existence of a pool of uncoupled LHCII in *C. reinhardtii* has been discussed in many studies on state transitions [27, 48]. With the use of time-resolved fluorescence, we have now demonstrated that such an LHCII pool indeed exists, regardless of the state of the cell.

It is important to mention that the results obtained in the present study in fact agree with an early proposal by Allen who, measuring cells of another green alga named *S. obliquus*, at that time claimed that during state transitions dissociated LHCII does not attach to PSI but instead is thermally deactivated, which means nothing else than that the fluorescence is quenched [49]. Our results can also explain why Minagawa et al. could follow the detachment of LHCII from PSII with the use of FLIM but did not report on what was happening after the detachment [27]. Although it was reported in several studies that at least CP26, CP29, and LhcbM5 attach to PSI in state 2 [21-23, 48], our current data demonstrate that this can only be true for a relatively small fraction. As was stated above, even if only one LHCII trimer would move from PSII to PSI this would already lead to an increase of PSI amplitude by 6%, which is more than is experimentally observed. Therefore, it should be concluded that for the state-1 to state-2 transition on average less than one 1 LHCII trimer is moving from PSII to PSI. In fact, we have to conclude from our data that even if LHCII detaches from PSII, only a fraction attaches to PSI and in fact most of the detached antenna complexes aggregate, leading to a shortening of the excited-state lifetime. This shortening ensures that there is no increase in photodamage of the antenna complexes upon detachment which would otherwise occur if quenching would be absent [50]. The fact that only a small amount of antenna attaches to PSI in state 2 also explains why the amount of fluorescence of PSI at 77K hardly increases (Figure 1). In contrast, the PSII (and LHC) fluorescence drops substantially, in line with the observed decrease of the average lifetime at room temperature.

State transitions: Chlamydomonas reinhardtii vs. Arabidopsis thaliana

Despite the fact that state transitions are present in plants and green algae, clear differences can be observed between this process in the model organisms *A. thaliana* and *C. reinhardtii.* In the plant *A. thaliana* the amount of LHCII involved in the process is relatively small (around 10-15% of the population) and this mobile pool is part of the LHCII population that transfers energy relatively slowly to the PSII core in state 1 [6] but once it is attached to PSI (state 2) the transfer is extremely fast and efficient [6]. The amount of LHCII that dissociates from PSII is identical to the amount that re-associates with PSI and serves to maintain a balance between PSI and PSII excitation. In the case of *C. reinhardtii* we demonstrate here that state transitions seem to reduce the antenna size of PSII, while

the effect on PSI is rather small, less than one LHCII trimer attaches per PSI complex on average. It has recently been demonstrated that in case of *A.thaliana*, the association of LHCII to PSI plays an important role in long term acclimation to different intensities of growth light because the antenna size of both PSI and PSII can be modulated simply by the change in the amount of LHCII (Lhcb1 and Lhcb2) which in most conditions serve as antenna for both PSs [6]. On the other hand, recent data on *C. reinhardtii* have underlined the important role of state transitions as a short term response mechanism to increase photoprotection [51]. This different role of state transitions in algae and plants seems to be related to the different mechanisms of non-photochemical quenching (NPQ) in the two organisms. Whereas *A. thaliana* can switch on its photoprotective mechanism of NPQ within seconds in dangerous high-light conditions, due to the presence of the so-called PsbS protein in the membranes [52], this is not the case for *C. reinhardtii*, where the protein that is required for NPQ is expressed with a delay of several hours when the alga is put in high-light conditions [53]. In this time period photoprotection is assured by state transitions [51]. Within this context it makes sense that state transitions in *C. reinhardii* are mainly affecting the antenna size of PSII, which indeed needs to be immediately reduced in high-light conditions to avoid photodamage. A concomitant increase of the antenna size of PSI is not necessary, and it would even be detrimental creating PSI damage [54]. In this respect there is again a resemblance with *A. thaliana* where high-light stress is one of the very few conditions in which LHCII does not attach to PSI [6]. Very interestingly, it has been found for *A. thaliana* that in high light, as part of the NPQ mechanism, PsbS induces the detachment of a significant fraction of the outer antenna from PSII, which gets concomitantly quenched [55]. This is very much reminiscent to what is now observed for *C. reinhardtii* during the process that has always been denoted as state transitions.

In conclusion, in contrast to what is generally believed, not 80% of the LHCII is moving from PSII to PSI upon the transition from state 1 to state 2 but only a small fraction (in the order of 10%). The rest of LHCII that detaches from PSII becomes quenched and this detachment seems to play an important role in NPQ that protects PSII against dangerous over-excitation in high-light conditions, similar to what is happening in plants when PsbS is activated in high light.

2.6 REFERENCES

[1] P. Jordan, P. Fromme, H.T. Witt, O. Klukas, W. Saenger, N. Krauss, Three-dimensional structure of cyanobacterial photosystem I at 2.5 angstrom resolution, Nature, 411 (2001) 909-917.
[2] Z.F. Liu, H.C. Yan, K.B. Wang, T.Y. Kuang, J.P. Zhang, L.L. Gui, X.M. An, W.R. Chang, Crystal structure of spinach major light-harvesting complex at 2.72 angstrom resolution, Nature, 428 (2004) 287-292.
[3] R. Croce, H. van Amerongen, Light-harvesting and structural organization of Photosystem II: From individual complexes to thylakoid membrane, Journal of Photochemistry and Photobiology B-Biology, 104 (2011) 142-153.
[4] E. Wientjes, H. van Amerongen, R. Croce, Quantum Yield of Charge Separation in Photosystem II: Functional Effect of Changes in the Antenna Size upon Light Acclimation, The Journal of Physical Chemistry B, (2013).
[5] A. Ben-Shem, F. Frolow, N. Nelson, Crystal structure of plant photosystem I, Nature, 426 (2003) 630-635.
[6] E. Wientjes, H. van Amerongen, R. Croce, LHCII is an antenna of both photosystems after long-term acclimation, Biochimica et biophysica acta, 1827 (2013) 420-426.
[7] B. Drop, M. Webber-Birungi, F. Fusetti, R. Kouril, K.E. Redding, E.J. Boekema, R. Croce, Photosystem I of Chlamydomonas reinhardtii Contains Nine Light-harvesting Complexes (Lhca) Located on One Side of the Core, Journal of Biological Chemistry, 286 (2011) 44878-44887.
[8] D. Elrad, A.R. Grossman, A genome's-eye view of the light-harvesting polypeptides of Chlamydomonas reinhardtii, Current Genetics, 45 (2004) 61-75.
[9] R. Tokutsu, N. Kato, K.H. Bui, T. Ishikawa, J. Minagawa, Revisiting the Supramolecular Organization of Photosystem II in Chlamydomonas reinhardtii, Journal of Biological Chemistry, 287 (2012) 31574-31581.
[10] N. Murata, Control of Excitation Transfer in Photosynthesis .I. Light-Induced Change of Chlorophyll a Fluorescence in Porphyridium Cruentum, Biochimica Et Biophysica Acta, 172 (1969) 242-&.
[11] Bonavent.C, J. Myers, Fluorescence and Oxygen Evolution from Chlorella Pyrenoidosa, Biochimica Et Biophysica Acta, 189 (1969) 366-+.
[12] J.F. Allen, J. Bennett, K.E. Steinback, C.J. Arntzen, Chloroplast Protein-Phosphorylation Couples Plastoquinone Redox State to Distribution of Excitation-Energy between Photosystems, Nature, 291 (1981) 25-29.
[13] J.F. Allen, Protein-Phosphorylation in Regulation of Photosynthesis, Biochimica Et Biophysica Acta, 1098 (1992) 275-335.
[14] R. Kouril, A. Zygadlo, A.A. Arteni, C.D. de Wit, J.P. Dekker, P.E. Jensen, H.V. Scheller, E.J. Boekema, Structural characterization of a complex of photosystem I and light-harvesting complex II of Arabidopsis thaliana, Biochemistry, 44 (2005) 10935-10940.
[15] S. Bellafiore, F. Barneche, G. Peltier, J.D. Rochaix, State transitions and light adaptation require chloroplast thylakoid protein kinase STN7, Nature, 433 (2005) 892-895.
[16] N. Depege, S. Bellafiore, J.D. Rochaix, Role of chloroplast protein kinase Stt7 in LHCII phosphorylation and state transition in Chlamydomonas, Science, 299 (2003) 1572-1575.
[17] V. Bonardi, P. Pesaresi, T. Becker, E. Schleiff, R. Wagner, T. Pfannschmidt, P. Jahns, D. Leister, Photosystem II core phosphorylation and photosynthetic acclimation require two different protein kinases, Nature, 437 (2005) 1179-1182.
[18] A. Shapiguzov, B. Ingelsson, I. Samol, C. Andres, F. Kessler, J.D. Rochaix, A.V. Vener, M. Goldschmidt-Clermont, The PPH1 phosphatase is specifically involved in LHCII dephosphorylation and state transitions in Arabidopsis, Proceedings of the National Academy of Sciences of the United States of America, 107 (2010) 4782-4787.
[19] R.H. Wijffels, M.J. Barbosa, An Outlook on Microalgal Biofuels, Science, 329 (2010) 796-799.
[20] R. Delosme, J. Olive, F.A. Wollman, Changes in light energy distribution upon state transitions: An in vivo photoacoustic study of the wild type and photosynthesis mutants from Chlamydomonas reinhardtii, Biochimica Et Biophysica Acta-Bioenergetics, 1273 (1996) 150-158.
[21] M. Iwai, Y. Takahashi, J. Minagawa, Molecular remodeling of photosystem II during state transitions in Chlamydomonas reinhardtii, Plant Cell, 20 (2008) 2177-2189.

[22] H. Takahashi, M. Iwai, Y. Takahashi, J. Minagawa, Identification of the mobile light-harvesting complex II polypeptides for state transitions in Chlamydomonas reinhardtii, Proceedings of the National Academy of Sciences of the United States of America, 103 (2006) 477-482.
[23] R. Tokutsu, M. Iwai, J. Minagawa, CP29, a Monomeric Light-harvesting Complex II Protein, Is Essential for State Transitions in Chlamydomonas reinhardtii, Journal of Biological Chemistry, 284 (2009) 7777-7782.
[24] J. Kargul, M.V. Turkina, J. Nield, S. Benson, A.V. Vener, J. Barber, Light-harvesting complex II protein CP29 binds to photosystem I of Chlamydomonas reinhardtii under State 2 conditions, Febs Journal, 272 (2005) 4797-4806.
[25] M. Hodges, I. Moya, Time-Resolved Chlorophyll Fluorescence Studies on Photosynthetic Mutants of Chlamydomonas-Reinhardtii - Origin of the Kinetic Decay Components, Photosynthesis Research, 13 (1987) 125-141.
[26] J. Wendler, A.R. Holzwarth, State Transitions in the green-alga Scenedesmus-obliquus probed by time-resolved chlorophyll fluorescence spectroscopy and global data-analysis, Biophysical Journal, 52 (1987) 717-728.
[27] M. Iwai, M. Yokono, N. Inada, J. Minagawa, Live-cell imaging of photosystem II antenna dissociation during state transitions, Proceedings of the National Academy of Sciences of the United States of America, 107 (2010) 2337-2342.
[28] K. Amarnath, J. Zaks, S.D. Park, K.K. Niyogi, G.R. Fleming, Fluorescence lifetime snapshots reveal two rapidly reversible mechanisms of photoprotection in live cells of Chlamydomonas reinhardtii, Proceedings of the National Academy of Sciences of the United States of America, 109 (2012) 8405-8410.
[29] B. van Oort, M. Alberts, S. de Bianchi, L. Dall'Osto, R. Bassi, G. Trinkunas, R. Croce, H. van Amerongen, Effect of Antenna-Depletion in Photosystern II on Excitation Energy Transfer in Arabidopsis thaliana, Biophysical Journal, 98 (2010) 922-931.
[30] A.R. Holzwarth, D. Lenk, P. Jahns, On the analysis of non-photochemical chlorophyll fluorescence quenching curves I. Theoretical considerations, Biochimica Et Biophysica Acta-Bioenergetics, 1827 (2013) 786-792.
[31] M.M. Fleischmann, S. Ravanel, R. Delosme, J. Olive, F. Zito, F.A. Wollman, J.D. Rochaix, Isolation and characterization of photoautotrophic mutants of Chlamydomonas reinhardtii deficient in state transition, Journal of Biological Chemistry, 274 (1999) 30987-30994.
[32] D.S. Gorman, R.P. Levine, Cytochrome F and Plastocyanin - Their Sequence in Photosynthetic Electron Transport Chain of Chlamydomonas Reinhardi, Proceedings of the National Academy of Sciences of the United States of America, 54 (1965) 1665-&.
[33] F.A. Wollman, P. Delepelaire, Correlation between Changes in Light Energy-Distribution and Changes in Thylakoid Membrane Polypeptide Phosphorylation in Chlamydomonas-Reinhardtii, Journal of Cell Biology, 98 (1984) 1-7.
[34] G. Finazzi, R.P. Barbagallo, E. Bergo, R. Barbato, G. Forti, Photoinhibition of Chlamydomonas reinhardtii in State 1 and State 2 - Damages to the photosynthetic apparatus under linear and cyclic electron flow, Journal of Biological Chemistry, 276 (2001) 22251-22257.
[35] O.J.G. Somsen, L.B. Keukens, M.N. de Keijzer, A. van Hoek, H. van Amerongen, Structural heterogeneity in DNA: Temperature dependence of 2-aminopurine fluorescence in dinucleotides, Chemphyschem, 6 (2005) 1622-1627.
[36] B. van Oort, A. Amunts, J.W. Borst, A. van Hoek, N. Nelson, H. van Amerongen, R. Croce, Picosecond Fluorescence of Intact and Dissolved PSI-LHCI Crystals, Biophysical Journal, 95 (2008) 5851-5861.
[37] B. van Oort, A. van Hoek, A.V. Ruban, H. van Amerongen, Aggregation of Light-Harvesting Complex II leads to formation of efficient excitation energy traps in monomeric and trimeric complexes, Febs Letters, 581 (2007) 3528-3532.
[38] E. Russinova, J.W. Borst, M. Kwaaitaal, A. Cano-Delgado, Y.H. Yin, J. Chory, S.C. de Vries, Heterodimerization and endocytosis of Arabidopsis brassinosteroid receptors BRI1 and AtSERK3 (BAK1), Plant Cell, 16 (2004) 3216-3229.
[39] K. Broess, G. Trinkunas, C.D. van der Weij-de Wit, J.P. Dekker, A. van Hoek, H. van Amerongen, Excitation energy transfer and charge separation in photosystem II membranes revisited, Biophysical Journal, 91 (2006) 3776-3786.

[40] K. Broess, G. Trinkunas, A. van Hoek, R. Croce, H. van Amerongen, Determination of the excitation migration time in Photosystem II - Consequences for the membrane organization and charge separation parameters, Biochimica Et Biophysica Acta-Bioenergetics, 1777 (2008) 404-409.
[41] V. Barzda, C.J. de Grauw, J. Vroom, F.J. Kleima, R. van Grondelle, H. van Amerongen, H.C. Gerritsen, Fluorescence lifetime heterogeneity in aggregates of LHCII revealed by time-resolved microscopy, Biophysical Journal, 81 (2001) 538-546.
[42] S.B. Krumova, S.P. Laptenok, J.W. Borst, B. Ughy, Z. Gombos, G. Ajlani, H. van Amerongen, Monitoring Photosynthesis in Individual Cells of Synechocystis sp. PCC 6803 on a Picosecond Timescale, Biophysical Journal, 99 (2010) 2006-2015.
[43] J. Bennett, K.E. Steinback, C.J. Arntzen, Chloroplast phosphoproteins: Regulation of excitation energy transfer by phosphorylation of thylakoid membrane polypeptides, Proc.Natl.Acad.Sci.USA, 77 (1980) 5253-5257.
[44] A. Shapiguzov, B. Ingelsson, I. Samol, C. Andres, F. Kessler, J.D. Rochaix, A.V. Vener, M. Goldschmidt-Clermont, The PPH1 phosphatase is specifically involved in LHCII dephosphorylation and state transitions in Arabidopsis, Proceedings of the National Academy of Sciences of the United States of America, 107 (2010) 4782-4787.
[45] M. Pribil, P. Pesaresi, A. Hertle, R. Barbato, D. Leister, Role of Plastid Protein Phosphatase TAP38 in LHCII Dephosphorylation and Thylakoid Electron Flow, Plos Biology, 8 (2010) -.
[46] M. Tikkanen, M. Grieco, S. Kangasjarvi, E.M. Aro, Thylakoid protein phosphorylation in higher plant chloroplasts optimizes electron transfer under fluctuating light, Plant physiology, 152 (2010) 723-735.
[47] M. Tikkanen, M. Piippo, M. Suorsa, S. Sirpio, P. Mulo, J. Vainonen, A.V. Vener, Y. Allahverdiyeva, E.M. Aro, State transitions revisited-a buffering system for dynamic low light acclimation of Arabidopsis, Plant molecular biology, 62 (2006) 779-793.
[48] J. Minagawa, State transitions-The molecular remodeling of photosynthetic supercomplexes that controls energy flow in the chloroplast, Biochimica Et Biophysica Acta-Bioenergetics, 1807 (2011) 897-905.
[49] J.F. Allen, A. Melis, The Rate of P-700 Photooxidation under Continuous Illumination Is Independent of State-1 State-2 Transitions in the Green-Alga Scenedesmus-Obliquus, Biochimica Et Biophysica Acta, 933 (1988) 95-106.
[50] A.V. Ruban, R. Berera, C. Ilioaia, I.H.M. van Stokkum, J.T.M. Kennis, A.A. Pascal, H. van Amerongen, B. Robert, P. Horton, R. van Grondelle, Identification of a mechanism of photoprotective energy dissipation in higher plants, Nature, 450 (2007) 575-U522.
[51] G. Allorent, R. Tokutsu, T. Roach, G. Peers, P. Cardol, J. Girard-Bascou, D. Seigneurin-Berny, D. Petroutsos, M. Kuntz, C. Breyton, F. Franck, F.A. Wollman, K.K. Niyogi, A. Krieger-Liszkay, J. Minagawa, G. Finazzi, A Dual Strategy to Cope with High Light in Chlamydomonas reinhardtii, Plant Cell, 25 (2013) 545-557.
[52] X.P. Li, O. Bjorkman, C. Shih, A.R. Grossman, M. Rosenquist, S. Jansson, K.K. Niyogi, A pigment-binding protein essential for regulation of photosynthetic light harvesting, Nature, 403 (2000) 391-395.
[53] G. Peers, T.B. Truong, E. Ostendorf, A. Busch, D. Elrad, A.R. Grossman, M. Hippler, K.K. Niyogi, An ancient light-harvesting protein is critical for the regulation of algal photosynthesis, Nature, 462 (2009) 518-U215.
[54] M. Grieco, M. Tikkanen, V. Paakkarinen, S. Kangasjarvi, E.-M. Aro, Steady-State Phosphorylation of Light-Harvesting Complex II Proteins Preserves Photosystem I under Fluctuating White Light, Plant Physiology, 160 (2012) 1896-1910.
[55] A.R. Holzwarth, Y. Miloslavina, M. Nilkens, P. Jahns, Identification of two quenching sites active in the regulation of photosynthetic light-harvesting studied by time-resolved fluorescence, Chemical Physics Letters, 483 (2009) 262-267.

Supplementary Information:

LHCII:PSI:PSII stoichiometry in the membranes of *Chlamydomonas reinhardtii*

It has been proposed that in *C. reinhardtii* 80% of the LHCII population moves from PSII to PSI during the transition from state 1 to state 2. However, to fully understand the extent of the transition it is important to know the number of LHCII complexes present in the membranes.

We have measured the PSI:PSII ratio (in terms of reaction centers) with a Joliot-type spectrophotometer (Bio-Logic SAS JTS-10) using the carotenoid electrochromic shift as reported previously(1-4). The data indicate that in our cells the PSI/PSII ratio is 0.93, in agreement with previous reports indicating that in most conditions this value for *C. reinhardtii* is close to 1 (3, 5).

The Chl *a*/*b* ratio of the cells was 2.25, also in agreement with previous data (5). The pigment composition of the complexes was analyzed by fitting the spectrum of the 80% acetone extracted pigments with the spectra of the individual pigments in acetone and by HPLC, as described previously (6). Some of us have recently shown that the PSI-LHCI complex of *C. reinhardtii* is composed of a core complex together with 9 Lhca's, binding in total around 240 Chls, of which 196 are Chls *a* and 44 are Chls *b* (7).

The PSII core contains 35 Chls *a*, whereas one LHCII trimer binds 42 Chls (24 Chls *a* and 18 Chls *b*) (8). For CP29 we use the stoichiometry obtained from the crystal structure (9) (meaning 9 Chls *a* and 4 Chls *b*) and for CP26 we use the same stoichiometry as for monomeric LHCII (8 Chls *a* and 6 Chls *b*). We assume that CP29 and CP26 are present in a 1:1 stoichiometry with the PSII core like in plants, meaning that PSII core + CP29 + CP26 together bind 53 Chls *a* and 8 Chls *b*

Using these data we can calculate the relative number *x* of LHCII trimers according to the equation:

$$2.25\pm0.05 = ((0.93\pm0.10) * 196 + 52 + 24\,x)/((0.93\pm0.10) * 44 + 10 + 18x)$$

leading to 7.5±1.0 LHCII (estimated uncertainty at most 1 LHCII) per PSII RC in the membranes of *C. reinhardtii*. Thus, if in state 1 all LHCII trimers (for instance 7) are associated with PSII, then there are 250 Chls *a* and 155 Chls *b* per PSII RC.

If, as suggested, 80% of the outer antenna moves to PSI in state 2, 2/3 of the Chls *a* of PSII would disappear, leading to a large decrease of the PSII amplitude and a concomitant increase of the PSI amplitude. Using the numbers above, this would mean that in state 1 45% of the Chls *a* would be attached to PSI and in state 2 this percentage would be 83%, an increase of 38%. However, as shown in the main text, the experimentally observed percentage is at most 4%. Even if we assume that one out of seven LHCII trimers would move from PSII to PSI, the ratio of the number of Chls *a* in PSI and

PSII would change from 196 and 226 to 220 and 202, respectively. This would correspond to an increase of the PSI amplitude of around 6%, more than is experimentally observed.

Global Analysis for *C. reinhardtii* cells grown in "normal" light conditions

C. reinhardtii cells were grown under continuous white light illumination in TAP medium(10). Cells were shaken in a rotary shaker (100 rpm) at 30^0C and illuminated by a white lamp at **normal** light intensity (**100 µmol.photons $m^2.s^{-1}$**). All cells were grown in 250 ml flasks with a growing volume of 50 ml, and they were maintained in the logarithmic growth phase. The global analysis results are shown in table S1.

Table S1. *Global analysis results for TCSPC data obtained upon excitation at 400 nm at RT for state-locked C. reinhardtii grown in normal light conditions.*

State 1			State 2		
condition : Normal Light			condition : Normal Light		
Detection	**680 nm**	**707 nm**	**Detection**	**680 nm**	**707 nm**
τ (ps)	*p*	*p*	τ (ps)	*p*	*p*
73	0.48	0.64	61	0.44	0.54
258	0.19	0.21	173	0.26	0.26
612	0.33	0.15	520	0.28	0.18
1553	0.004	0.004	1066	0.02	0.02
τ_{avg}	289.1 ps	198.0 ps	τ_{avg}	234.5 ps	191.4 ps

Confidence intervals of fluorescence lifetimes (τ) as calculated by exhaustive search were <5%, lifetimes were calculated with 2–4 repeats, p represents relative amplitudes. The fit results were interpreted in terms of the overall average fluorescence lifetime (τ_{avg}) for τ_1, τ_2, τ_3 and τ_4 according to $\tau_{avg} = \sum_{i=1}^{4} p_i \tau_i$ *where* $\sum_{i=1}^{4} p_i = 1$

Residuals for analysis performed in Tables 1 and 2

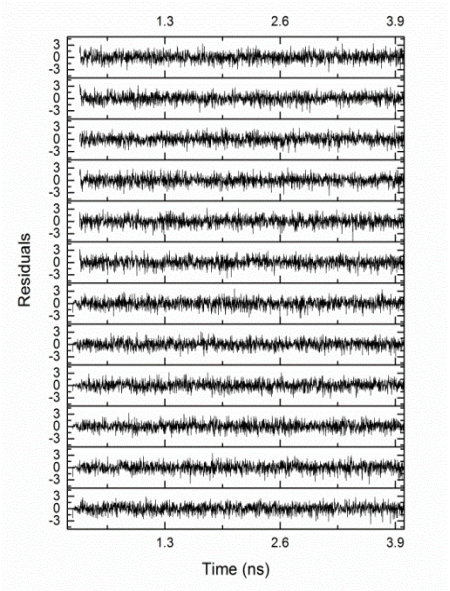

Figure S1.*Weighted residual plots of fluorescence decay curves in Figure 2. The residuals show that 5 decay components are sufficient for a successful fit.*

77 K Steady State Excitation Spectra for state-1-locked and state-2-locked cells

For steady-state fluorescence excitation spectra a Jobin Yvon Fluorolog FL3A22 spectrofluorimeter was used. The fluorescence excitation spectra were recorded at 77 K, with excitation and emission bandwidths of 2 nm and 1 nm, respectively. The emission was collected at 680 and 712 nm. An integration time of 0.4 s was used. Each spectrum was measured 6 times in a run and then averaged. The state-1 and state-2 spectrum for PSI, detected at 712 nm, are very similar and only show a small difference around 650 nm, indicating a small increase of excitation energy transfer from LHCII to PSI (see Fig. S2). Also the state-1 and state-2 spectrum for detection at 680 nm (PSII and detached LHCII), are very similar and only show a small difference around 475 nm, indicating a small decrease of excitation energy transfer from LHCII to PSI.

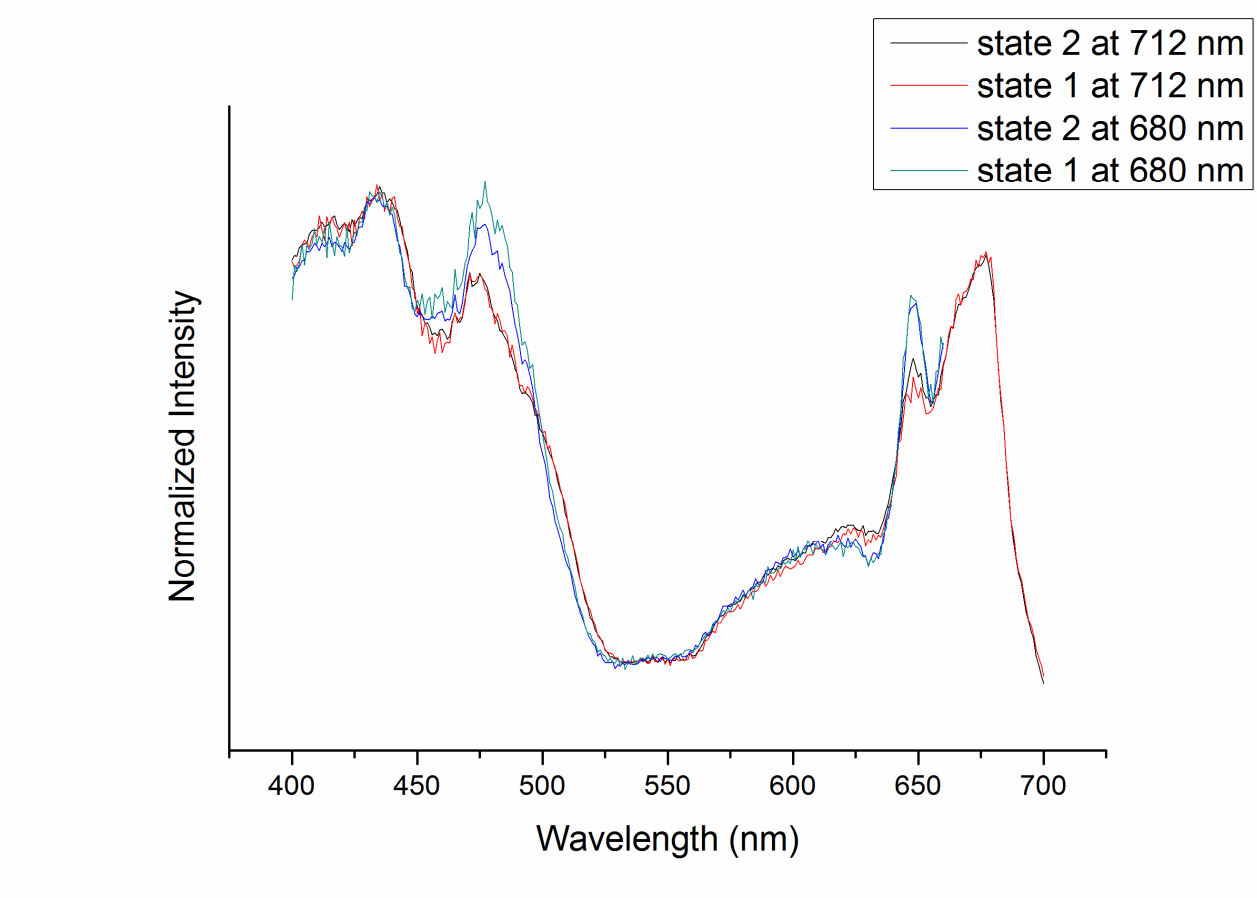

Figure S2. *Excitation spectra of state-1-locked and state-2-locked C. reinhardtii cells. The spectra are recorded at 77K at 2 different emission wavelengths (680 nm and 712 nm).*

In Fig. S3 the 77K emission spectra are shown for state 1 and state 2 after excitation at 440 nm (absorption peak of Chl *a*) and 475 nm (Chl *b*). For state 1 the relative height of the PSI peak around

710 nm is somewhat lower for 475 nm excitation than for 440 nm excitation. This indicates that the amount of Chl *b* which is present in the outer antenna complexes is somewhat lower for PSI than for PSII. Upon going to state 2 the spectra are completely different with a substantial relative increase of the PSI peak for both excitation wavelengths. Nevertheless, the PSI peak is still somewhat (although less) smaller for 475 nm excitation and also these results do not indicate massive movement of outer antenna complexes from PSII to PSI.

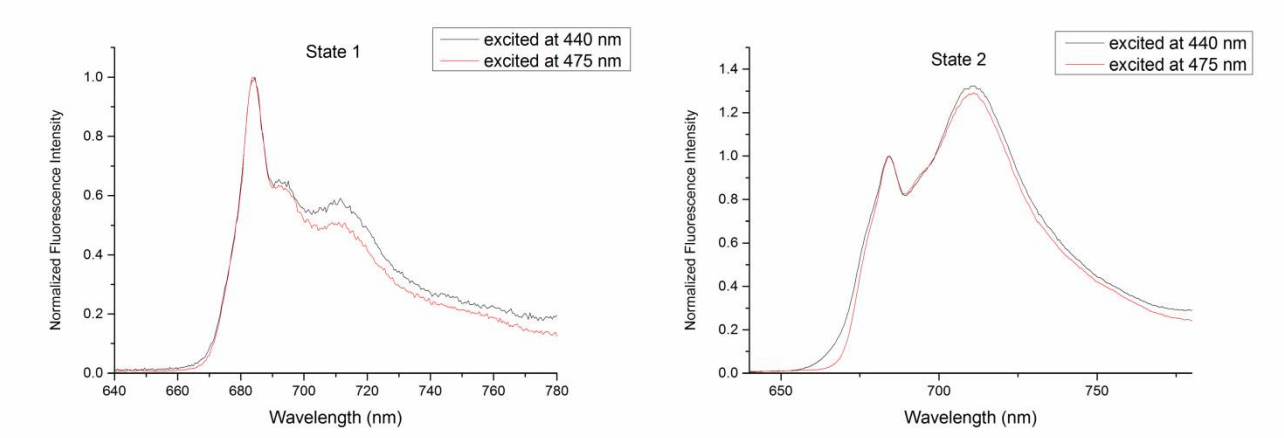

Figure S3. *Emission spectra of state-1-locked and state-2-locked C. reinhardtii cells. The spectra are recorded at 77K for 2 different excitation wavelengths (440 nm and 475 nm).*

The average lifetime distribution for FLIM image - Figure 3

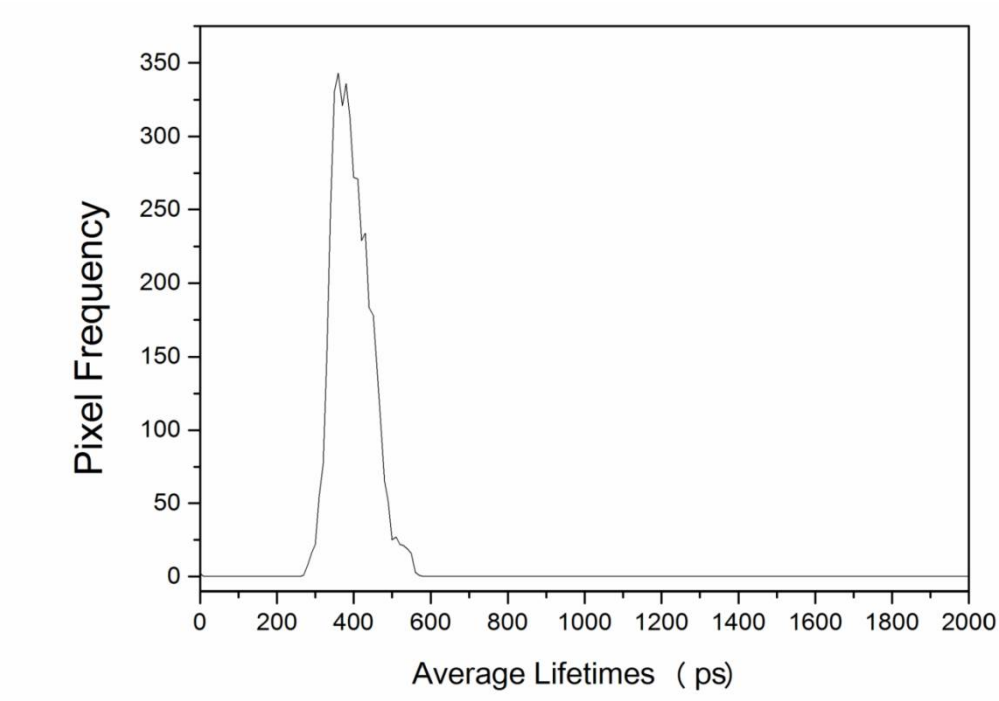

Figure S4. *The average lifetime distribution for Figure 3.*

References

1. Petroutsos D*, et al.* (2009) PGRL1 Participates in Iron-induced Remodeling of the Photosynthetic Apparatus and in Energy Metabolism in Chlamydomonas reinhardtii. *Journal of Biological Chemistry* 284(47):32770-32781 .
2. Bailleul B, Cardol P, Breyton C, & Finazzi G (2010) Electrochromism: a useful probe to study algal photosynthesis. *Photosynthesis Research* 106(1-2):179-189 .
3. Cardol P*, et al.* (2009) Impaired respiration discloses the physiological significance of state transitions in Chlamydomonas. *Proceedings of the National Academy of Sciences of the United States of America* 106(37):15979-15984 .
4. Joliot P & Delosme R (1974) Flash-Induced 519nm Absorption Change in Green-Algae. *Biochimica Et Biophysica Acta* 357(2):267-284 .
5. Bonente G, Pippa S, Castellano S, Bassi R, & Ballottari M (2012) Acclimation of Chlamydomonas reinhardtii to Different Growth Irradiances. *Journal of Biological Chemistry* 287(8):5833-5847 .
6. Croce R, Canino G, Ros F, & Bassi R (2002) Chromophore organization in the higher-plant photosystem II antenna protein CP26. *Biochemistry* 41(23):7334-7343 .
7. Drop B*, et al.* (2011) Photosystem I of Chlamydomonas reinhardtii Contains Nine Light-harvesting Complexes (Lhca) Located on One Side of the Core. *Journal of Biological Chemistry* 286(52):44878-44887 .
8. Liu ZF*, et al.* (2004) Crystal structure of spinach major light-harvesting complex at 2.72 angstrom resolution. *Nature* 428(6980):287-292 .
9. Pan XW*, et al.* (2011) Structural insights into energy regulation of light-harvesting complex CP29 from spinach. *Nature Structural & Molecular Biology* 18(3):309-U394 .
10. Gorman DS & Levine RP (1965) Cytochrome F and Plastocyanin - Their Sequence in Photosynthetic Electron Transport Chain of Chlamydomonas Reinhardi. *Proceedings of the National Academy of Sciences of the United States of America* 54(6):1665-& .

Chapter 3

Origin of the strong changes in fluorescence at 77K upon state transitions in *Chlamydomonas reinhardtii*.

Caner Ünlü [a], Iryna Polukhina [b], Herbert van Amerongen [a,c]

[a] Laboratory of Biophysics, Wageningen University, 6703 HA Wageningen, The Netherlands, [b] Department of Physics and Astronomy, Faculty of Sciences, VU University Amsterdam, De Boelelaan 1081, 1081 HV Amsterdam, The Netherlands [c] MicroSpectroscopy Centre, Wageningen University, 6703 HA Wageningen, The Netherlands.

CHAPTER 3

3.1 ABSTRACT:

In response to changes in the reduction state of the plastoquinone pool in its thylakoid membrane, the green alga *Chlamydomonas reinhardtti* is performing state transitions: Remodelling of its thylakoid membrane leads to a redistribution of excitations over photosystems I and II (PSI and PSII). The signature of these transitions is formed by marked changes in the 77K fluorescence spectrum. These changes are generally thought to reflect a redistribution of light-harvesting complexes (LHCs) over PSII (680) and PSI (720). Here we studied the picosecond fluorescence properties of *Chlamydomonas reinhardtti* over a broad range of wavelengths. It is observed that upon going from state 1 (relatively high 680nm/720nm fluorescence ratio) to state 2 (low ratio), a large part of the fluorescence of LHC/PSII becomes substantially quenched, probably because of LHC detachment from PSII, whereas the fluorescence of PSI hardly changes. These results are in agreement with our recent proposal that the amount of LHC moving from PSII to PSI upon going from state 1 to state 2 is very limited (Unlu et al. *Proceedings of the National Academy of Sciences of the United States of America* (2014). 111 (9):3460-3465).

3.2 INTRODUCTION

In oxygen-evolving photosynthetic organisms light energy is captured by photosystem I (PSI) and photosystem II (PSII). PSI and PSII both contain a pigment-protein core complex surrounded by outer light-harvesting complexes (LHCs). Light absorption by the LHCs induces electronic excitations, which lead to charge separation in the reaction centres (RCs) of PSI and PSII located in the cores of the photosystems. [1-7]. These photosystems are essential for photosynthetic electron transport, which operates in two different modes, cyclic electron flow and linear electron flow, providing ATP and NADPH for the Benson-Calvin cycle. [8, 9]. To ensure optimal efficiency in the electron transport chain, the distribution of absorbed light energy over both photosystems needs to be balanced, and if one of the photosystems is over-excited due to short-term environmental changes (like changes in spectral composition of light), the balance of absorbed light between both photosystems is regulated via the so-called state transitions and it involves the reorganization of LHCs between PSII and PSI [10-14].

The possible mechanisms for reorganisation of outer LHCs of PSII (LHCII) upon state transitions in *Chlamydomonas reinhardtii* have been discussed for several decades [11-13, 15-24]. For a long time people adhered to the opinion that upon the transition from state 1 to state 2, 80% of LHCII detaches from PSII and attaches completely to PSI in *Chlamydomonas reinhardtii* [12, 16]. Recently, this was disputed by us based on *in vivo* time-resolved fluorescence kinetics for state-locked cells [23]. In this study, it was observed that the amplitudes of PSII-LHCII and PSI fluorescence kinetics change only slightly upon state transitions [23]. These observations were important, because slightly earlier Wientjes et al. had shown that even small changes in the structure of the photosystems due to

migration of LHCII lead to significant changes in the amplitudes of the fluorescence kinetics of both photosystems in plants [14]. Moreover, it was observed that the PSII-LHCII fluorescence kinetics becomes faster whereas the PSI lifetimes hardly changed [14, 25]. Therefore, it was concluded that the changes in the PSI structure upon state transitions are minor, whereas LHCII is most likely partly detaching from PSII and becoming quenched [23] although also those changes are not very large. Even more recently, Nagy et al. confirmed this conclusion [24]. Also, in an early fluorescence kinetics study on the green alga *Scenedesmus obliquus*, it was shown that the changes in the PSI structure are minor upon state transitions [26]. Altogether, these studies do not support the view that the detached LHCII completely attaches to PSI [12] but they support an early view of Allen, who suggested that the detached LHCII goes into a thermal energy dissipative mode upon state transitions [27].

Chlorophyll fluorescence is often used to investigate the photosynthetic performance *in vivo* or *in vitro* [28-30], making use of the fact that it has its own characteristic emission behaviour [28-30]. At room temperature, the fluorescence emission of PSI around 720 nm is rather weak, but at cryogenic temperatures, the PSI fluorescence becomes far stronger and is easily discernible from the fluorescence of PSII, also because the fluorescence bands become sharper [31, 32]. Low-temperature emission spectra of photosynthetic organisms in different states are traditionally used to demonstrate the occurrence of state transitions [10, 11, 13]. In photosynthetic organisms, the occurrence of a state 1 to state 2 transition corresponds to a characteristic decrease of the ratio of the fluorescence intensity at 680 nm (PSII-LHCII emission peak) and 720 nm (PSI emission peak) at 77 K [10, 11, 13]. It has been thought that the detachment of LHCII from PSII upon going to state 2 decreases the number of excitations arriving at PSII, whereas the attachment of LHCII to PSI increases the number of excitations in PSI [13], thereby explaining the change in ratio. As was mentioned above, we recently concluded that changes in amplitudes and lifetimes of PSII-LHCII and PSI fluorescence kinetics are small upon state transitions [23], meaning that also the ratio in fluorescence of PSI and PSII does not change a lot, at least at room temperature. This seems to be in conflict with the low-temperature steady-state emission results, where the PSII/PSI emission ratio changes substantially upon state transitions. Therefore, we have performed picosecond fluorescence measurements on state–locked WT *Chlamydomonas reinhardtii* cells at 77 K by using a streak-camera setup in order to investigate in detail the changes in fluorescence kinetics for different states. Our data show that the changes in 77 K fluorescence upon state transitions are mostly related to the changes in PSII and LHCII fluorescence, whereas PSI fluorescence hardly changes. These results support on the one hand our recent conclusion that LHCII detaches from PSII in state 2 conditions but only a fraction attaches to PSI while the detached antenna becomes quenched [23, 24], and on the other hand reveals the origin of the characteristic change in the ratio of the fluorescence intensity at 680 nm and 720 nm at 77 K, thereby resolving the apparent discrepancy between room temperature and 77K results.

3.3 MATERIALS AND METHODS:

Strain and Growth Conditions. Wild-type (WT) (Strain 137c) and the STT7 kinase mutant *Chlamydomonas reinhardtii* cells were grown under continuous white light illumination in TAP medium [33-35] like before [23]. Cells were shaken in a rotary shaker (100 rpm) at 30^0C and illuminated by a white lamp at low light intensity (10 µmol photons.m^{-2}.s^{-1}). All cells were grown in 250 ml flasks with a growing volume of 50 ml, and were maintained in the logarithmic growth phase.

State Locking.

Cells were locked in state 1 or 2 in the following ways, commonly used for state transitions studies on *C. reinhardtii* [12, 15-17, 19]: State 1 was obtained by incubating the cells in the dark while vigorously shaking for 2 hours (to oxidize the plastoquinone pool with the oxygen present) and state 2 was obtained by dark incubation in anaerobic conditions achieved by nitrogen bubbling for 25 min (to over-reduce the plastoquinone pool in the absence of oxygen) starting from cells in state 1, a method that was also applied by Delosme et al. [12, 16, 17]. Cells were directly used for time-resolved fluorescence measurements at 77K without further treatment.

Fluorescence Measurements

Streak Camera at 77K

Time-resolved fluorescence spectra at 77K were recorded with a picosecond streak-camera system combined with a grating (50 grooves/mm, blaze wavelength 600 nm) with the central wavelength set at 700 nm, having a spectral width of 260 nm (for details see [36-38]). Excitation light was vertically polarized, the spot size diameter was typically ~100 μm, and the laser repetition rate was 250 kHz. The detection polarizer was set at magic-angle orientation. The excitation wavelength was 400 nm and the laser power was adjusted to 50 ± 5 μW. The sample was put in liquid nitrogen. Images with a 2-ns time window were obtained for all samples. A high signal-to-noise ratio was achieved by averaging 100 single images, each obtained after analogue integration of 10 exposures of 1.112 s. Images were corrected for background and photocathode shading. The instrument response function (IRF) was described with a Gaussian of ≈11 ps fwhm. Extreme care was taken during measurements (see SI)

Data Analysis.

Data obtained with the streak-camera setup were globally analyzed with Glotaran, the graphical user interface of the R package TIMP (for details, see [39-41]). The method of global analysis is e.g. described by van Stokkum et al. [42]. With global analysis, the data were fitted to a sum of exponential decay curves convolved with an IRF and the amplitudes of each decay component as a function of wavelength are called "decay-associated spectra" (DAS).

3.4 RESULTS:

To determine the difference in fluorescence kinetics of state-1 and state-2-locked samples at 77 K, time-resolved fluorescence of samples in liquid nitrogen was measured with a picosecond streak-camera system, using 400-nm excitation. Figures 1a and 1b represent the streak-camera images for

state-1- and state-2- locked cells, respectively. The time-integrated fluorescence spectra, which are obtained by summing up the fluorescence spectra at all time points of the streak images, differs substantially for state 1 and state 2 (Figure 2): In particular, the ratio of the fluorescence intensity at 680 nm and 720 nm, i.e. F680/F720, changes to a large extent. The occurrence of this change is the accepted way to demonstrate that cells are in

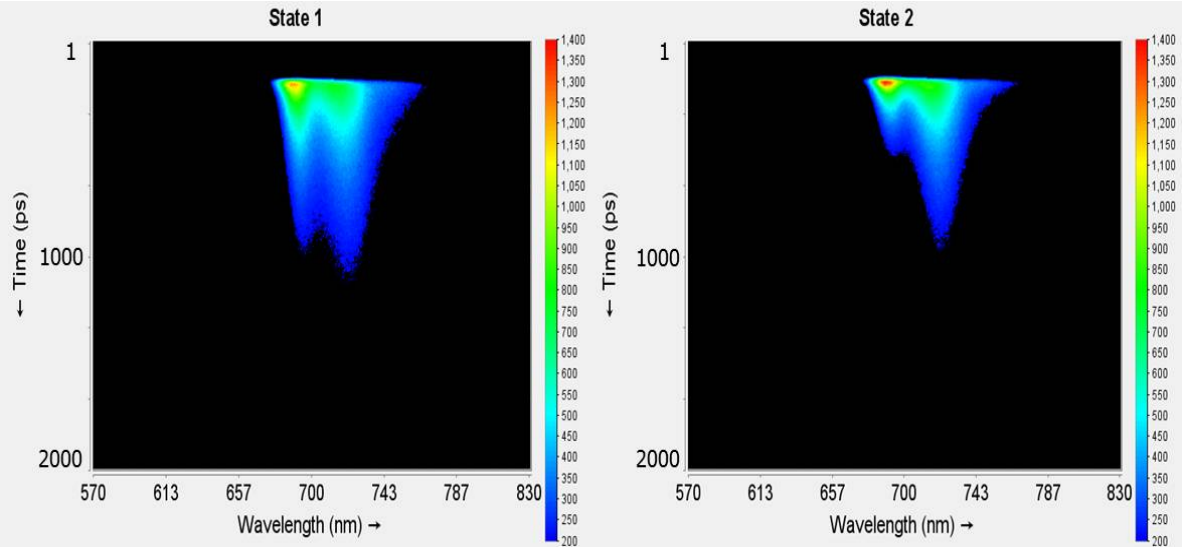

Figure 1. *Streak-camera images of state-1- and state-2-locked Chlamydomonas reinhardtii cells. The images were recorded at 77K with excitation wavelength 400 nm. The time scale is 2 ns. The cells from the same batch was used for recording streak images after state transitions (from state 1 to state 2) without any further modification. In these images, the fluorescence intensity (with the color code) is represented as a function of time (vertical axis) and wavelength (horizontal axis).*

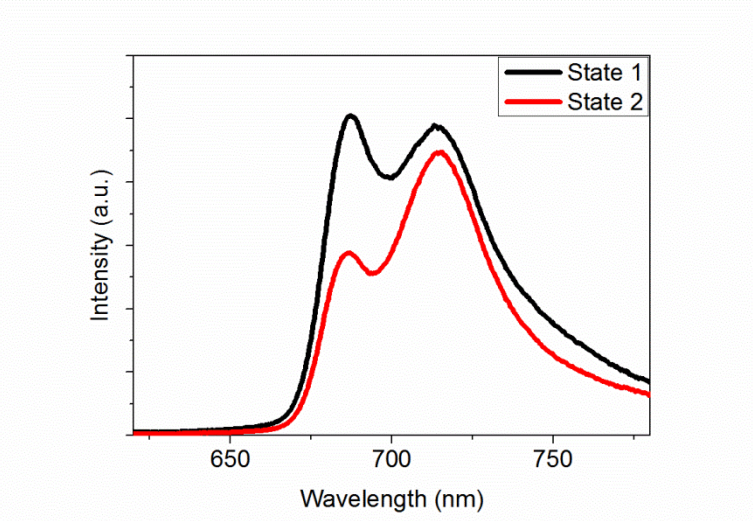

Figure 2. *Integrated fluorescence spectra of state-1- (black) and state-2-locked (red) Chlamydomonas reinhardtii cells. The spectra were recorded at 77K with excitation wavelength 400 nm. The same cell sample is used for recording fluorescence spectra after state transitions (from state 1 to state 2) without any further modification.*

different states [12, 13, 20-23, 27, 43-45]. The PSII peak around 695 nm is less emphasized in the present study as compared to our previous study [23], which is largely due to the fact that the spectral bandwidth of our streak camera set up is wider (6 nm) than the one of the steady-state fluorescence

spectrophotometer used in our previous study (2 nm). Global analysis of the fluorescence data required 5 lifetimes (Figure 3). The black DAS corresponds to the fastest lifetime of 7 ps for both state-1- and state-2-locked cells. This value is not extremely accurate because the fwhm of the IRF is around 11 ps. Although both DAS display a positive/negative signature, characteristic for excitation energy transfer (EET), their shapes are different (Figure 4a). Also for the next component (red DAS, 45 ps) the spectra differ for both states although, probably somewhat fortuitously, the lifetimes are

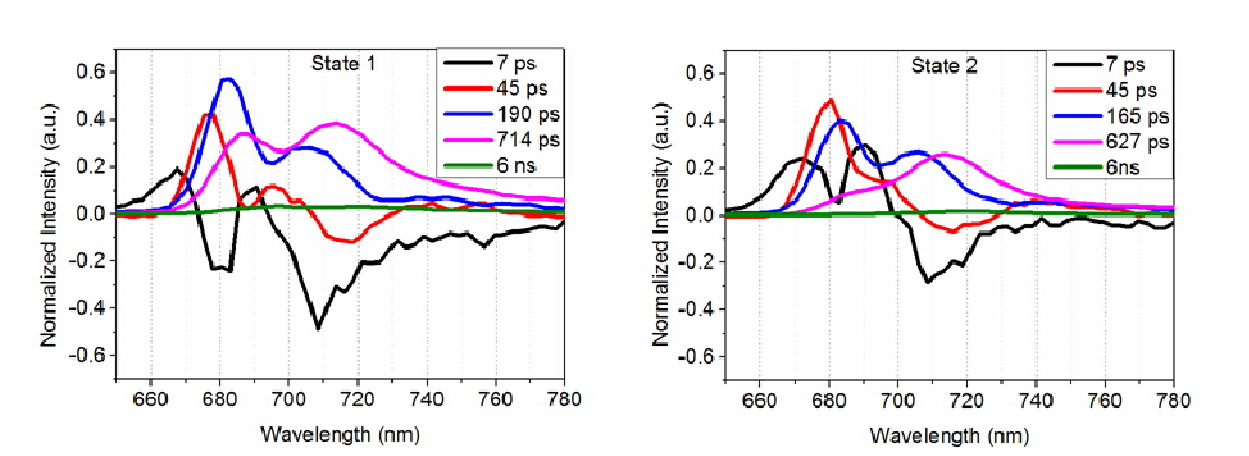

Figure 3. *The decay associated spectra (DAS) for state-1- and state-2-locked cells. The lifetimes are indicated in the figure. For a detailed explanation of the normalization procedure, see results.*

again the same. Both spectra display a positive/negative signature (Figure 3). But unlike the black DAS, these DAS show more contribution in the positive zone (between 675 – 705 nm) for both states. The negative part of the red DAS covers the interval 705 – 730 nm (Figure 4b). The blue DAS corresponds to a 190 ps lifetime for state-1-locked cells with positive peaks at 683 nm and 708 nm (Figure 3). The peak at 683 nm is almost twice as high as the one at 708 nm (Figure 4c). For state-2-locked cells the blue DAS corresponds to a 165 ps lifetime, also with 2 positive peaks at 683 nm and 708 nm, but the ratio between the peaks at 682 and 705 nm is considerably lower than for state 1 (Figure 4c). The cyan DAS for state-1-locked cells corresponds to a 714 ps lifetime with 2 positive peaks around 685 nm and 715 nm, whereas the contribution of the 715 nm peak is slightly higher (Figure 3, Figure 4d). The cyan DAS for state-2-locked cells corresponds to a 627 ps lifetime with 2 positive peaks around 685 nm and 715 nm. In this case, the peak at 715 nm is the dominant one (Figure 3, Figure 4d). The green DAS with very long lifetime (–6 ns) has very low amplitude (around 1%) for both states. It should be noted that this long lifetime is rather inaccurate, and should mainly be ascribed to red chlorophylls in PSI (Figure 3). It is important to note that the spectra in figures 3 and 4 were normalized in such a way that the fluorescence spectra immediately upon excitation (i.e. at time zero, t=0) are the same for state 1 and state 2. This is a necessary requirement because the pigment composition should be identical for both states. The spectrum at t=0 is obtained in a straightforward way by summing all the DAS obtained for a particular measurement. The shape of the t=0 spectrum indeed appears to be (nearly) identical for state 1 and 2 and normalization of the DAS is then

straightforward: If the t=0 spectrum for state 1 is higher by a factor x than the t=0 spectrum for state 2, then all the DAS for state 2 are multiplied by this factor x in order to obtain the proper normalization. The only way in which the spectra at t=0 might differ for state 1 and state 2 would be the presence of one or more ultrafast processes that would be too fast to capture when applying the fitting procedure and that would differ for state 1 and 2. However, the fact that both spectra at t=0 have very similar shapes shows that this is not the case (see supplementary information, figure S1).

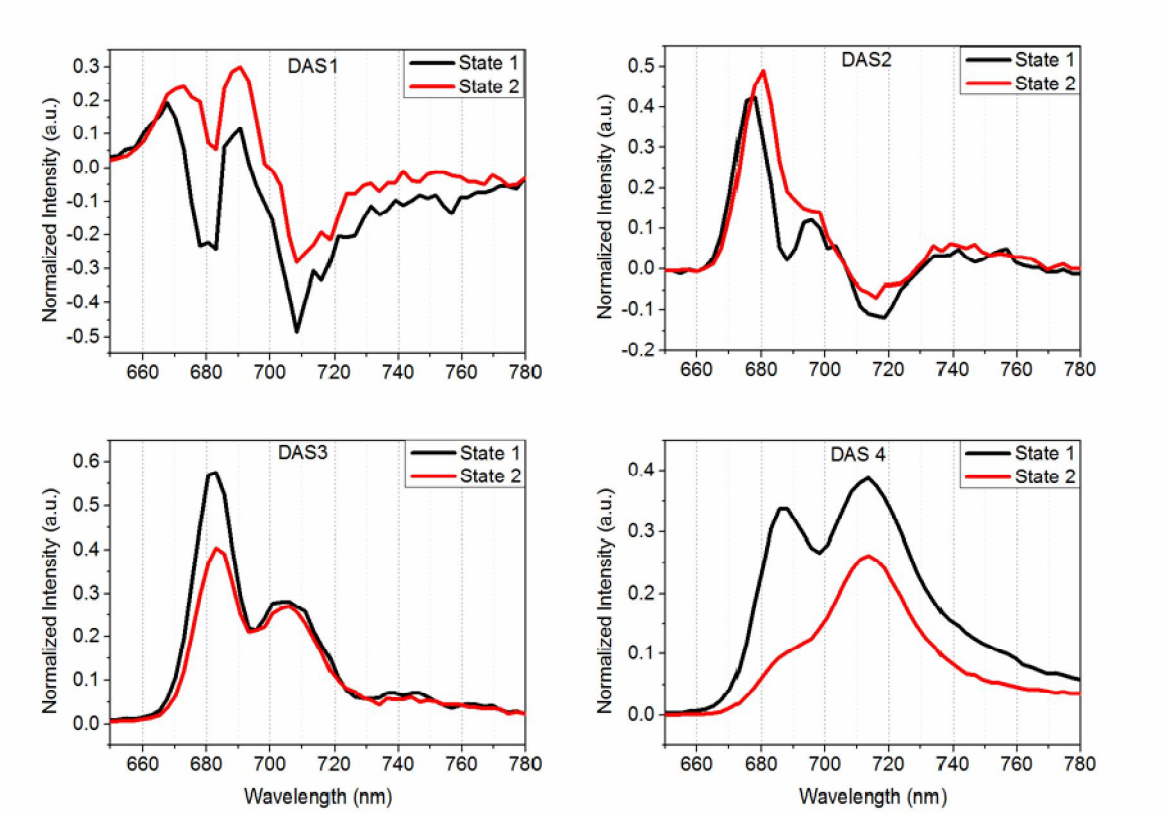

Figure 4. *Comparison of the DAS for each component for cells in different states. For a detailed explanation of the normalization procedure, see results.*

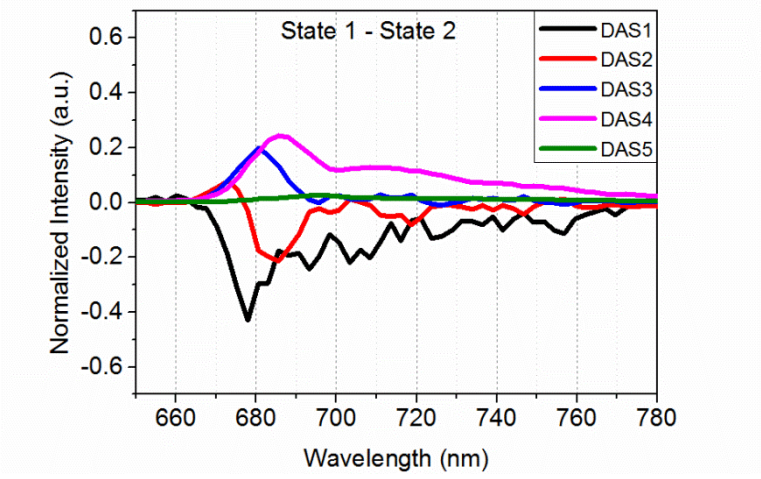

Figure 5. *Subtraction of DAS of State–2–locked cells from those of state–1–locked cells after normalization (For detailed explanation of normalization process, see results).*

In figure 5 the subtraction of each state 2 DAS from the corresponding state 1 DAS is shown after normalization, in order to visualize the differences in fluorescence kinetics for both states. The subtraction in case of the fastest component (7 ps) gives a negative peak at 678 nm without any positive contribution. The difference spectrum for the 45 ps component displays a negative peak around 685 nm. Apparently, for state-2-locked cells there is a large contribution of rapidly disappearing excitations, with fluorescence spectra peaking at 678 (for the 7 ps component) and 685 nm (for the 45 ps component), which do not show a concomitant fluorescence rise at other wavelengths, demonstrating that these excitations are quenched either chemically or non-photochemically. For the blue (3^{rd}) and cyan (4^{th}) DAS, the situation is completely different than for the fastest components. The subtraction of the blue DAS of state-2-locked cells from the blue DAS of state-1-locked cells displays a single peak around 683 nm. The subtraction of the cyan DAS of state-2-locked cells from the cyan DAS of state-1-locked cells displays a dominant peak at 685 nm with a broad and less pronounced contribution between 710 nm and 760 nm. These differences in blue and cyan DAS are apparently due to substantial changes in the PSII-LHCII fluorescence region during state transitions and the same is true for the differences in the corresponding lifetimes. In conclusion, the most pronounced differences between state 1 and state 2 can be observed in the PSII-LHCII region, whereas the fluorescence in the PSI region (around 720 nm) is rather similar for both states.

3.5 DISCUSSION

Recently, the change in fluorescence kinetics for state-1- and state-2-locked *C. reinhardtii* cells at room temperature was studied in detail with the use of the time-correlated single-photon counting technique [23]. It was shown that the fluorescence amplitude and lifetime of PSI do not show major changes upon state transitions, whereas the lifetimes in the PSII region become somewhat faster in state-2-locked cells [23]. This is important because in a different study on *A. thaliana*, it had been demonstrated that the amplitude of the fluorescence component that is due to PSI increases significantly when LHCII becomes attached to it [14]. It was thus remarkable that in *C. reinhardtii* only relatively minor differences could be observed between the PSI fluorescence kinetics for state 1 and 2 whereas the percentage of moving antenna had been concluded to be much higher in earlier studies [12, 16].

In the present study, the fluorescence kinetics of state-locked cells were investigated at 77K with a picosecond streak-camera setup. In the streak-camera image and the time-integrated fluorescence spectra, it is observed that the fluorescence intensity around 680 nm (PSII-LHCII fluorescence region) decreases in state-2-locked cells. On the other hand, the fluorescence intensity around 720 nm (PSI region) remains rather similar. Although the integrated fluorescence spectra show that there are significant differences between the cells locked in both states, they do not provide information on excitation energy transfer (EET) processes and time-resolved data are required for further insight. In order to understand the changes in fluorescence kinetics in more detail, global analysis was performed

of the streak-camera data. It reveals substantial differences in the DAS of the two fastest components for both states whereas the corresponding lifetimes are the same. In state-1-locked cells, EET is observed from pigments emitting at 670 nm (positive feature) to pigments emitting at 680 nm (negative feature) with a time constant of 7 ps. In state-2-locked cells, the emission at 670 nm disappears with a similar time constant but no EET to 680 nm pigments can be observed (no negative peak at 680 nm). Either the 670 nm pigments are directly quenched or the excitations are still transferred with a similar time constant but are immediately quenched after transfer. In either case a significant fraction of the excitations originating from 670 nm pigments are lost and less excitation energy remains in PSII. These excitations also do not arrive in PSI, since there is no significant change in the PSI fluorescence region in any DAS for state 1 and state 2.

The fact that less energy transfer to 680 nm pigments (PSII-LHCII fluorescence region) takes place in state 2 is also reflected in the blue DAS. The blue DAS (165/190 ps) show 2 major positive peaks at 683 nm and 708 nm, which are due to PSII-LHCII and PSI, respectively. The intensity of the peak at 683 nm has dropped by 35 % for state 2 whereas the peak at 708 nm is the same. This is possibly due to the detachment of LHCII from PSII in state 2 [23, 24], while it is accompanied by instantaneous quenching. Such detached LHCII should be highly quenched, otherwise a long-lived fluorescence component (around 4 ns) should be observed. The quenching originates most likely from aggregation since aggregated LHCII is known to be heavily quenched as compared to monomeric and trimeric LHCII [46]. Moreover, such detachment of LHCII from PSII also causes a decrease in size of the PSII-LHCII complex with a concomitant decrease in lifetime of the blue DAS in state-2-locked cells, as is indeed observed.

Differences are also observed between the second (red) DAS for state 1 and 2, although the lifetimes are the same, i.e. 45 ps. In state-2-locked cells, less excitations are transferred from 680 nm to 690 nm pigments. As a result, the cyan DAS (627/714 ps), which has 2 major positive peaks at 685 nm and 715 nm, which are due to PSII-LHCII and PSI, respectively, shows a drastic decrease at 685 nm for state-2-locked cells. It should be mentioned that in the cyan DAS, the peak at 715 nm also becomes somewhat smaller in state 2 but this change is minor when compared to the one at 685 nm. The decrease of EET from 680 nm to 690 nm pigments can also be explained by the detachment of LHCII from PSII in state 2, like was argued for the changes in the black and blue DAS. Also, the detachment of LHCII from PSII, which is accompanied by very fast LHCII quenching, causes a decrease in size of the PSII-LHCII complex and concomitantly a decrease in the lifetime of the cyan DAS for state-2-locked cells.

Not only the long lifetimes, corresponding to the blue and cyan DAS, become shorter for state 2, also the DAS of each lifetime differs in structure for different states because of changes in the EET process. However, the changes in the DAS mostly occur in the PSII-LHCII fluorescence region whereas the change in the PSI fluorescence region is minor. In order to check to which extent the changes in the fluorescence kinetics were cause by the state transitions, the same procedures to induce

state 1 and state 2 were applied to STT7 kinase mutant cells. This mutant is unable to perform state transitions [34, 35]. The fluorescence kinetics for these cells were also studied at 77 K, for conditions that induce state 1 and state 2 in WT cells (See supplementary information, Figure S2 and Figure S3). However, the fluorescence kinetics for STT7 cells are very similar for both conditions and the pronounced changes, which are observed for WT cells are absent (see supplementary information, Figure S2 and Figure S3). This convincingly demonstrates that indeed the changes in fluorescence kinetics for different states as observed for wild-type cells originate from state transitions. In conclusion, our current 77K data perfectly fit with the recent models by Unlu et al. and Nagy et al., which propose that LHCII indeed detaches from PSII like proposed before but the majority does not attach to PSI. Moreover, the detached LHCII becomes heavily quenched, probably after aggregating. This is in contrast to what was generally believed before, namely that the changes in the 77 K steady-state emission spectra of *C. reinhardtii* occur largely due to dissociation of LHCII from PSII and attachment to PSI.

Acknowledgements: This work was supported financially by the Netherlands Organization for Scientific Research (NWO) via the Council for Chemical Sciences (HvA) and also partly supported by the BioSolar Cells Programme of the Netherlands ministry of Economic Affairs Agriculture and Innovation, and by the Foundation for Fundamental Research on Matter (FOM).

The authors would like to thank Roberta Croce (VU University Amsterdam) for useful discussions and financial support for I.P

3.6 REFERENCES

[1] G.H. Schatz, H. Brock, A.R. Holzwarth, Kinetic and Energetic Model for the Primary Processes in Photosystem-Ii, Biophysical Journal, 54 (1988) 397-405.
[2] A.N. Melkozernov, S. Lin, R.E. Blankenship, Excitation dynamics and heterogeneity of energy equilibration in the core antenna of photosystem I from the cyanobacterium Synechocystis sp. PCC 6803, Biochemistry, 39 (2000) 1489-1498.
[3] B. Gobets, R. van Grondelle, Energy transfer and trapping in photosystem I, Biochimica Et Biophysica Acta-Bioenergetics, 1507 (2001) 80-99.
[4] N. Nelson, C.F. Yocum, Structure and function of photosystems I and II, Annual Review of Plant Biology, 57 (2006) 521-565.
[5] A. Busch, M. Hippler, The structure and function of eukaryotic photosystem I, Biochimica Et Biophysica Acta-Bioenergetics, 1807 (2011) 864-877.
[6] R. Croce, H. van Amerongen, Light-harvesting in photosystem I, Photosynthesis Research, 116 (2013) 153-166.
[7] H. van Amerongen, R. Croce, Light harvesting in photosystem II, Photosynthesis Research, 116 (2013) 251-263.
[8] R. Croce, H. van Amerongen, Natural strategies for photosynthetic light harvesting, Nature Chemical Biology, 10 (2014) 492-501.
[9] H. Takahashi, S. Clowez, F.A. Wollman, O. Vallon, F. Rappaport, Cyclic electron flow is redox-controlled but independent of state transition, Nature Communications, 4 (2013).
[10] N. Murata, Control of excitation transfer in photosynthesis I. Light-induced change of chlorophyll a fluoresence in Porphyridium cruentum, Biochimica et Biophysica Acta (BBA) - Bioenergetics, 172 (1969) 242-251.
[11] W.P. Williams, J.F. Allen, State-1/State-2 Changes in Higher-Plants and Algae, Photosynthesis Research, 13 (1987) 19-45.
[12] R. Delosme, J. Olive, F.A. Wollman, Changes in light energy distribution upon state transitions: An in vivo photoacoustic study of the wild type and photosynthesis mutants from Chlamydomonas reinhardtii, Biochimica Et Biophysica Acta-Bioenergetics, 1273 (1996) 150-158.
[13] J. Minagawa, State transitions-The molecular remodeling of photosynthetic supercomplexes that controls energy flow in the chloroplast, Biochimica Et Biophysica Acta-Bioenergetics, 1807 (2011) 897-905.
[14] E. Wientjes, H. van Amerongen, R. Croce, LHCII is an antenna of both photosystems after long-term acclimation, Biochimica et biophysica acta, 1827 (2013) 420-426.
[15] F.A. Wollman, P. Delepelaire, Correlation between Changes in Light Energy-Distribution and Changes in Thylakoid Membrane Polypeptide Phosphorylation in Chlamydomonas-Reinhardtii, Journal of Cell Biology, 98 (1984) 1-7.
[16] M.M. Fleischmann, S. Ravanel, R. Delosme, J. Olive, F. Zito, F.A. Wollman, J.D. Rochaix, Isolation and characterization of photoautotrophic mutants of Chlamydomonas reinhardtii deficient in state transition, Journal of Biological Chemistry, 274 (1999) 30987-30994.
[17] G. Finazzi, R.P. Barbagallo, E. Bergo, R. Barbato, G. Forti, Photoinhibition of Chlamydomonas reinhardtii in State 1 and State 2 - Damages to the photosynthetic apparatus under linear and cyclic electron flow, Journal of Biological Chemistry, 276 (2001) 22251-22257.
[18] G. Forti, G. Caldiroli, State transitions in Chlamydomonas reinhardtii. The role of the Mehler reaction in state 2-to-state 1 transition, Plant Physiology, 137 (2005) 492-499.
[19] J. Kargul, M.V. Turkina, J. Nield, S. Benson, A.V. Vener, J. Barber, Light-harvesting complex II protein CP29 binds to photosystem I of Chlamydomonas reinhardtii under State 2 conditions, Febs Journal, 272 (2005) 4797-4806.
[20] H. Takahashi, M. Iwai, Y. Takahashi, J. Minagawa, Identification of the mobile light-harvesting complex II polypeptides for state transitions, Plant and Cell Physiology, 47 (2006) S105-S105.
[21] M. Iwai, M. Yokono, N. Inada, J. Minagawa, Live-cell imaging of photosystem II antenna dissociation during state transitions, Proceedings of the National Academy of Sciences of the United States of America, 107 (2010) 2337-2342.

[22] B. Drop, K.N.S. Yadav, E.J. Boekema, R. Croce, Consequences of state transitions on the structural and functional organization of Photosystem I in the green alga Chlamydomonas reinhardtii, Plant Journal, 78 (2014) 181-191.
[23] C. Unlu, B. Drop, R. Croce, H. van Amerongen, State transitions in Chlamydomonas reinhardtii strongly modulate the functional size of photosystem II but not of photosystem I, Proceedings of the National Academy of Sciences of the United States of America, 111 (2014) 3460-3465.
[24] G. Nagy, R. Unnep, O. Zsiros, R. Tokutsu, K. Takizawa, L. Porcar, L. Moyet, D. Petroutsos, G. Garab, G. Finazzi, J. Minagawa, Chloroplast remodeling during state transitions in Chlamydomonas reinhardtii as revealed by noninvasive techniques in vivo, Proceedings of the National Academy of Sciences of the United States of America, 111 (2014) 5042-5047.
[25] P. Galka, S. Santabarbara, K. Thi Thu Huong, H. Degand, P. Morsomme, R.C. Jennings, E.J. Boekema, S. Caffarri, Functional Analyses of the Plant Photosystem I-Light-Harvesting Complex II Supercomplex Reveal That Light-Harvesting Complex II Loosely Bound to Photosystem II Is a Very Efficient Antenna for Photosystem I in State II, Plant Cell, 24 (2012) 2963-2978.
[26] J. Wendler, A.R. Holzwarth, State Transitions in the green-alga Scenedesmus-obliquus probed by time-resolved chlorophyll fluorescence spectroscopy and global data-analysis, Biophysical Journal, 52 (1987) 717-728.
[27] J.F. Allen, Protein-Phosphorylation in Regulation of Photosynthesis, Biochimica Et Biophysica Acta, 1098 (1992) 275-335.
[28] K. Maxwell, G.N. Johnson, Chlorophyll fluorescence - a practical guide, Journal of Experimental Botany, 51 (2000) 659-668.
[29] H. Van Amerongen, L. Valkunas, R. Van Grondelle, Photosynthetic Excitons, 2000, World Scientific, Singapore, 2000.
[30] R.E. Blankenship, Molecular mechanisms of photosynthesis, Blackwell Science Ltd, 2002.
[31] F. Cho, Govindje., Fluorescence Spectra of Chlorella in 295-77 Degrees K Range, Biochimica Et Biophysica Acta, 205 (1970) 371-&.
[32] F. Cho, Govindje., Low-Temperature (4-77 Degrees K) Spectroscopy of Anacystis - Temperature Dependence of Energy Transfer Efficiency, Biochimica Et Biophysica Acta, 216 (1970) 151-+.
[33] D.S. Gorman, R.P. Levine, Cytochrome F and Plastocyanin - Their Sequence in Photosynthetic Electron Transport Chain of Chlamydomonas Reinhardi, Proceedings of the National Academy of Sciences of the United States of America, 54 (1965) 1665-&.
[34] S. Bellafiore, F. Barneche, G. Peltier, J.D. Rochaix, State transitions and light adaptation require chloroplast thylakoid protein kinase STN7, Nature, 433 (2005) 892-895.
[35] N. Depege, S. Bellafiore, J.D. Rochaix, Role of chloroplast protein kinase Stt7 in LHCII phosphorylation and state transition in Chlamydomonas, Science, 299 (2003) 1572-1575.
[36] B. van Oort, A. Amunts, J.W. Borst, A. van Hoek, N. Nelson, H. van Amerongen, R. Croce, Picosecond Fluorescence of Intact and Dissolved PSI-LHCI Crystals, Biophysical Journal, 95 (2008) 5851-5861.
[37] B. Van Oort, S. Murali, E. Wientjes, R.B.M. Koehorst, R.B. Spruijt, A. van Hoek, R. Croce, H. van Amerongen, Ultrafast resonance energy transfer from a site-specifically attached fluorescent chromophore reveals the folding of the N-terminal domain of CP29, Chemical Physics, 357 (2009) 113-119.
[38] I.H. Van Stokkum, B. Van Oort, F. Van Mourik, B. Gobets, H. Van Amerongen, (Sub)-picosecond spectral evolution of fluorescence studied with a synchroscan streak-camera system and target analysis, in: Biophysical techniques in photosynthesis, Springer, 2008, pp. 223-240.
[39] S.P. Laptenok, J.W. Borst, K.M. Mullen, I.H.M. van Stokkum, A.J.W.G. Visser, H. van Amerongen, Global analysis of Forster resonance energy transfer in live cells measured by fluorescence lifetime imaging microscopy exploiting the rise time of acceptor fluorescence, Physical Chemistry Chemical Physics, 12 (2010) 7593-7602.
[40] K.M. Mullen, I.H.M. van Stokkum, TIMP: An R package for modeling multi-way spectroscopic measurements, Journal of Statistical Software, 18 (2007).
[41] J.J. Snellenburg, S.P. Laptenok, R. Seger, K.M. Mullen, I.H.M. van Stokkum, Glotaran: A Java-Based Graphical User Interface for the R Package TIMP, Journal of Statistical Software, 49 (2012) 1-22.

[42] I.H.M. van Stokkum, D.S. Larsen, R. van Grondelle, Global and target analysis of time-resolved spectra (vol 1658, pg 82, 2004), Biochimica Et Biophysica Acta-Bioenergetics, 1658 (2004) 262-262.
[43] M. Iwai, Y. Takahashi, J. Minagawa, Molecular remodeling of photosystem II during state transitions in Chlamydomonas reinhardtii, Plant Cell, 20 (2008) 2177-2189.
[44] M. Iwai, J. Minagawa, Dissociation of light-harvesting complex II from photosystem II supercomplex during state transitions in Chlamydomonas reinhardtii, Photosynthesis Research, 91 (2007) 252-252.
[45] H. Takahashi, M. Iwai, Y. Takahashi, J. Minagawa, Identification of the mobile light-harvesting complex II polypeptides for state transitions in Chlamydomonas reinhardtii, Proceedings of the National Academy of Sciences of the United States of America, 103 (2006) 477-482.
[46] B. van Oort, A. van Hoek, A.V. Ruban, H. van Amerongen, Aggregation of Light-Harvesting Complex II leads to formation of efficient excitation energy traps in monomeric and trimeric complexes, Febs Letters, 581 (2007) 3528-3532.

Supplementary Information

1) **Comparison of spectra at t=0 obtained from different state-locked WT cells**

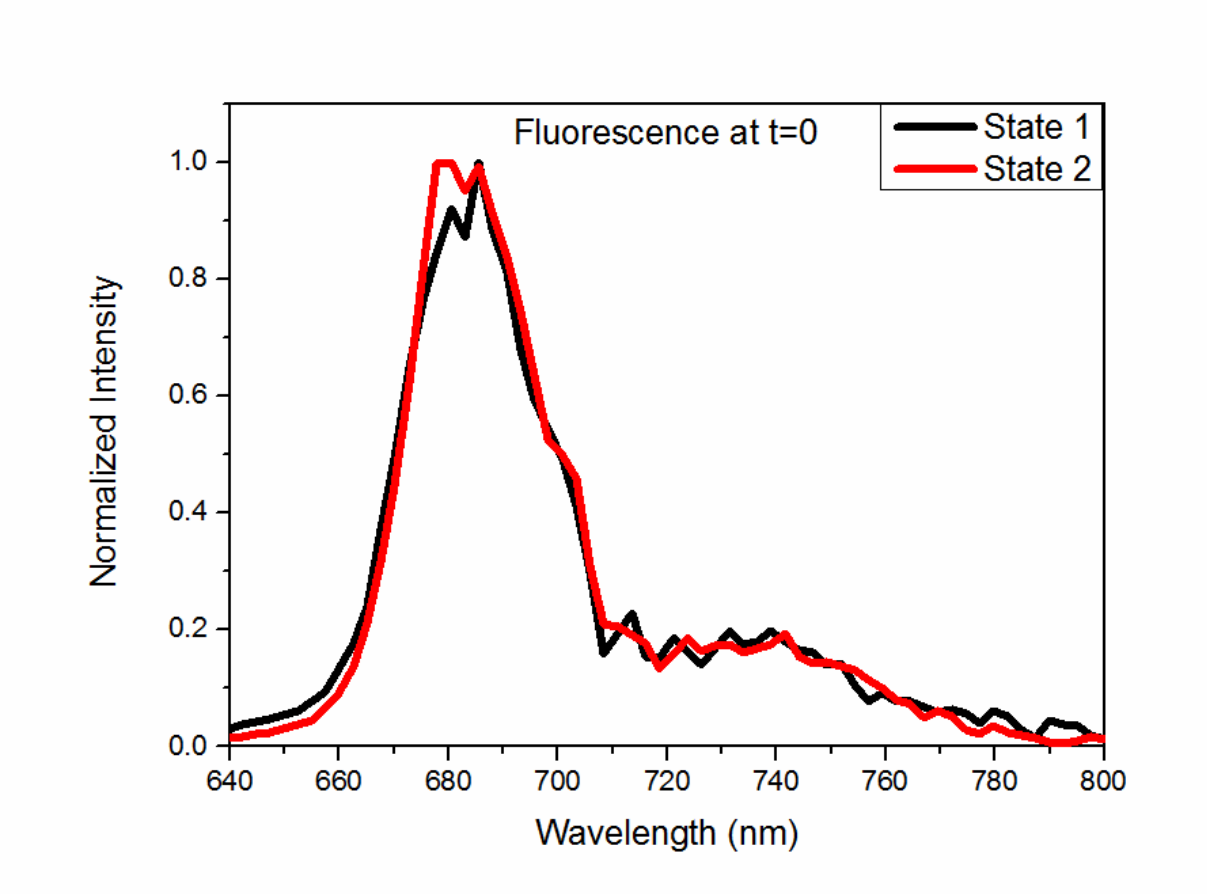

Figure S1. *Comparison of estimated spectra at t=0 obtained from state-1-locked and state-2-locked cells. For explanation see main text (results).*

2) **Comparison of state transitions in WT and STT7 kinase mutant**

In order to confirm that the observed differences observed for cells with either an oxidized (state 1) or an overreduced plastoquinone pool (state 2) are indeed due to state transitions we repeated the measurement under identical conditions with STT7 mutant cells, which are lacking the kinase that is responsible for the phosphorylation required for state transitions. The results could only be fitted in a meaningful way using 4 decay components, in contrast to the results obtained for WT cells which required 5 components. In order to allow a direct comparison between mutant and WT cells, we also fitted the time-resolved fluorescence data on WT cells with 4 decay components and the results are shown in Figure S2.

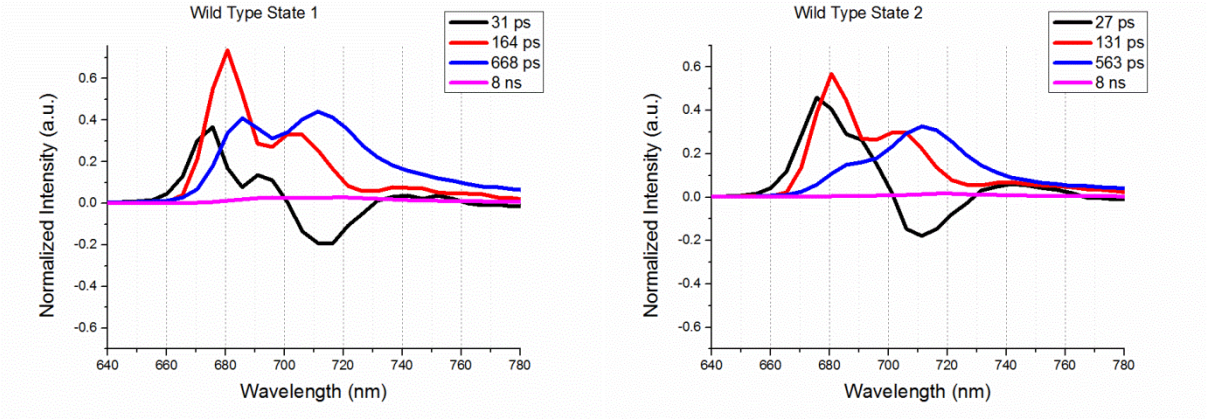

Figure S2. *The decay associated spectra (DAS) for state-1- and state-2-locked cells using 4 exponentials for the fitting. The lifetimes are indicated in the figure. All spectra are normalized and for a detailed explanation of the normalization process, we refer to the Results section in the main text.*

As before one can observe clear differences for all DAS in state 1 and state 2 and in particular the 3rd (blue) DAS shows that the long-lived PSII contribution (around 685 nm) has largely decreased whereas the PSI contribution around 710 nm hardly has changed.

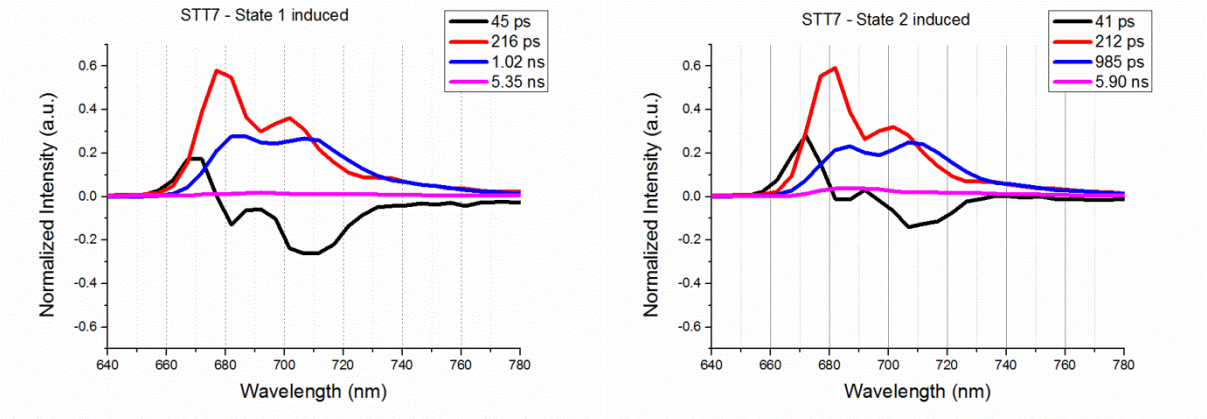

Figure S3. *The decay associated spectra (DAS) for "state-1- and state-2-locked" STT7 mutant cells with 4 exponentials. The lifetimes are indicated in the figure. All spectra are normalized and for a detailed explanation of the normalization process we refer to the Results section in the main text.*

In sharp contrast to what is observed for the WT cells, the STT7 cells show hardly any differences for the conditions that are responsible for state 1 and 2 in WT cells. Both the lifetimes and the shapes of the different components are very similar, although not entirely identical. However, all the major changes that are discussed for the WT cells are missing for these mutant cells.

3) Precautions during Streak camera measurements at 77 K

All streak measurements in this study were performed with extreme care; the most important precautions are listed below.

- The same culture was used for streak camera measurements after and before state transitions.
- Pasteur pipettes were kept in 77 K before they were used for experiments.
- Pipettes were cleansed by ethanol before their use in streak camera measurements to get rid of humidity.
- Always clear samples, which mean samples without any ice formation in the solution, were used for streak measurements.

Chapter 4

Disturbed Excitation Energy Transfer in *Arabidopsis Thaliana* Mutants Lacking Minor Antenna Complexes of Photosystem II

Luca Dall'Osto [a*], Caner Ünlü [b*], Stefano Cazzaniga [a], Herbert van Amerongen [b,c]

[a] Dipartimento di Biotecnologie, Università di Verona, 37134 Verona, Italy, [b] Laboratory of Biophysics, Wageningen University, 6703 HA Wageningen, The Netherlands, [c] MicroSpectroscopy Centre, Wageningen University, 6703 HA Wageningen, The Netherlands.

[*] Both authors equally contributed to this work

Based on:

Dall'Osto, L. and Ünlü, C., Cazzaniga, S., & van Amerongen, H. (2014). Disturbed excitation energy transfer in< i> Arabidopsis thaliana</i> mutants lacking minor antenna complexes of photosystem II. *Biochimica et Biophysica Acta (BBA)-Bioenergetics*, *1837*(12), 1981-1988.

CHAPTER 4

4.1 ABSTRACT

Minor light-harvesting complexes (Lhcs) CP24, CP26 and CP29 occupy a position in photosystem II (PSII) of plants between the major light-harvesting complexes LHCII and the PSII core subunits. Lack of minor Lhcs *in vivo* causes impairment of PSII organization, and negatively affects electron transport rates and photoprotection capacity. Here we used picosecond-fluorescence spectroscopy to study excitation-energy transfer (EET) in thylakoids membranes isolated from *A. thaliana* wild-type plants and knockout lines depleted of either two (koCP26/24 and koCP29/24) or all minor Lhcs (NoM). In the absence of all minor Lhcs, the functional connection of LHCII to the PSII cores appears to be seriously impaired whereas the "disconnected" LHCII is substantially quenched. For both double knock-out mutants, excitation trapping in PSII is faster than in NoM thylakoids but slower than in WT thylakoids. In NoM thylakoids, the loss of all minor Lhcs is accompanied by an over-accumulation of LHCII, suggesting a compensating response to the reduced trapping efficiency in limiting light, which leads to a photosynthetic phenotype resembling that of low-light-acclimated plants. Finally, fluorescence kinetics and biochemical results show that the missing minor complexes are not replaced by other Lhcs, implying that they are unique among the antenna subunits and crucial for the functioning and macro-organization of PSII.

4.2 INTRODUCTION

Oxygenic photosynthesis is performed in the chloroplast by a series of reactions which transform sunlight energy into chemical energy [1]. Absorption of light, excitation energy transfer (EET) and electron transfer are the primary events of the photosynthetic light phase and take place in Photosystems (PS) I and II [2-10]. PSII is a large supramolecular pigment-protein complex located in the thylakoid membranes of plants, algae and cyanobacteria. Its reaction center (RC) consists of several subunits carrying the cofactors for electron transport and forms, together with the proteins CP43 and CP47 a so-called core complex [11, 12]. Core complexes form dimers (C_2), which bind a system of nuclear-encoded light-harvesting proteins (Lhcbs): CP29 and CP26 are monomeric antennae located in close connection to the core, and seem to mediate the binding of an LHCII trimer (the major antenna complex of PSII) called LHCII-S (strongly bound), thus forming the basic PSII supercomplex structure C_2S_2 [13]. Moreover, in higher plants another monomeric subunit (CP24) and one more trimeric LHCII (LHCII-M, 'moderately' bound) bind the PSII core to extend the light-harvesting capacity of the supercomplex (called $C_2S_2M_2$). Besides light harvesting, the outer antenna of PSII plays a crucial role in photoprotective and regulatory mechanisms such as limiting the level of Chl triplet states [14-16], scavenging of reactive oxygen species [17] and activating non-radiative de-excitation pathways [18].

Excitations are used to induce primary charge separation (CS) within the RC, after which electrons are transferred in succession to the acceptors Q_A and Q_B, while the oxidizing equivalents in the Mn cluster

are used to catalyze water splitting [1]. The quantum efficiency of CS depends on the rate constants of different molecular events, namely 1) EET from outer antenna to RC; 2) CS and charge recombination; 3) secondary electron transfer to Q_A, and 4) relaxation processes, such as intersystem crossing, internal conversion and fluorescence emission [19].

Among the antenna complexes of PSII, monomeric Lhcs CP24, CP26 and CP29 are of particular interest, because the location of these complexes in between LHCII and the RC makes them crucial for facilitating EET from LHCII, forming the major part of the antenna system, to the core subunits, although it seems that also direct EET from LHCII-S to the core is possible [20, 21]. Indeed, depletion of specific monomeric Lhcs *in vivo* was shown to impair the organization of photosynthetic complexes within grana partitions, and to negatively affect electron transport rates and photoprotection capacity [22]. Evidence that these gene products have been conserved over at least 350 million years of evolution [23] strongly indicates that each complex has a specific role in the PSII function over the highly variable conditions of the natural environment.

CS in the reaction centers of PSI and PSII occurs within tens to hundreds of picoseconds (ps) after light absorption. A great challenge in studying EET and charge separation in thylakoid membranes is to disentangle the kinetics related to both photosystems. Broess et al. [24] and Caffari et al. [20] recently provided a more detailed picture of EET in PSII membranes and supercomplexes of plants while van Oort et al.[25] investigated EET in entire thylakoids of WT and mutant Arabidopsis with the use of ps-fluorescence spectroscopy, using different combinations of excitation/detection wavelengths, in order to distinguish PSI and PSII kinetics. The exciton/radical-pair-equilibrium (ERPE) model has often been used to describe the kinetics of EET in PSII preparations with open RCs, i.e. with the electron acceptor Q_A fully oxidized [26, 27]. This model assumes that EET to the RC is too fast to contribute substantially to the charge separation time [26]. To provide a more accurate description for grana-enriched membranes, the ERPE model was extended after analyzing ps-fluorescence measurements using different excitation wavelengths and applying a coarse-grained model to determine the excitation migration time to the RC [24]. Comparison of the fluorescence kinetics obtained for 412 nm (more excitations in the core) and 484 nm excitation (more excitations in the outer antenna), led to the conclusion that the average migration time of an excitation toward the RC contributes 20–25% to the average trapping time in PSII membranes and around 50% in full thylakoid membranes [25, 28, 29] and the overall migration time to the RC is around 150 ps in WT thylakoids, four times longer than for grana-enriched membranes [24] which is likely due to additional antenna complexes that are less well connected to the PSII RC [21, 25, 28-30] and that are lost during preparation of grana membranes [21]. Recently, also models were presented that assume excitation trapping the time of which is entirely dominated by migration of excitations to the RC [31, 32].

Recent studies on EET dynamics focused on the behavior of specific pigment-protein complexes that constitute either PSI or PSII [33-35]. Reverse genetic approaches in model organisms such as

Arabidopsis thaliana allowed to isolate knock-out lines devoid of specific components of PSII [36, 37] and have been instrumental in order to dissect the function of each subunit *in vivo*. Hopefully, applying time-resolved spectroscopy on thylakoid membranes of different composition can provide new knowledge on the primary events of the light phase at the molecular level.

In this work, thylakoid membranes of *A. thaliana* have been studied with time-resolved fluorescence spectroscopy using different combinations of excitation and detection wavelengths, in order to (partly) separate PSI and PSII/LHCII contributions. In particular, PSII/LHCII fluorescence decay kinetics have been measured on thylakoids isolated from wild-type Arabidopsis, from the double knock-out mutants koCP26/24 and koCP29/24, and from a mutant depleted of all minor antennae (NoM). The main goal of this study was to investigate how the depletion of specific Lhcs affects the excitation- and electron-transfer parameters of PSII. In the absence of all minor Lhcs of PSII, the functional connection between LHCII from the PSII cores appears to be strongly impaired and LHCII is substantially quenched which is probably related to the fact that the NoM plants are strongly hampered in their growth as compared to WT plants. For double knock-out mutants, the outer antenna is better connected to the PSII core and the corresponding plants also grow significantly better than the NoM plants.

4.3 MATERIALS AND METHODS:

Plant material and growth conditions

WT plants of *Arabidopsis thaliana* ecotype Col-0 and mutants *koLhcb4.1*, *koLhcb4.2*, *koLhcb5* and *koLhcb6* were obtained as previously described [36, 37]. Multiple mutants *koLhcb5 koLhcb6* (koCP26/24), *koLhcb4.1 koLhcb4.2* (koCP29/24) and *koLhcb4.1 koLhcb4.2 koLhcb5* (NoM) were isolated by crossing single mutant plants and by selecting the progeny through immunoblotting, using antibodies specific for the different Lhcb subunits. Double mutant *koLhcb4.1 koLhcb4.2* is devoid of both CP29 and CP24 minor antennae, since accumulation of CP24 is hampered when CP29 is missing, as previously reported[36]. Seedlings were grown for 5 weeks at 100 μmol photons m^{-2} s^{-1}, 23°C, 70% humidity, and 8 h of daylight.

Membrane isolation

Dark-adapted leaves were rapidly homogenized using mortar and pestle, and stacked thylakoids were isolated as previously described [38], with the following modifications aimed at preserving thylakoids functionality: protease inhibitors (2 mM ε-aminocaproic acid, 2 mM benzamidine-hydrochloride, 0.5 mM PMSF) were added to the buffers; maximum 1 g of leaves was grinded in 100 ml of GB; thylakoids were resuspended in B4 buffer (0.4 M sorbitol, 15 mM NaCl, 10 mM KCl, 5 mM $MgCl_2$, 15 mM Hepes pH 7.8) before being frozen in liquid nitrogen

.

Pigment analysis

Pigments were extracted from leaf discs with 85% acetone buffered with Na_2CO_3, then separated and quantified by HPLC [39].

In vivo fluorescence measurements

PSII maximal photochemical efficiency was measured through Chl fluorescence on dark-adapted leaves at room temperature with a PAM 101 fluorimeter (Walz, Germany); saturating light pulses (4500 μmol photons m^{-2} s^{-1}, 0.6 s) were supplied by a KL1500 halogen lamp (Schott, UK) (for results, please see supplementary information).

Gel electrophoresis and immunoblotting

SDS-PAGE analysis was performed with the Tris-Tricine buffer system [40], with the addition of 7M urea to the running gel when needed to separate Lhcb4 isoforms [36]. For fractionation of pigment-protein complexes, membranes corresponding to 500 μg of Chls were washed with 5 mM EDTA and then solubilized in 1 ml of 0.7% α-DM, 10 mM HEPES, pH 7.8. Solubilized samples were then fractionated by ultracentrifugation in a 0.1–1 M sucrose gradient containing 0.06% α-DM, 10 mM HEPES, pH 7.8 (22 h at 280,000 *g*, 4 ^{0}C). Non-denaturing Deriphat-PAGE was performed following the method developed in [41] with the modification described in [42]. The thylakoids concentrated at 1 mg/ml chlorophylls were solubilised with a final concentration of 1% α/β-DM, whereas 25 μg of Chls was loaded in each lane. Bands corresponding to trimeric LHCII and monomeric PSII core were excised from the gel, and purified complexes were then eluted by grinding gel slices in a buffer containing 10 mM Hepes pH 7.5, 0.05% α- DM. LHCII/PSII core ratios were quantified by loading thylakoids (15 μg of Chls), PSII core (0.25-0.5-0.75-1.0 μg of Chls) and trimeric LHCII (1.0-2.0-3.0-4.0 μg of Chls) in the same slab gels. After staining with coomassie blue, the signal amplitude of LHCII and CP43/CP47 bands were quantified (n=4) by GelPro 3.2 software (Bio-Rad, USA). By using the pigment composition of the individual subunits [12, 43] and the OD of each protein band, the number of LHCII trimers per monomeric PSII core was calculated. For immunotitration, thylakoid samples corresponding to 0.1, 0.25, 0.5, and 1 μg of chlorophyll were loaded for each sample and electroblotted on nitrocellulose membranes; proteins were detected with alkaline phosphatase-conjugated antibody, according to Towbin et al. [44], and signal amplitude was quantified by densitometric analysis (n = 4). In order to avoid any deviation between different immunoblots, samples were compared only when loaded in the same slab gel.

Photosystems activity measured with artificial donors and acceptors

These measurements were performed as previously described [38]. PSI electron transport from the artificial donor ($TMPDH_2$, N,N,N,N-tetramethyl-p-phenylene-diamine, reduced form) to $NADP^+$ was measured at 22°C on functional thylakoids in the dual-wavelength spectrophotometer Unicam AA

(Thermo Scientific, USA), while PSII electron transport to DMBQ (dimethyl-benzoquinone) was measured following the O_2 evolution in a Clark-type oxygen electrode system (DW2/2, Hansatech Instruments, UK) both under red light illumination (200 µmol photons m^{-2} s^{-1}, λ>600 nm). Concentrations used were as follows: 0.1 sorbitol, 5 mM $MgCl_2$, 10 mM NaCl, 20 mM KCl, 10 mM Hepes pH 7.8, 0.5 mM $NADP^+$, 10 µM ferredoxin, either 300 mM DMBQ or 250 mM $TMPDH_2$ and thylakoids to a final Chl concentration of 10 µg/ml. When $TMPDH_2$ was used, the reaction mixture contained 5 mM ascorbic acid, and after 1.5 min of illumination 1 μM DCMU was added, followed by the artificial donor.

Time-resolved fluorescence

Time-correlated single photon counting (TCSPC) measurements were performed with a home-built setup [45, 46]. In brief, samples were kept at room temperature (RT, 22°C) in a flow cuvette coupled to a sample reservoir. The samples were flown from reservoir to cuvette with a speed of 2.5 ml/s and the optical path length of the cuvette was 3 mm. The samples were excited with 412 nm and 484 nm pulses of 0.2 ps duration at a repetition rate of 3.8 MHz. In order to avoid the closure of reaction centers the excitation intensity was kept low (0.5 – 1.5 µW), which resulted in a count rate of 30000 photons per second or lower (See Supplementary Information for details, Figure S1) The diameter of the excitation spot was 2 mm. The instrument response function or IRF (70 – 80 ps FWHM) was obtained with pinacyanol iodide in methanol with a 6 ps fluorescence lifetime [47, 48]. Measurements were done by collecting photons for 5 minutes. Fluorescence was detected at 679 nm, 701 nm and 720 nm using interference filters (15 nm width). The data were collected using a multichannel analyser with a maximum time window of 4096 channels typically at 5 or 2 ps/channel. One complete experiment for a fluorescence decay measurement consisted of the recording of data sets of the reference compound, isolated thylakoid and again the reference compound, which was done at least three times in this order with a fresh sample for each condition, in order to check the reproducibility.

Data analysis.

Data obtained with the TCSPC setup were globally analysed using the "TRFA Data Processing Package" of the Scientific Software Technologies Center (Belarusian State University, Minsk, Belarus). Fluorescence decay curves were fitted to a sum of exponentials that was convoluted with the IRF. The quality of a fit was judged from the χ^2 value and by visual inspection of the residuals and the autocorrelation thereof. The number of exponentials was 5 in all cases, whereas one of these components was an artefact with a very fast lifetime (between 0.1 ps and 1 ps), which was mainly used to improve the fitting quality at early times. These artefacts are not further considered or discussed below.

4.4 RESULTS:

In order to isolate knock-out (KO) lines of *Arabidopsis thaliana* lacking two or three minor antennae, kolhcb4.1, kolhcb4.2, kolhcb5 and kolhcb6 homozygous KO lines were identified in seed pools obtained from NASC by immunoblot analysis using specific antibodies raised against CP29, CP26 and CP24 antenna proteins, as previously described [36, 37]. KO double mutants kolhcb5 kolhcb6 retain Lhcb4 (CP29) as the only minor antenna [37], while deletion of both CP29 isoforms in the kolhcb4.1 kolhcb4.2 double mutant results in a plant retaining CP26 as the only minor antenna, since accumulation of CP24 is hampered in this genotype [36]. Triple mutant kolhcb4.1 kolhcb4.2 kolhcb5 is lacking all minor antennae: indeed, deletion of both lhcb4.1 and lhcb4.2 yielded a plant devoid of CP29, and lack of CP29 hampered CP24 stability and accumulation [37]; thus the triple KO only retains subunits of the major antenna complex LHCII. In the following, we will refer to these genotypes as koCP26/24 (kolhcb5 kolhcb6), koCP29/24 (kolhcb4.1 kolhcb4.2) and NoM (kolhcb4.1 kolhcb4.2 kolhcb5). When grown in control conditions (100 µmol photons m^{-2} s^{-1}, 23°C, 8/16 h day/night) for 4 weeks, koCP26/24 and koCP29/24 plants did not show significant reduction in growth with respect to the WT plants, while NoM plants were much smaller than WT plants (Figure 1A). Thylakoid membranes were isolated from WT and mutant plants, and the lack of the corresponding gene product was confirmed by SDS-PAGE (Figure 1B) and western blotting (see Supplementary Information, Figure S2). The pigment content of mutant thylakoids showed a significant decrease in the Chl *a*/Chl *b* ratio with respect to the membranes from WT (reflecting a relative increase of the amount of outer antenna complexes): double mutants koCP26/24 and koCP29/24 showed a ratio of 2.61 and 2.64 respectively, *vs.* 2.75 for WT thylakoids. The lowest ratio (2.35) was observed for NoM (Table 1). In order to detect possible alterations in the relative amount of protein components of the photosynthetic apparatus upon removal of minor antennae, we determined the stoichiometry of the main subunits of both Photosystems by immunoblotting titration, using antibodies specific for the subunits CP47 (PsbB, inner antenna of PSII core complex), PsaA (main subunit of PSI core complex) and LHCII (the major outer antenna of PSII). The PSI/PSII (PsaA/CP47) ratio was essentially the

Table 1. *Chlorophyll composition and LHCII content determined on thylakoids from wild-type and KO mutants.*

Sample	Chl a/b	LHCII trimeric / PSII monomeric
WT	2.75 ± 0.05	4.2 ± 0.3
NoM	2.35 ± 0.04	6.1 ± 0.3
KoCP29/24	2.64 ± 0.03	4.8 ± 0.3
KoCP26/24	2.61 ± 0.02	5.1 ± 0.3

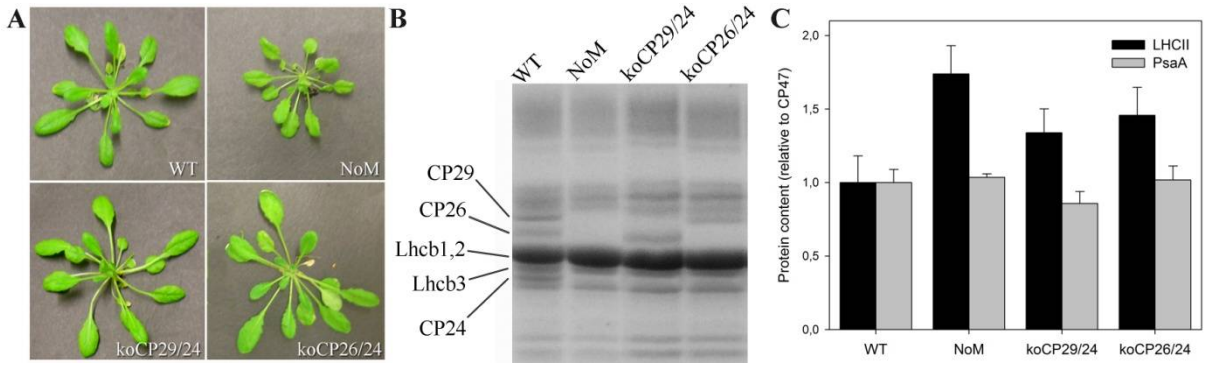

Figure 1. Characterization of the KO mutants. *(A) Phenotype of wild-type and mutant plants grown in control conditions (100 µmol photons m^{-2} s^{-1}, 23°C, 8/16 h day/night) for 4 weeks . (B) SDS/PAGE analysis of wild-type and mutants thylakoid proteins. Selected apoprotein bands are marked. Fifteen micrograms of Chls were loaded in each lane. (C) Immunotitration of thylakoid proteins. Data of LHCII and PsaA subunits were normalized to the PSII core amount, CP47 content, and normalized to the corresponding WT content.*

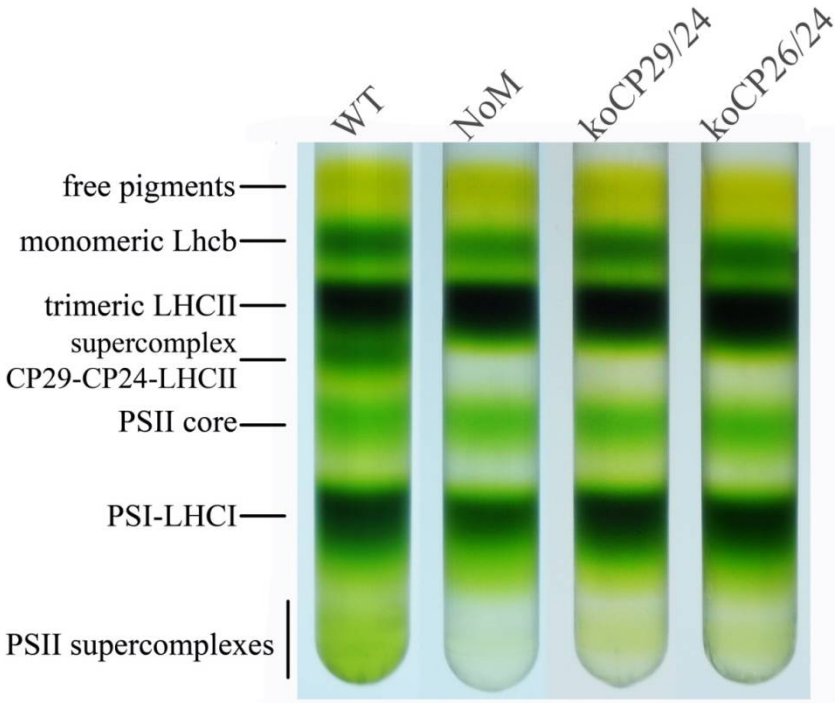

Figure 2. Sucrose density gradient fractionation of wild-type and KO mutants solubilized thylakoids. *Solubilization was performed with 0.7% α-DM. Composition of the green bands are indicated.*

same in WT, koCP26/24 and NoM membranes, while a slight increase in CP47 relative content was detected for koCP29/24 as compared to WT. The LHCII/PSII ratio increased with the removing of monomeric antennae: both koCP26/24 and koCP29/24 had a significantly higher amount of LHCII with respect to WT, while the LHCII content was even higher in NoM (Figure 1C). The stoichiometric ratio of trimeric LHCII and monomeric PSII core complex was determined by quantifying the coomassie staining of the corresponding bands on an SDS/PAGE, by integrating the optical density of each band (see supplementary information, Figure S3, see Methods for details). Results confirmed a

far higher LHCII content in NoM (6.1 trimeric LHCII per monomeric PSII) with respect to the WT (4.2 trimers), while koCP29/24 and koCP26/24 showed an intermediate content (respectively, 4.8 and 5.1 trimers per monomeric PSII) (Table 1).

To analyze the organization of pigment-protein complexes, thylakoid membranes isolated from WT and KO mutants were solubilized with 0.7% dodecyl-α-D-maltoside (α-DM), then Chl-binding proteins were fractionated by sucrose gradient ultracentrifugation. The fractionation patterns are shown in Figure 2. Six major green bands were obtained for the wild type: the PSI-LHCI complex was found as a major band in the lower part of the gradient, corresponding to a complex more stable than PSII that does not dissociate into smaller complexes upon mild solubilization of thylakoids; the PSII-LHCII components are visible as multiple green bands, namely PSII core complex, CP29-CP24-LHCII-M antenna supercomplex, trimeric LHCII and monomeric Lhcb; a large band with apparent molecular mass higher than PSI-LHCI, which contained undissociated PSII supercomplexes of different LHCII composition, was detected in the lower part of the gradient. The major difference detected in KO mutants with respect to the wild type was the lack of the antenna supercomplex CP29-

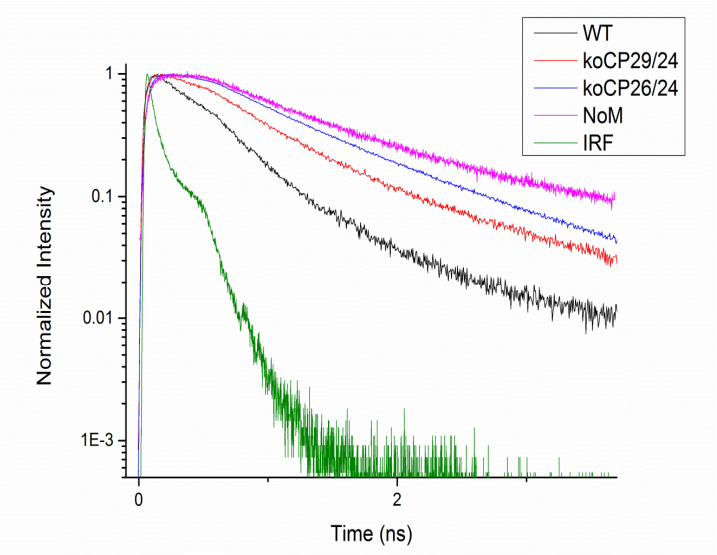

Figure 3. Time-resolved fluorescence decays of thylakoid membranes from WT, KoCP29/24, KoCP26/24 and NoM strains*. The excitation wavelength is 412 nm and the detection wavelength is 680 nm.*

Table 2*. Fitted lifetimes (and amplitudes in brackets) for thylakoids at room temperature with excitation wavelength 412 nm and detection wavelength 680 nm.*

	WT	koCP2624	koCP29CP24	NoM
τ_1	52 ps (25%)	64 ps (23%)	66 ps (21%)	59 ps (30%)
τ_2	166 ps (32%)	273 ps (23%)	278 ps (23%)	294 ps (20%)
τ_3	409 ps (42%)	912 ps (53%)	732 ps (52%)	1.001 ns (48%)
τ_4	5.6 ns (1%)	2.8 ns (1%)	2.1 ns (4%)	2.9 ns (2%)

Confidence intervals of fluorescence lifetimes (τ) as calculated by exhaustive search were <5%, lifetimes were calculated from 2–6 repeats.

CP24-LHCII. Moreover, PSII supercomplexes were differentially represented in these genotypes: faint bands of PSII supercomplexes were still detectable in the lower part of the gradient in both koCP29/24 and koCP26/24, although their amounts were strongly reduced as compared to WT, while NoM thylakoids were completely devoid of PSII supercomplexes.

To test the photosynthetic activity of both photosystems in our thylakoid preparations, artificial electron donors and acceptors were used. The rate of linear electron transport (ET) from H_2O to DMBQ, which accepts electrons at the Q_B site, was measured polarographically as the rate of O_2 evolution, while the ET capacity of PSI was measured spectrophotometrically as the rate of $NADP^+$ reduction, upon addition of the plastocyanin electron donor $TMPDH_2$ (see Methods for details). Results reported in Table S1 show that all photosystems retained their ET capacity, which clearly indicates that all the preparations are active and can efficiently drive photosynthesis. However, a reduction in O_2 evolution and NADPH accumulation on a Chl basis was observed in the membranes of NoM mutants (respectively, -30% and -20% as compared with the WT); this result might be ascribed to a lower PSII efficiency due to the presence of badly connected LHCII in the NoM mutant as compared to WT.

Fluorescence decay curves were measured with the TCSPC setup stacked thylakoids from *Arabidopsis thaliana*. This approach aimed to be close to the native situation and was preferred above measuring on grana-enriched membranes (BBYs), which are known to constitute a heterogeneous system and to retain a far lower amount of trimeric LHCII than the number generally reported to be bound per RC in thylakoid preparations. Either 412-nm laser pulses, exciting relatively more PSII core complexes, or 484 nm laser pulses, exciting relatively more outer antenna complexes, were used. For detection 679 nm-, 701 nm- and 720 nm-interference band filters were used. By combining the results for different excitation and detection wavelengths it is in principle possible to differentiate between PSI and PSII kinetics and to estimate the average migration time of excitations to the PSII reaction centers [25].

The fluorescence decay curves of thylakoid preparations from WT, NoM, koCP29/24 and koCP26/24 mutants were strikingly different from each other (Figure 3). The decay of WT thylakoids was the fastest followed by those of koCP29/24, koCP26/24 and NoM, in that order. To get more quantitative information from the decay curves, they were fitted to a sum of exponential decay functions. The fitting results are given in Table 2 (more detailed results are given in Supplementary Information, see Table S2, Table S3, Table S4 and Table S5).

The lifetime τ_1, which is in the range of 50 ps – 70 ps, is largely due to PSI, although also PSII does contribute to some extent [25, 28, 49]. Because PSI fluorescence is red-shifted as compared to PSII fluorescence, the relative amplitude of this component increases upon going from detection wavelength 679 to 720 nm. The value of τ_1 and the corresponding amplitude only differ to a limited extent for the different thylakoid preparations. WT *Arabidopsis* shows the shortest value for τ_1 with 52

ps, whereas the τ_1 value for the NoM mutant is only 7 ps slower (59 ps). The τ_1 value is somewhat slower for koCP26/24 and koCP29/24 with 64 ps and 66 ps, respectively. The relative amplitude of τ_1 ranges from 21 to 30 % for the different thylakoid preparations (for λ_{exc}=412 nm, λ_{det}=679 nm; more detailed results are given in Supplementary Information, see Table S2, Table S3, Table S4 and Table S5).

The lifetimes τ_2 and τ_3 in Table 2 are mainly due to PSII–LHCII (and possibly some detached antenna with the highest amplitude at λ_{det}=679 nm, as expected for PSII – LHCII [25]. WT thylakoids show the lowest values for both τ_2 (166 ps) and τ_3 (409 ps). These lifetimes become considerably longer for the mutants. The τ_2 values for the various mutants are very similar to each other, ranging from 273 ps to 294 ps. On the other hand, the difference in τ_3 for the mutants is significantly more pronounced. τ_3 is 732 ps for the koCP29/24 mutant, whereas it is 905 ps for koCP26/24 and 1.00 ns for NoM. In comparison to WT, the amplitude for τ_3 becomes rather high in all mutants whereas the amplitudes for τ_2 decrease substantially. Finally, the slowest component (τ_4) can be ascribed to free chlorophyll and/or disconnected light-harvesting complexes with very low amplitudes and possibly some closed RCs although this is rather unlikely with the current excitation conditions (total amplitude is at most 4%) [25]. It should be noted that the amplitude for τ_4 is lower than 1% for WT thylakoids (detailed results are given in Supplementary Information, see Table S2, Table S3, Table S4 and Table S5).

To estimate the PSII – LHCII kinetics, PSI and PSII kinetics were separated from each other using the method recently presented by van Oort et al [25]. In brief, the PSII – LHCII contribution to the sub-100 ps component was determined by using different excitation and detection wavelengths [25] and together with the long lifetimes τ_2 and τ_3, which are solely attributed to PSII – LHCII, the kinetics of PSII–LHCII, with possibly some free LHCII, can be calculated [25]. The obtained PSII–LHCII kinetics differ considerably for WT and mutant thylakoids. For excitation at 412 nm, the WT

Table 3. *PSII – LHCII (with possible free LHCII) kinetics for thylakoid membranes*

	τ_{avg} (ps)		
Excitation	**412 nm**	**484 nm**	**Difference (ps)**
WT	259	285	26
KoCP29/24	523	565	42
KoCP26/24	617	687	70
NoM	601	778	178

The PSII – LHCII (with possible free LHCII) kinetics were derived from the kinetics of thylakoid membranes by removing the PSI contribution, as explained in van Oort et al [23]before.

preparation shows the fastest PSII–LHCII kinetics with an average lifetime of 259 ps, whereas the mutants are significantly slower; 523 for koCP29/24, 617 ps for koCP26/24, and 601 ps for NoM. For excitation at 484 nm, the PSII–LHCII kinetics of all mutant and WT preparations become slower. The PSII–LHCII average lifetime for WT cells is then 285 ps. For the mutant preparations, the average lifetimes are 565 ps, 687 ps and 771 ps for koCP29/24, koCP26/24 and NoM, respectively (Table 3).

The difference in PSII–LHCII average lifetime for different excitation wavelengths is approximately proportional to the average migration time of excitons needed to reach the RC for the first time, but also the presence of detached antennae affects this difference. The difference is 26 ps for WT thylakoids, whereas it becomes larger for the mutants: 41 ps and 70 ps for koCP29/24 and koCP26/24, respectively, whereas it is even 170 ps for NoM mutants. It should be noted that detached or loosely bound antennae cause a significant increase of the difference between PSII–LHCII kinetics for different excitation wavelengths (Table 3). In addition, it should be mentioned that the difference between overall average lifetimes (i.e. without correction for PSI) with different excitation wavelengths for WT and mutant strains has the same trend as the difference in PSII–LHCII average lifetime for different excitation wavelengths (See Supplementary Information Table S2, Table S3, Table S4 and Table S5), which shows that the differences between corrected lifetimes upon different excitation wavelengths are not artificially created or exaggerated because of corrections and calculations. The calculated PSII–LHCII average lifetime values will be discussed hereafter.

4.5 DISCUSSION

The monomeric antennae CP24, CP26, and CP29 are three of the six light-harvesting subunits that compose the PSII peripheral antenna system of higher plants. They are the only Lhc subunits that can occupy the position between the inner antennae CP43/CP47 and the outer LHCII trimers within the PSII supercomplex [50] (Figure 4). Although these pigment-protein complexes are homologous and

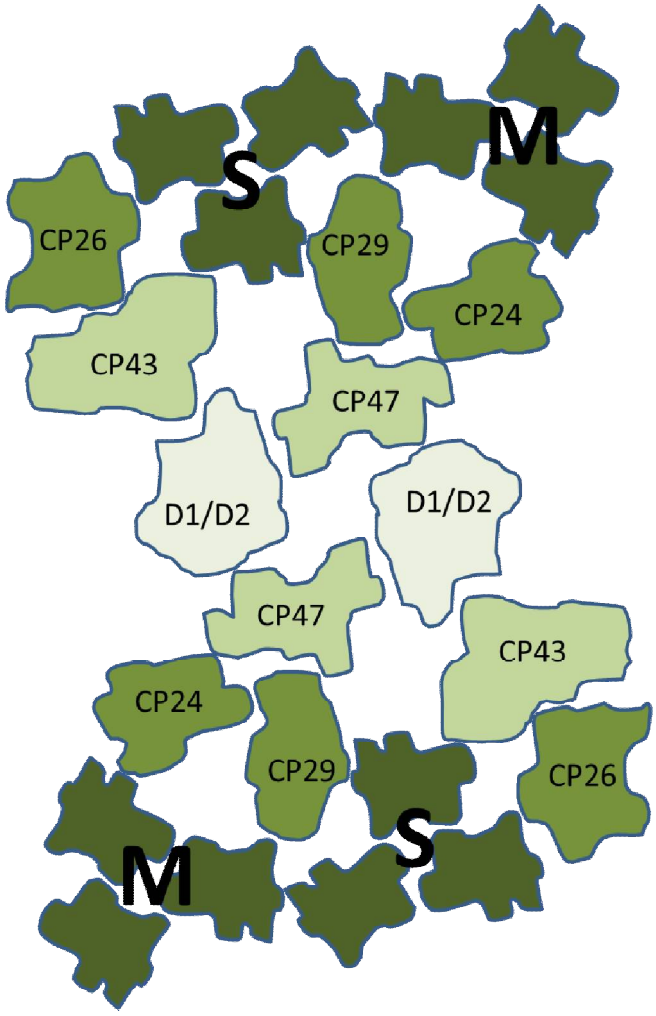

Figure 4. Membrane organization of PSII in Arabidopsis Thaliana*. The core of PSII consists of reaction center (D1/D2) together with CP47 and CP43. Minor antenna complexes (CP24, CP26 and CP29) with the major antenna complexes LHCII (dark green) form peripheral antenna that surrounds the core. The binding strength of trimeric LHCII at different locations is strong (S) or moderate (M) PSII structure is based on the study of Caffari et al. [21]*

are expected to share a common three-dimensional organization on the basis of the structural data available [43, 51], they cannot be exchanged between each other in the supercomplexes [50].

Earlier work [52] has characterized Arabidopsis plants devoid of LHCII, and proposed a high degree of redundancy among Lhcb subunits; indeed, the PSII supercomplex organization was maintained in the absence of LHCII by over-accumulating Lhcb5. Instead, the knock-out of monomeric antennae leads to destabilization of PSII-Lhcb supercomplexes, meaning that the minor antennae are essential for PSII organization. This conclusion is supported by the fact that removal of two or more different monomeric Lhcb's increases the trapping time of excitons in the RCs substantially as compared to WT thylakoids, meaning that the absence of minor antenna complexes leads to badly connected or disconnected LHCII as will be discussed further below.

Recently, time-resolved fluorescence kinetic studies were performed on different knockout mutants of *A. thaliana.* It was shown that, in the absence of specific minor antenna complexes in most cases the overall average lifetimes become longer as compared to those of WT cells [25, 30] and in particular the migration time of excitations to the RCs increases [25, 30]. These results confirm that there are disruptions of the PSII–LHCII complex organization in the absence of minor antenna complexes resulting in the formation of badly connected or disconnected LHCII [25, 30]. Amongst the mutants studied here, the most explicit slowdown of the fluorescence kinetics is observed for the NoM mutant as might have been expected since all minor antenna complexes are missing. For koCP26/24 the slowdown of the fluorescence kinetics is more pronounced than for koCP29/24. This observation is in good agreement with previous work in [30], which indicates that both double mutants have disconnected LHCII, but the koCP26/24 mutant has more, although the mutant that was lacking CP26 showed faster fluorescence kinetics than mutants lacking either CP24 or CP29 or both [25].

The most significant increase concerns the lifetimes of decay components 2 and 3 for all mutants, and this must originate from a reorganization or "disassembly" of PSII–LHCII, in agreement with earlier studies [25, 30]. The increase in the lifetime of the PSII–LHCII components can be explained by the existence of badly connected or disconnected LHCII due to the absence of several minor antenna complexes. In the presence of disconnected LHCII, long-lived fluorescence components (around 4 ns) are expected, unless the LHCII complexes aggregate [48] which leads to a shortening of the fluorescence lifetime [48]. In a previous picosecond fluorescence study on thylakoid membranes from *A. thaliana*, it was shown that not only lifetime components 2 and 3 are responsible for the PSII-LHCII kinetics, but component 1 is also partly due to PSII-LHCII [25]. In that study, van Oort et al. used two excitation wavelengths in order to vary the relative amount of excitations in the core and outer antenna of PSII [25]. Applying this method, we find that the average lifetime of PSII-LHCII for the NoM mutant is 2.3 times longer than the average lifetime of PSII-LHCII for WT. This huge difference is attributed to the disruption of PSII supercomplexes and the presence of detached LHCII. Furthermore, from the biochemical analysis it is concluded that the LHCII/PSII ratio is increased by 50% in the NoM mutant as compared to WT cells, which means that the number of PSII pigments per RC in the NoM mutant is about 20% higher than in WT, since monomeric antennae are lacking. This should lead to an increase of the average lifetime of approximately 20% if all LHCII would be connected equally well to the PSII RC as in WT thylakoids [25]. To figure out the reason behind the increase of the average lifetime, the migration time for the WT and NoM mutant are calculated by the method van Oort et al. [25]. According to this method, the difference $\Delta\tau$ in the average lifetime of PSII for the two excitation wavelengths is approximately proportional to the migration time[25]. For WT cells we find $\Delta\tau$ = 26 ps, whereas for the NoM mutant the value of $\Delta\tau$ is far larger, i.e. 170 ps. This dramatic increase cannot be explained by an increase of the migration time because of badly connected LHCII only but there should also be a significant fraction of disconnected LHCII (see also Van Oort et

al. 2010). The (partial) detachment of LHCII is confirmed by the absence in NoM mutants of PSII supercomplexes containing LHCII-S, as shown upon mild solubilization of thylakoids and fractionation of pigment-protein complexes by ultracentrifugation (Figure 2). Therefore, CP29 and CP26 play a crucial role in mediating the association of trimeric LHCII with the PSII complex. Moreover, the loss of all monomeric Lhcbs was accompanied by an over-accumulation of LHCII (+45% as compared to WT), suggesting compensation within the group of Lhcb proteins as a general regulatory mechanism for PSII antenna size. The phenotype of NoM is consistent with a recent study of *Arabidopsis thaliana* acclimation to low- vs. high-light [53], which showed that LHCII is among the Lhcb's the major one responsible for the regulation of the PSII antenna size during acclimation.

The efficiency of light harvesting, directly related to the plastoquinone redox state, might play a role in antenna-size regulation. Indeed, the redox state is an indicator of the overall efficiency of photosynthetic electron transport, and it was suggested to play a key role in the modulation of antenna size through regulation of the Lhc genes expression [54]. More recent results [55] showed than upon long-term acclimation, despite a lack of Lhcb transcriptional regulation, the level of LHCII is tuned to environmental conditions, thus suggesting that the steady-state level of LHCII depends on post-transcriptional, rather than on transcriptional regulation, as assessed by the finding of a strong differential translational control on individual Lhcb mRNAs [56]. Thus, overaccumulation of LHCII in NoM would represent an adaptation response: depletion of minor antennae leads to reduced trapping efficiency in limiting light, and would trigger a compensative response leading to a photosynthetic phenotype with high LHCII/PSII ratio, namely resembling that of low light-acclimated leaves.

Accumulation of a large amount of disconnected antenna proteins in the NoM thylakoids suggests that LHCII is independently folded into membranes, irrespective from its assembly with the PSII core complex later on [57]. Therefore, even when the assembly is prevented, LHCII is stable in the membrane and does not undergo proteolytic degradation. This evidence is consistent with the phenotype of PSII mutants such as *viridis-zd*^{69} of barley [58] and of lincomycin-treated plants [59], which revealed the stability of free LHCII in the thylakoids.

Isolation of the C_2S_2 supercomplex from koCP29/24 thylakoid membranes [36] has shown that LHCII-S can be associated with the core complex when CP26 is the only monomeric subunit present. This evidence is consistent with the isolation of a stable monomeric core with CP26 and the LHCII-S trimer[20]. In the absence of both CP29 and CP24, some $C_2S_2M_2$ complexes can assemble in grana membranes, but they are less stable and the molecular interactions are rather weak [36]. Moreover, koCP29/24 plants shows a 15% increase in LHCII content with respect to the wild-type level (similar to the 20% for the koCP26/24 mutant). Thus, it is likely that a large part of the outer antenna is not directly bound to the PSII supercomplexes; rather, other trimers are interspersed among the C_2S_2 particles. This is confirmed by the time-resolved fluorescence data. The PSII–LHCII kinetics slows down significantly (average lifetime is almost doubled as compared to WT) while the value of $\Delta\tau$ is 42

ps as compared to 26 ps for WT. In a previous study, a CP29 antisense line was studied with the same method that we used here and the results are slightly different [25]. In that case $\Delta\tau$ was 30 ps instead of 42 ps [25]. However, it should be mentioned that in the CP29as mutant CP29 expression was only partially blocked [60] as shown by detection of CP24 unlike the present mutant [36]. For koCP29/24 a large fraction of uncoupled LHCII is observed, giving rise to a long lifetime of 732 ps (see τ_3 in table 2 and table S3). In addition, after correcting for the PSI contribution and the 2 ns component the corresponding amplitude is around 65%, depending somewhat on excitation wavelength. For koCP26/24 the fitted lifetime is 912 ps with a similar amplitude around 64 % after correcting for the PSI contribution. These amplitudes might correspond to the percentage of badly connected Chls *a* and since there are 5 LHCII trimers per PSII core in each mutant, this implies that at most one LHCII trimer plus one minor antenna, either CP29 or CP26 depending on the type of mutant, would be closely associated with the PSII core. This is in excellent agreement with earlier work in which it was shown that LHCII-S can be associated with the core complex when CP26 is the only monomeric subunit present [36]. Such an interpretation of the lifetime data would be in agreement with electron-microscopy observations, which show a high number of LHCII complexes interposed between rows of connected PSII cores in grana membranes [37]. These results would also be consistent with recent biochemical characterization of PSII supercomplexes in Arabidopsis [20], which indicate that LHCII-S binding is far less stable in a mutant devoid of CP26. The absence of a PSII supercomplex binding LHCII-M indicates that CP26 and CP24 have an important function in mediating the association of $C_2S_2M_2$ complex.

A key consideration for the efficiency of primary productivity in plants and algae is the size of the light-harvesting system. Ort et al. have proposed antenna size reduction as a valuable strategy for the optimisation of the light reactions: theoretical simulation of net CO_2 uptake suggested that a smaller antenna size would significantly improve photosynthetic efficiency on crop canopies [61]. Even biomass yield of microalgal cultures at industrial scale is currently limited by several biological constraints, including the uneven light distribution into photobioreactors [62]; therefore, the successful implementation of biofuel production facilities requires domestication strategies, such as decreasing the absorption cross section to enhance light penetration and increase the size of metabolic sinks per chlorophyll [63, 64].

However, strategies to improve light penetration must ensure that truncated antenna mutants are not photosynthetically impaired in ways other than reduced LHC content: indeed in higher plants, an extreme reduction in LHC complement lead to a lower photochemical yield and increases photoinhibition [65].

The present results show that depletion of even a sub-group of LHCs strongly affects the PSII light-harvesting efficiency and thus the photoautotrophic growth. To ensure that truncated-antenna strains will operate with improved light use efficiency, biotechnological approaches aimed at reducing

antenna cross-section must focus on trimeric LHCII, rather than monomeric Lhcb content: the latter leads to a strong impairment of PSII light-use efficiency, thus cancelling out benefits of optical density reduction, although only for the NoM mutant this leads to strongly reduced growth under continuous-light conditions.

In summary, we have found in this study that in the absence of all minor antenna complexes of PSII, the functional connection of LHCII to the PSII cores is strongly diminished. A large part of this LHCII has a long excited-state lifetime although far shorter than the 4 ns of isolated LHCII trimers. Most likely, the detached LHCII is aggregated which leads to a shortening of the excited-state lifetime. In koCP26/24 and koCP29/24 mutants, it seems likely that only one LHCII trimer is directly (specifically) connected to the PSII core (or two LHCII trimers per PSII core dimer) whereas all other trimers are interspersed between the supercomplexes and still lead to relatively good EET, not hampering plant growth during continuous growth light conditions.

Acknowledgements: We thank Roberto Bassi for helpful discussions and support. This work was supported financially by the Netherlands Organization for Scientific Research (NWO) via the Council for Chemical Sciences (HvA).

4.6 REFERENCES:

[1] N. Nelson, A. Ben-Shem, The complex architecture of oxygenic photosynthesis, Nature Reviews Molecular Cell Biology, 5 (2004) 971-982.
[2] R. Croce, H. van Amerongen, Natural strategies for photosynthetic light harvesting, Nature Chemical Biology, 10 (2014) 492-501.
[3] N. Nelson, C.F. Yocum, Structure and function of photosystems I and II, Annual Review of Plant Biology, 57 (2006) 521-565.
[4] J. Veerman, F.K. Bentley, J.J. Eaton-Rye, C.W. Mullineaux, S. Vasil'ev, D. Bruce, The PsbU subunit of photosystem II stabilizes energy transfer and primary photochemistry in the phycobilisome - Photosystem II assembly of Synechocystis sp PCC 6803, Biochemistry, 44 (2005) 16939-16948.
[5] H. van Amerongen, R. Croce, Light harvesting in photosystem II, Photosynthesis Research, 116 (2013) 251-263.
[6] G.H. Schatz, H. Brock, A.R. Holzwarth, Kinetic and Energetic Model for the Primary Processes in Photosystem-Ii, Biophysical Journal, 54 (1988) 397-405.
[7] R. Croce, H. van Amerongen, Light-harvesting in photosystem I, Photosynthesis Research, 116 (2013) 153-166.
[8] A. Busch, M. Hippler, The structure and function of eukaryotic photosystem I, Biochimica Et Biophysica Acta-Bioenergetics, 1807 (2011) 864-877.
[9] A.N. Melkozernov, S. Lin, R.E. Blankenship, Excitation dynamics and heterogeneity of energy equilibration in the core antenna of photosystem I from the cyanobacterium Synechocystis sp. PCC 6803, Biochemistry, 39 (2000) 1489-1498.
[10] B. Gobets, R. van Grondelle, Energy transfer and trapping in photosystem I, Biochimica Et Biophysica Acta-Bioenergetics, 1507 (2001) 80-99.
[11] K.N. Ferreira, T.M. Iverson, K. Maghlaoui, J. Barber, S. Iwata, Architecture of the photosynthetic oxygen-evolving center, Science, 303 (2004) 1831-1838.
[12] Y. Umena, K. Kawakami, J.R. Shen, N. Kamiya, Crystal structure of oxygen-evolving photosystem II at a resolution of 1.9 angstrom, Nature, 473 (2011) 55-U65.
[13] E.J. Boekema, H. van Roon, J.F.L. van Breemen, J.P. Dekker, Supramolecular organization of photosystem II and its light-harvesting antenna in partially solubilized photosystem II membranes, European Journal of Biochemistry, 266 (1999) 444-452.
[14] S.S. Lampoura, V. Barzda, G.M. Owen, A.J. Hoff, H. van Amerongen, Aggregation of LHCII leads to a redistribution of the triplets over the central xanthophylls in LHCII, Biochemistry, 41 (2002) 9139-9144.
[15] M. Mozzo, L. Dall'Osto, R. Hienerwadel, R. Bassi, R. Croce, Photoprotection in the antenna complexes of photosystem II - Role of individual xanthophylls in chlorophyll triplet quenching, Journal of Biological Chemistry, 283 (2008) 6184-6192.
[16] V. Barzda, E.J.G. Peterman, R. van Grondelle, H. van Amerongen, The influence of aggregation on triplet formation in light-harvesting chlorophyll a/b pigment-protein complex II of green plants, Biochemistry, 37 (1998) 546-551.
[17] N. Betterle, M. Ballottari, S. Zorzan, S. de Bianchi, S. Cazzaniga, L. Dall'Osto, T. Morosinotto, R. Bassi, Light-induced Dissociation of an Antenna Hetero-oligomer Is Needed for Non-photochemical Quenching Induction, Journal of Biological Chemistry, 284 (2009) 15255-15266.
[18] P. Horton, A.V. Ruban, R.G. Walters, Regulation of light harvesting in green plants, Annual Review of Plant Physiology and Plant Molecular Biology, 47 (1996) 655-684.
[19] E.C.M. Engelmann, G. Zucchelli, F.M. Garlaschi, A.P. Casazza, R.C. Jennings, The effect of outer antenna complexes on the photochemical trapping rate in barley thylakoid Photosystem II, Biochimica Et Biophysica Acta-Bioenergetics, 1706 (2005) 276-286.
[20] S. Caffarri, R. Kouril, S. Kereiche, E.J. Boekema, R. Croce, Functional architecture of higher plant photosystem II supercomplexes, Embo Journal, 28 (2009) 3052-3063.
[21] S. Caffarri, K. Broess, R. Croce, H. van Amerongen, Excitation Energy Transfer and Trapping in Higher Plant Photosystem II Complexes with Different Antenna Sizes, Biophysical Journal, 100 (2011) 2094-2103.
[22] S. de Bianchi, M. Ballottari, L. Dall'Osto, R. Bassi, Regulation of plant light harvesting by thermal dissipation of excess energy, Biochemical Society Transactions, 38 (2010) 651-660.

[23] D.G. Durnford, J.A. Price, S.M. McKim, M.L. Sarchfield, Light-harvesting complex gene expression is controlled by both transcriptional and post-transcriptional mechanisms during photoacclimation in Chlamydomonas reinhardtii, Physiologia Plantarum, 118 (2003) 193-205.
[24] K. Broess, G. Trinkunas, A. van Hoek, R. Croce, H. van Amerongen, Determination of the excitation migration time in Photosystem II - Consequences for the membrane organization and charge separation parameters, Biochimica Et Biophysica Acta-Bioenergetics, 1777 (2008) 404-409.
[25] B. van Oort, M. Alberts, S. de Bianchi, L. Dall'Osto, R. Bassi, G. Trinkunas, R. Croce, H. van Amerongen, Effect of Antenna-Depletion in Photosystern II on Excitation Energy Transfer in Arabidopsis thaliana, Biophysical Journal, 98 (2010) 922-931.
[26] G.H. Schatz, H. Brock, A.R. Holzwarth, Picosecond Kinetics of Fluorescence and Absorbance Changes in Photosystem II Particles Excited at Low Photon Density, Proceedings of the National Academy of Sciences of the United States of America, 84 (1987) 8414-8418.
[27] R. Vangrondelle, Excitation-Energy Transfer, Trapping and Annihilation in Photosynthetic Systems, Biochimica Et Biophysica Acta, 811 (1985) 147-195.
[28] E. Wientjes, H. van Amerongen, R. Croce, LHCII is an antenna of both photosystems after long-term acclimation, Biochimica et biophysica acta, 1827 (2013) 420-426.
[29] E. Wientjes, H. van Amerongen, R. Croce, Quantum Yield of Charge Separation in Photosystem II: Functional Effect of Changes in the Antenna Size upon Light Acclimation, The Journal of Physical Chemistry B, (2013).
[30] Y. Miloslavina, S. de Bianchi, L. Dall'Osto, R. Bassi, A.R. Holzwarth, Quenching in Arabidopsis thaliana Mutants Lacking Monomeric Antenna Proteins of Photosystem II, Journal of Biological Chemistry, 286 (2011) 36830-36840.
[31] D.I.G. Bennett, K. Amarnath, G.R. Fleming, A Structure-Based Model of Energy Transfer Reveals the Principles of Light Harvesting in Photosystem II Supercomplexes, Journal of the American Chemical Society, 135 (2013) 9164-9173.
[32] J. Chmeliov, G. Trinkunas, H. van Amerongen, L. Valkunas, Light Harvesting in a Fluctuating Antenna, Journal of the American Chemical Society, 136 (2014) 8963-8972.
[33] J.P. Dekker, R. Van Grondelle, Primary charge separation in Photosystem II, Photosynthesis Research, 63 (2000) 195-208.
[34] V.I. Novoderezhkin, E.G. Andrizhiyevskaya, J.P. Dekker, R. van Grondelle, Pathways and timescales of primary charge separation in the photosystem II reaction center as revealed by a simultaneous fit of time-resolved fluorescence and transient absorption, Biophysical Journal, 89 (2005) 1464-1481.
[35] M.K. Sener, C. Jolley, A. Ben-Shem, P. Fromme, N. Nelson, R. Croce, K. Schulten, Comparison of the light-harvesting networks of plant and cyanobacterial photosystem I, Biophysical Journal, 89 (2005) 1630-1642.
[36] S. de Bianchi, N. Betterle, R. Kouril, S. Cazzaniga, E. Boekema, R. Bassi, L. Dall'Osto, Arabidopsis Mutants Deleted in the Light-Harvesting Protein Lhcb4 Have a Disrupted Photosystem II Macrostructure and Are Defective in Photoprotection, Plant Cell, 23 (2011) 2659-2679.
[37] S. de Bianchi, L. Dall'Osto, G. Tognon, T. Morosinotto, R. Bassi, Minor antenna proteins CP24 and CP26 affect the interactions between photosystem II Subunits and the electron transport rate in grana membranes of Arabidopsis, Plant Cell, 20 (2008) 1012-1028.
[38] A.P. Casazza, D. Tarantino, C. Soave, Preparation and functional characterization of thylakoids from Arabidopsis thaliana, Photosynthesis Research, 68 (2001) 175-180.
[39] A.M. Gilmore, H.Y. Yamamoto, Zeaxanthin Formation and Energy-Dependent Fluorescence Quenching in Pea-Chloroplasts under Artificially Mediated Linear and Cyclic Electron-Transport, Plant Physiology, 96 (1991) 635-643.
[40] H. Schagger, G. Vonjagow, Tricine Sodium Dodecyl-Sulfate Polyacrylamide-Gel Electrophoresis for the Separation of Proteins in the Range from 1-Kda to 100-Kda, Analytical Biochemistry, 166 (1987) 368-379.
[41] G.F. Peter, J.P. Thornber, Biochemical-Composition and Organization of Higher-Plant Photosystem-Ii Light-Harvesting Pigment-Proteins, Journal of Biological Chemistry, 266 (1991) 16745-16754.

[42] M. Havaux, L. Dall'Osto, S. Cuine, G. Giuliano, R. Bassi, The effect of zeaxanthin as the only xanthophyll on the structure and function of the photosynthetic apparatus in Arabidopsis thaliana, Journal of Biological Chemistry, 279 (2004) 13878-13888.
[43] Z.F. Liu, H.C. Yan, K.B. Wang, T.Y. Kuang, J.P. Zhang, L.L. Gui, X.M. An, W.R. Chang, Crystal structure of spinach major light-harvesting complex at 2.72 angstrom resolution, Nature, 428 (2004) 287-292.
[44] H. Towbin, T. Staehelin, J. Gordon, Electrophoretic Transfer of Proteins from Polyacrylamide Gels to Nitrocellulose Sheets - Procedure and Some Applications, Proceedings of the National Academy of Sciences of the United States of America, 76 (1979) 4350-4354.
[45] O.J.G. Somsen, L.B. Keukens, M.N. de Keijzer, A. van Hoek, H. van Amerongen, Structural heterogeneity in DNA: Temperature dependence of 2-aminopurine fluorescence in dinucleotides, Chemphyschem, 6 (2005) 1622-1627.
[46] J.W. Borst, M.A. Hink, A. van Hoek, A.J.W.G. Visser, Effects of refractive index and viscosity on fluorescence and anisotropy decays of enhanced cyan and yellow fluorescent proteins, Journal of Fluorescence, 15 (2005) 153-160.
[47] B. van Oort, A. Amunts, J.W. Borst, A. van Hoek, N. Nelson, H. van Amerongen, R. Croce, Picosecond Fluorescence of Intact and Dissolved PSI-LHCI Crystals, Biophysical Journal, 95 (2008) 5851-5861.
[48] B. van Oort, A. van Hoek, A.V. Ruban, H. van Amerongen, Aggregation of Light-Harvesting Complex II leads to formation of efficient excitation energy traps in monomeric and trimeric complexes, Febs Letters, 581 (2007) 3528-3532.
[49] R. Croce, H. van Amerongen, Light-harvesting and structural organization of Photosystem II: From individual complexes to thylakoid membrane, Journal of Photochemistry and Photobiology B-Biology, 104 (2011) 142-153.
[50] H. van Amerongen, J.P. Dekker, Light harvesting in photosystem II, in: Light-Harvesting Antennas in Photosynthesis, Kluwer Academic Publishers, 2003, pp. 219-251.
[51] X.W. Pan, M. Li, T. Wan, L.F. Wang, C.J. Jia, Z.Q. Hou, X.L. Zhao, J.P. Zhang, W.R. Chang, Structural insights into energy regulation of light-harvesting complex CP29 from spinach, Nature Structural & Molecular Biology, 18 (2011) 309-U394.
[52] A.V. Ruban, M. Wentworth, A.E. Yakushevska, J. Andersson, P.J. Lee, W. Keegstra, J.P. Dekker, E.J. Boekema, S. Jansson, P. Horton, Plants lacking the main light-harvesting complex retain photosystem II macro-organization, Nature, 421 (2003) 648-652.
[53] M. Ballottari, L. Dall'Osto, T. Morosinotto, R. Bassi, Contrasting behavior of higher plant photosystem I and II antenna systems during acclimation, Journal of Biological Chemistry, 282 (2007) 8947-8958.
[54] J.M. Escoubas, M. Lomas, J. Laroche, P.G. Falkowski, Light-Intensity Regulation of Cab Gene-Transcription Is Signaled by the Redox State of the Plastoquinone Pool, Proceedings of the National Academy of Sciences of the United States of America, 92 (1995) 10237-10241.
[55] S. Frigerio, C. Campoli, S. Zorzan, L.I. Fantoni, C. Crosatti, F. Drepper, W. Haehnel, L. Cattivelli, T. Morosinotto, R. Bassi, Photosynthetic antenna size in higher plants is controlled by the plastoquinone redox state at the post-transcriptional rather than transcriptional level, Journal of Biological Chemistry, 282 (2007) 29457-29469.
[56] M. Floris, R. Bassi, C. Robaglia, A. Alboresi, E. Lanet, Post-transcriptional control of light-harvesting genes expression under light stress, Plant Molecular Biology, 82 (2013) 147-154.
[57] N.H. Chua, P. Bennoun, Thylakoid Membrane Polypeptides of Chlamydomonas-Reinhardtii - Wild-Type and Mutant Strains Deficient in Photosystem 2 Reaction Center, Proceedings of the National Academy of Sciences of the United States of America, 72 (1975) 2175-2179.
[58] O. Machold, D.J. Simpson, B.L. Moller, Chlorophyll-Proteins of Thylakoids from Wild-Type and Mutants of Barley (Hordeum-Vulgare-L), Carlsberg Research Communications, 44 (1979) 235-254.
[59] L. Gaspar, E. Sarvari, F. Morales, Z. Szigeti, Presence of 'PSI free' LHCI and monomeric LHCII and subsequent effects on fluorescence characteristics in lincomycin treated maize, Planta, 223 (2006) 1047-1057.
[60] J. Andersson, R.G. Walters, P. Horton, S. Jansson, Antisense inhibition of the photosynthetic antenna proteins CP29 and CP26: Implications for the mechanism of protective energy dissipation, Plant Cell, 13 (2001) 1193-1204.

[61] D.R. Ort, X.G. Zhu, A. Melis, Optimizing Antenna Size to Maximize Photosynthetic Efficiency, Plant Physiology, 155 (2011) 79-85.
[62] P.G. Stephenson, C.M. Moore, M.J. Terry, M.V. Zubkov, T.S. Bibby, Improving photosynthesis for algal biofuels: toward a green revolution, Trends in Biotechnology, 29 (2011) 615-623.
[63] J.E.W. Polle, S.D. Kanakagiri, A. Melis, tla1, a DNA insertional transformant of the green alga Chlamydomonas reinhardtii with a truncated light-harvesting chlorophyll antenna size, Planta, 217 (2003) 49-59.
[64] H. Kirst, J.G. Garcia-Cerdan, A. Zurbriggen, T. Ruehle, A. Melis, Truncated Photosystem Chlorophyll Antenna Size in the Green Microalga Chlamydomonas reinhardtii upon Deletion of the TLA3-CpSRP43 Gene, Plant Physiology, 160 (2012) 2251-2260.
[65] C.E. Espineda, A.S. Linford, D. Devine, J.A. Brusslan, The AtCAO gene, encoding chlorophyll a oxygenase, is required for chlorophyll b synthesis in Arabidopsis thaliana, Proceedings of the National Academy of Sciences of the United States of America, 96 (1999) 10507-10511.

Supplementary Information

Table S1. Photosynthetic capacity of PSII and PSI supercomplexes measured in vitro on thylakoids from WT and KO mutants. *Effect of electron donors and acceptors on the electron transport rate of the supercomplex were assessed as described in "Material and Methods". Concentration used were: 250 μM DMBQ, PSII artificial electron acceptors; 250 μM $TMPDH_2$, PSI artificial electron donors. When $TMPDH_2$ was used, the reaction mixture contained 5 mM ascorbic acid, and after 1.5 min of illumination 1 μM DCMU was added, followed by the artificial donor. Data are expressed as mean ± SD (n = 3). Values marked with the same letters within the same column are not significantly different from each other (Student's t test, $P < 0.05$).*

	$\mu mol\ O_2\ mg\ Chl^{-1}\ h^{-1}$ ($H_2O \rightarrow DMBQ$, PSII)	$\mu mol\ NADPH\ mg\ Chl^{-1}\ h^{-1}$ ($TMPDH_2 \rightarrow NADP^+$, PSI)
WT	53.2 ± 3.7 [a]	156.9 ± 6.5 [a]
NoM	37.0 ± 2.7 [b]	128.3 ± 7.3 [b]
koCP29/24	48.0 ± 1.7 [a]	141.6 ± 11.7 [a,b]
koCP26/24	47.8 ± 2.8 [a]	149.9 ± 7.8 [a]

Table S2. *Fluorescence kinetics of PSII in thylakoids of WT A. thaliana*

	Excitation					
	412 nm			**484 nm**		
Detection	*680 nm*	*700 nm*	*720 nm*	*680 nm*	*700 nm*	*720 nm*
τ (ps)	%	%	%	%	%	%
52	24.8	43.7	51.8	13.6	29.5	42.3
166	32.2	25.1	26.6	35.5	31.9	28.0
409	42.1	30.6	21.1	49.9	37.9	29.3
5602	0.9	0.6	0.4	1.0	0.6	0.5
τ_{avg}(ps)	**287**	**221**	**181**	**324**	**257**	**214**

	PSII amplitudes from 166 ps DAS				PSII amplitudes from 409 ps DAS			
Wavelengths used for PSI removal	*700/680 nm*		*720/680 nm*		*700/680 nm*		*720/680 nm*	
Excitation	**412 nm**	**484 nm**	**412 nm**	**484 nm**	**412 nm**	**484 nm**	**412 nm**	**484 nm**
τ (ps)	%	%	%	%	%	%	%	%
52	17	9	19	9	17	9	18	9
166	36	38	35	38	36	38	35	38
409	47	53	46	53	47	53	46	53
τ_{avg} (ps)	**261**	**284**	**255**	**284**	**262**	**285**	**258**	**285**

	τ_{avg} for PSII		
Excitation	**412 nm**	**484 nm**	*Difference*
WT	259 ps	285 ps	*26 ps*

The kinetics were derived from the kinetics of thylakoid membranes by removing the PSI contribution, as explained in van Oort et al [23] before. Confidence intervals of fluorescence lifetimes (τ) were <5% (calculated by exhaustive search), standard errors of amplitudes were generally <5% (calculated from 2–6 repeats).

Table S3. *Fluorescence kinetics of PSII in thylakoids of KoCP29/24 mutant of A. thaliana*

	Excitation					
	412 nm			**484 nm**		
Detection	*680 nm*	*700 nm*	*720 nm*	*680 nm*	*700 nm*	*720 nm*
τ (ps)	%	%	%	%	%	%
66	21.0	39.7	54.9	13.3	26.8	42.2
278	22.5	20.2	18.4	20.8	22.7	21.2
732	52.5	37.8	25.2	62.0	48.0	34.7
2099	4.0	2.3	1.6	4.0	2.5	1.9
τ_{avg} (ps)	**544**	**408**	**305**	**604**	**485**	**381**

	PSII amplitudes from 278 ps DAS				PSII amplitudes from 732 ps DAS			
Wavelengths used for PSI removal	*700/680 nm*		*720/680 nm*		*700/680 nm*		*720/680 nm*	
Excitation	**412 nm**	**484 nm**	**412 nm**	**484 nm**	**412 nm**	**484 nm**	**412 nm**	**484 nm**
τ (ps)	%	%	%	%	%	%	%	%
66	14	10	14	9	13	10	13	9
278	26	23	26	23	26	23	26	23
732	60	67	60	68	61	68	61	68
τ_{avg} (ps)	**521**	**561**	**520**	**566**	**525**	**565**	**525**	**569**

	τ_{avg} for PSII		
Excitation	**412 nm**	**484 nm**	*Difference*
KoCP29/24	523 ps	565 ps	*42 ps*

The kinetics were derived from the kinetics of thylakoid membranes by removing the PSI contribution, as explained in van Oort et al [23] before. Confidence intervals of fluorescence lifetimes (τ) were <5% (calculated by exhaustive search), standard errors of amplitudes were generally <5% (calculated from 2–6 repeats).

Table S4. *Fluorescence kinetics of PSII in thylakoids of KoCP26/24 mutant of A. thaliana*

	Excitation					
	412 nm			**484 nm**		
Detection	*680 nm*	*700 nm*	*720 nm*	*680 nm*	*700 nm*	*720 nm*
τ (ps)	%	%	%	%	%	%
64	22.9	43.4	46.1	13.4	24.7	34.4
273	22.6	18.6	20.4	20.4	18.1	16.6
912	53.5	36.2	31.2	64.1	52.3	44.8
2800	0.9	1.8	2.3	2.1	4.9	4.2
τ_{avg} (ps)	**591**	**460**	**433**	**707**	**680**	**593**

	PSII amplitudes from 273 ps DAS				PSII amplitudes from 912 ps DAS			
Wavelengths used for PSI removal	*700/680 nm*		*720/680 nm*		*700/680 nm*		*720/680 nm*	
Excitation	**412 nm**	**484 nm**	**412 nm**	**484 nm**	**412 nm**	**484 nm**	**412 nm**	**484 nm**
τ (ps)	%	%	%	%	%	%	%	%
64	15	10	18	10	14	10	17	10
273	25	22	24	22	26	22	25	22
912	60	68	57	68	61	68	58	68
τ_{avg} (ps)	626	686	602	686	631	687	609	687

	τ_{avg} for PSII		
Excitation	**412 nm**	**484 nm**	*Difference*
KoCP26/24	617 ps	687 ps	*70 ps*

The kinetics were derived from the kinetics of thylakoid membranes by removing the PSI contribution, as explained in van Oort et al [23] before. Confidence intervals of fluorescence lifetimes (τ) were <5% (calculated by exhaustive search), standard errors of amplitudes were generally <5% (calculated from 2–6 repeats).

Table S5. *Fluorescence kinetics of PSII in thylakoids of NoM mutant of A. thaliana*

	Excitation					
	412 nm			**484 nm**		
Detection	*680 nm*	*700 nm*	*720 nm*	*680 nm*	*700 nm*	*720 nm*
τ (ps)	%	%	%	%	%	%
59	30.0	43.4	53.8	17.2	29.1	40.1
294	19.9	21.3	21.1	12.0	13.8	15.0
1001	47.8	33.7	23.7	69.6	55.8	44.1
2862	2.2	1.5	1.3	1.3	1.3	0.8
τ_{avg} (ps)	**619**	**470**	**369**	**778**	**654**	**532**

	PSII amplitudes from 294 ps DAS				PSII amplitudes from 1001 ps DAS			
Wavelengths used for PSI removal	*700/680 nm*		*720/680 nm*		*700/680 nm*		*720/680 nm*	
Excitation	**412 nm**	**484 nm**	**412 nm**	**484 nm**	**412 nm**	**484 nm**	**412 nm**	**484 nm**
τ (ps)	%	%	%	%	%	%	%	%
59	28	15	27	15	25	14	25	13
294	21	12	21	13	22	13	22	13
1001	51	73	51	73	53	74	53	74
τ_{avg} (ps)	**590**	**771**	**594**	**775**	**608**	**782**	**610**	**786**

	τ_{avg} for PSII		
Excitation	**412 nm**	**484 nm**	*Difference*
NoM	601 ps	778 ps	*178 ps*

The kinetics were derived from the kinetics of thylakoid membranes by removing the PSI contribution, as explained in van Oort et al [23] before. Confidence intervals of fluorescence lifetimes (τ) were <5% (calculated by exhaustive search), standard errors of amplitudes were generally <5% (calculated from 2–6 repeats).

Table S6. Maximum quantum efficiency of PSII photochemistry determined on dark-adapted leaves of Arabidopsis WT and KO mutants. *Data are expressed as mean ± SD (n = 6). Values marked with the same letters are not significantly different from each other (Student's t test, P < 0.05).*

	F_v / F_m
WT	0.81 ± 0.01 [a]
NoM	0.56 ± 0.02 [b]
koCP29/24	0.75± 0.02 [c]
koCP26/24	0.74 ± 0.02 [c]

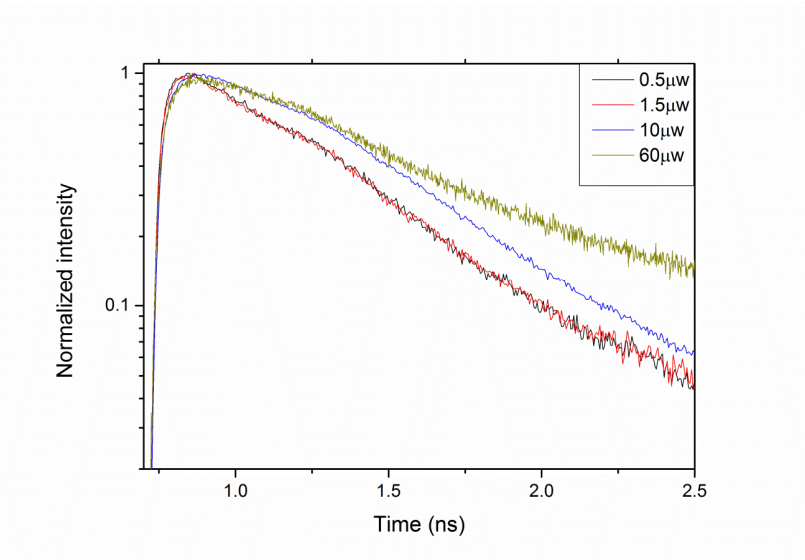

Figure S1. Fluorescence kinetics of thylakoid membranes of WT Arabidopsis Thaliana excited at 412 nm and detected at 680 nm at different excitation powers. *The resulting decay curves were indistinguishable for excitation powers 0.5 µW and 1.5 µW, which are used for the experiments.*

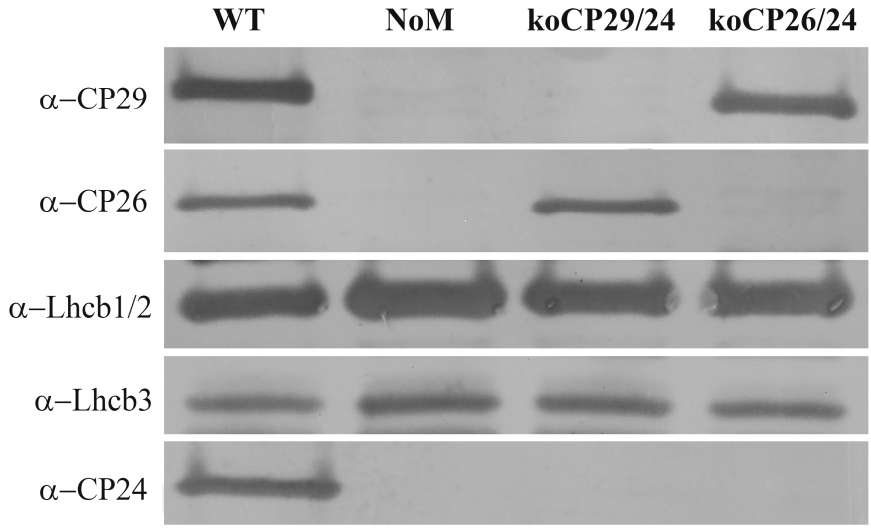

Figure S2. Polypeptide composition of thylakoids from WT and KO mutants. *Immunoblot analysis was carried out with antibodies against Lhcb subunits. Thylakoids corresponding to 1 µg of Chls were loaded for each sample.*

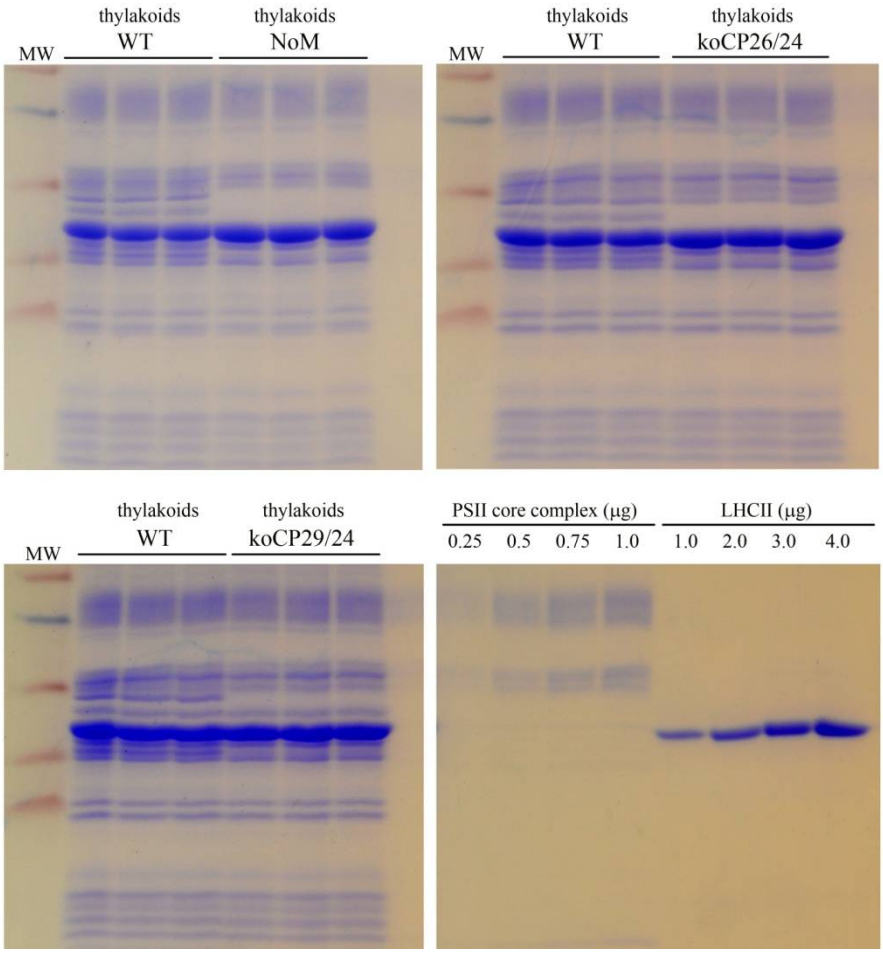

Figure S3. SDS-PAGE analysis of trimeric LHCII:monomeric PSII core stoichiometry in thylakoids from wild-type and KO mutants. *Absolute contents of LHCII and PSII core were quantified by loading thylakoids (15 µg of Chls/lane), PSII core (0.25-0.5-0.75-1.0 µg of Chls) and trimeric LHCII (1.0-2.0-3.0-4.0 µg of Chls) in the same slab gels. After staining with coomassie blue, the signal amplitude of LHCII and CP43/CP47 bands were quantified by densitometric analysis (n=4). By using the pigment composition of the individual subunits and the OD of each protein band, the number of LHCII trimers per monomeric PSII core was calculated. MW, pre-stained molecular weight marker.*

Chapter 5

Multi-Exciton Dynamics of ZnCdTe Quantum Dots

Caner Ünlü [a], Leyla Eral Dogan [b], Serdar Özçelik [b], Herbert van Amerongen [a,c]

[a]Laboratory of Biophysics, Wageningen University, 6703 HA Wageningen, The Netherlands, [b] Department of Chemistry, Izmir Institute of Technology, Gülbahçe Köyü, Urla, 35430 ˙Izmir, Turkey [c]MicroSpectroscopy Centre, Wageningen University, 6703 HA Wageningen, The Netherlands.

CHAPTER 5

5.1 ABSTRACT:

Quantum dots are semiconductor nanocrystals comprised of groups II–VI or III–V elements with unique photophysical properties. These semiconductor nanocrystals are of interest because they are used in many different application areas such as solar cells, cancer research, LEDs, lasers, artificial photosynthesis. Here, we have performed picosecond fluorescence measurements on ZnCdTe ternary quantum dots at room temperature by using a streak-camera setup in order to investigate in detail the fluorescence kinetics for ZnCdTe quantum dots with different size and structure at different excitation laser intensities. The fluorescence kinetics of ZnCdTe ternary quantum dots changes with the changes in structure and size. In heterogeneously structured ZnCdTe quantum dots, the fluorescence kinetics become faster as compared to homogeneously structured ZnCdTe quantum dots. Also, in both homogeneous and heterogeneous ZnCdTe quantum dots, a new peak is observed in the high-energy region of the emission spectrum when using high excitation intensities, which shows that the radiative processes that occur from higher energy states become more favoured as the excitation intensity increases.

5.2 INTRODUCTION:

Quantum dots are defined as semiconductor nanocrystals comprised of groups II–VI or III–V elements, and are described as particles with physical dimensions smaller than the exciton Bohr radius [1-4]. These semiconductor nanocrystals, possessing high fluorescence quantum efficiency, narrow spectral emission and easy color tenability, promise great potential as light-emitting nanomaterials for the next generation optoelectronic and biomedical applications [5-9]. The unique optical properties of the quantum dots are significantly challenging for the next generation displays, white-light illuminators, solar cells, photodetectors, image sensors, biosensors and drug delivery systems [5-9]. In addition, recent studies showed that quantum dots can serve as a good alternative for chlorophylls and carotenoids, (light-harvesting molecules in photosynthetic organisms) in artificial photosynthesis systems [9-11]. Moreover, surface properties of quantum dots can be modified [12] and quantum dots can be attached to complex biological photosynthetic systems, such as reaction centers, which can allow to tune or enhance light-harvesting properties of natural photosynthesis [9] .

Research efforts have mainly focused on the development of binary semiconductor colloidal nanocrystals such as CdS, CdTe, CdSe, etc…[13, 14]. The optical properties of the quantum dots can be tuned by adjusting the size of quantum dot. However, the size of quantum dot may lead to problems in some applications, especially in life sciences [6]. Therefore, producing the ternary quantum dots, such as CdSSe, CdHgTe, ZnCdTe…, become an alternative way to tailor the optical properties of quantum dots [6, 15, 16] . The optical behavior of the ternary quantum dots can be controlled by adjusting the size, composition and structure, and it is possible to produce ternary quantum dots that

have different optical properties with same size and same ingredients, but different composition and structure [6, 15-17].

Linear and nonlinear optical behavior of excitons in nanometer scale systems can be studied by time-resolved fluorescence techniques; with time-resolved fluorescence spectroscopy, it is possible to study electronic energies, the spectral distribution of photoexcited carriers (excitons), exciton-exciton interaction, carrier energy-relaxation and recombination dynamics [18-23]. The possible electron transitions in quantum dots can be defined by 6 basic processes [24]. Those are; 1) excitation from ground state to excited state 2) electronic relaxation within the conduction band,3) bandedge electron-hole recombination 4) exciton-exciton annihilation 5) trapping into trap states and 6) trapped electron-hole recombination. The trapped carriers can further recombine radiatively or nonradiatively with lifetimes from a few tens of picoseconds to nanoseconds or longer[24]. The exciton dynamics in quantum dots is related with scattering from phonons, impurities, defects, interfaces and surfaces, exciton-exciton scattering and also free excitons present in the crystal[24].

Unlike bulk semiconductor materials, multi-excitons can be generated in quantum dots [25-28]. The number of excitons formed in quantum dots is determined by the number of photons that is absorbed by the quantum dots[25-28] . Analysis of fluorescence dynamics of multi-excitons has shown that there is an increase in the weight of a fast component with a lifetime of a few picoseconds due to the formation of more than one exciton, which indicates that the relaxation rate of multi-exciton states can be extremely fast [26-28] . The relaxation of electrons in multi-exciton states can progress via several different paths such as relaxations from a biexciton state, triexciton state or upper energy level state like 1 P [26-28]. Each process corresponds to a different zone of the emission spectrum and the properties of these processes depend on the size and structure of the quantum dot[26-28] .

In this work, we have performed picosecond fluorescence measurements on ZnCdTe ternary quantum dots at room temperature by using a streak-camera setup in order to investigate in detail the fluorescence kinetics of ZnCdTe quantum dots with different size and structure by using different excitation laser intensities. Our data show that the changes in fluorescence kinetics are mostly related to the changes in structure and size.. In heterogeneous structured ZnCdTe quantum dots, the fluorescence kinetics become faster as compared to homogeneous structured ZnCdTe quantum dots. Also, in both homogeneous and heterogeneous ZnCdTe quantum dots, a new peak is observed in the high-energy region of the emission spectrum when using high excitation intensities, which shows that the radiative processes that occur from the higher energy states become more favoured when the excitation intensity increases.

5.3 MATERIALS & METHODS

ZnCdTe Quantum Dots

The ZnCdTe quantum dots were synthesized in aqueous medium by the one-pot synthesis method as described in [29]. The ZnCdTe quantum dots were classified into two groups (homogeneous and heterogeneous) according to their structural properties, and for both groups quantum dots were synthesized with two different sizes (4.5 nm and 9.5 nm in diameter) [29]. The ZnCdTe quantum dots with a homogeneous structure do not show a concentration gradient of any of the elements Zn, Cd and Te throughout the structure. The ZnCdTe quantum dots with heterogeneous structure possess a gradient crystal structure with Zn being more concentrated at the inner side and Cd more at the outer side. The structural composition, emission maxima, absorption maxima and quantum yields of the ZnCdTe quantum dots that are studied in this chapter are provided in Table 1. Their steady-state fluorescence spectra are given in the supplementary information (See Supporting information. Figure S1).

Time-resolved Fluorescence Measurements

Streak Camera

Time-resolved fluorescence spectra were recorded at room temperature with a picosecond streak-camera system combined with a grating (50 grooves/mm, blaze wavelength 600 nm) with central wavelength 600 nm and spectral width of 260 nm (for details see [30-32]). Excitation light was vertically polarized, the spot size diameter was typically ~100 μm, and the laser repetition rate was 250 kHz. The detection polarizer was set at magic-angle orientation. The excitation wavelength was 400 nm and the laser power was adjusted between 1 and 100 mW. The sample was put in a static cuvette and stirred during the measurements. Images with a 2-ns time window were obtained for all samples. A relatively high signal/noise ratio was achieved by averaging 100 single images, each obtained after analogue integration of 10 exposures of 1.112 s. Images were corrected for background and photocathode shading.

Data Analysis.

Data obtained with the streak-camera setup were globally analyzed with Glotaran, the graphical user interface of the R package TIMP (for details see [33-35]). The methods of global analysis are described by van Stokkum et al. [36]. With global analysis, the data were fitted to a sum of exponential decay curves convoluted with an IRF, which is described with a Gaussian of ~10 ps fwhm, and the amplitudes of each decay component as a function of wavelength are called “decay-associated spectra” (DAS).

Table.1. *Structural and photophysical parameters of analyzed $Zn_xCd_{1-x}Te$ quantum dots*

Nanoalloys	**λ_{abs} (nm)**	**λ_{ems} (nm)**	**Diameter (nm)**	**QY* (%)**	**Type of Structure**
$Zn_{0.21}Cd_{0.79}Te$	560	580	4.50	45	homogeneous
$Zn_{0.35}Cd_{0.65}Te$	540	590	4.50	20	heterogeneous
$Zn_{0.18}Cd_{0.82}Te$	570	590	9.50	41	homogeneous
$Zn_{0.46}Cd_{0.54}Te$	565	600	9.50	27	heterogeneous

**QY= quantum yield, λ_{abs} = Absorption peak, λ_{ems} = Emission peak*

5.4 RESULTS & DISCUSSION:

Figure 1 shows the streak-camera images at 10 mW excitation power for $Zn_{0.21}Cd_{0.79}Te$ (homogeneous, diameter: 4.5 nm), $Zn_{0.18}Cd_{0.82}Te$ (homogeneous, diameter: 9.5 nm), $Zn_{0.35}Cd_{0.56}Te$ (heterogeneous, diameter: 4.5 nm) and $Zn_{0.46}Cd_{0.54}Te$ (heterogeneous, diameter: 9.5 nm) quantum dots. The ZnCdTe quantum dots were excited with very high laser powers, ranging from 1 mW to 100 mW,

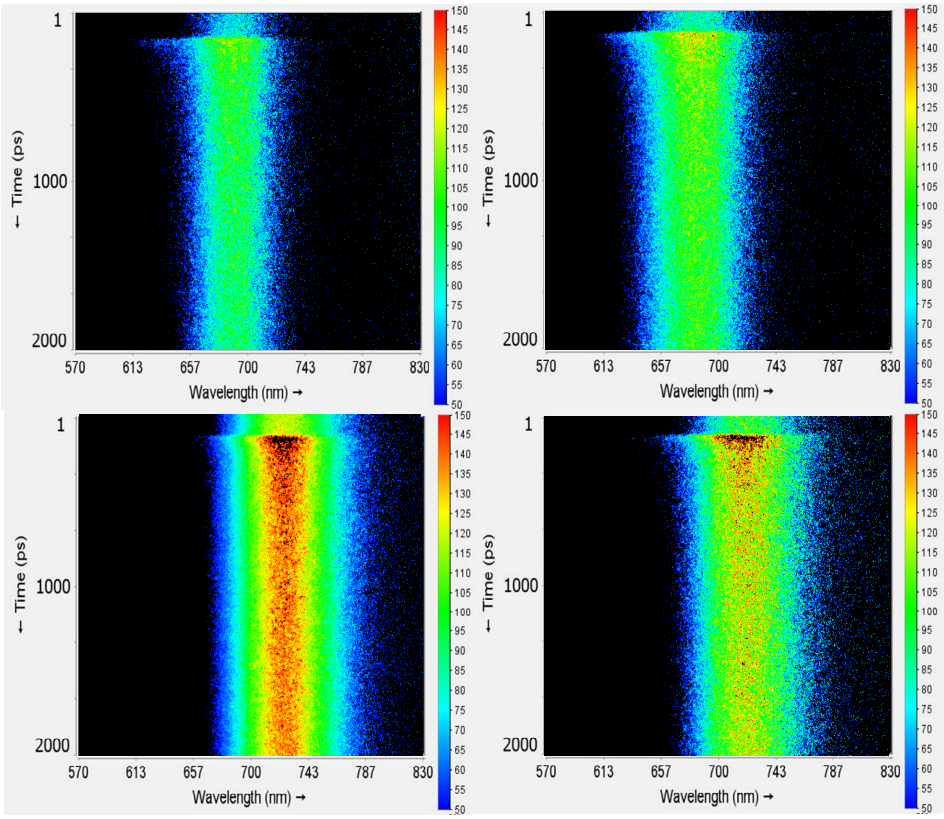

Figure 1. *Streak-camera images of ZnCdTe quantum dots with excitation wavelength 400 nm and excitation power 10 mW (up-left: $Zn_{0.21}Cd_{0.79}Te$, up-right: $Zn_{0.18}Cd_{0.82}Te$, down-left: $Zn_{0.35}Cd_{0.56}Te$ down-right: $Zn_{0.46}Cd_{0.54}Te$). The time scale is 2 ns. In these images, the fluorescence intensity (with the color code) is represented as a function of time (vertical axis) and wavelength (horizontal axis).*

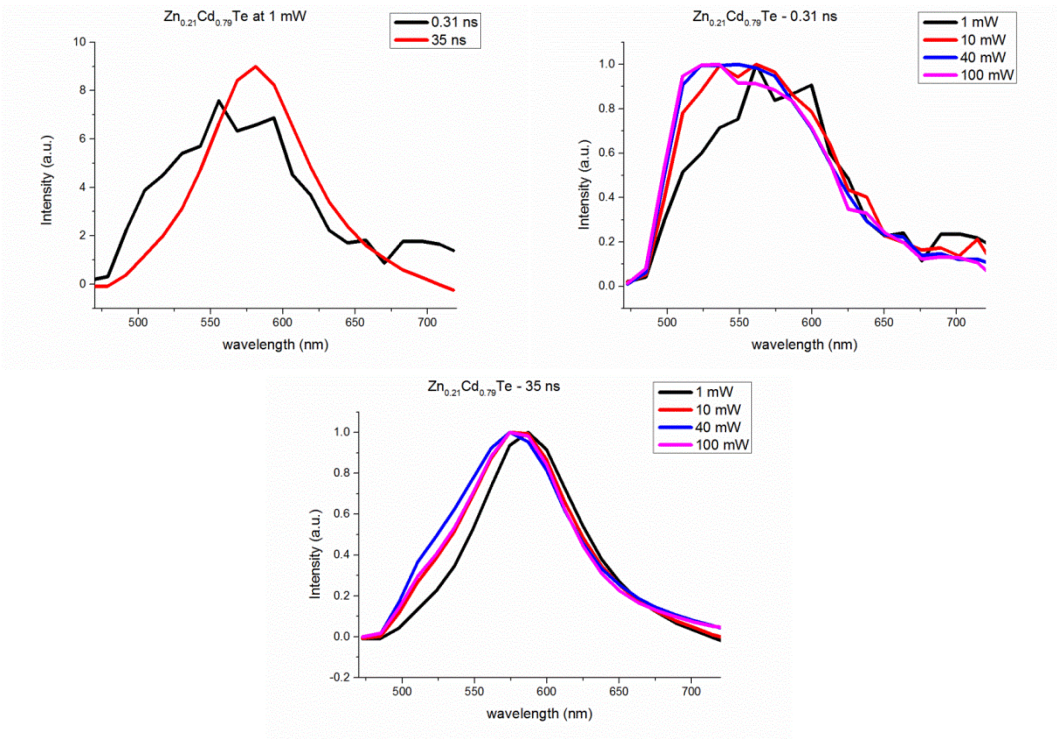

Figure 2. DAS with corresponding lifetimes for $Zn_{0.21}Cd_{0.79}Te$ at different excitation powers

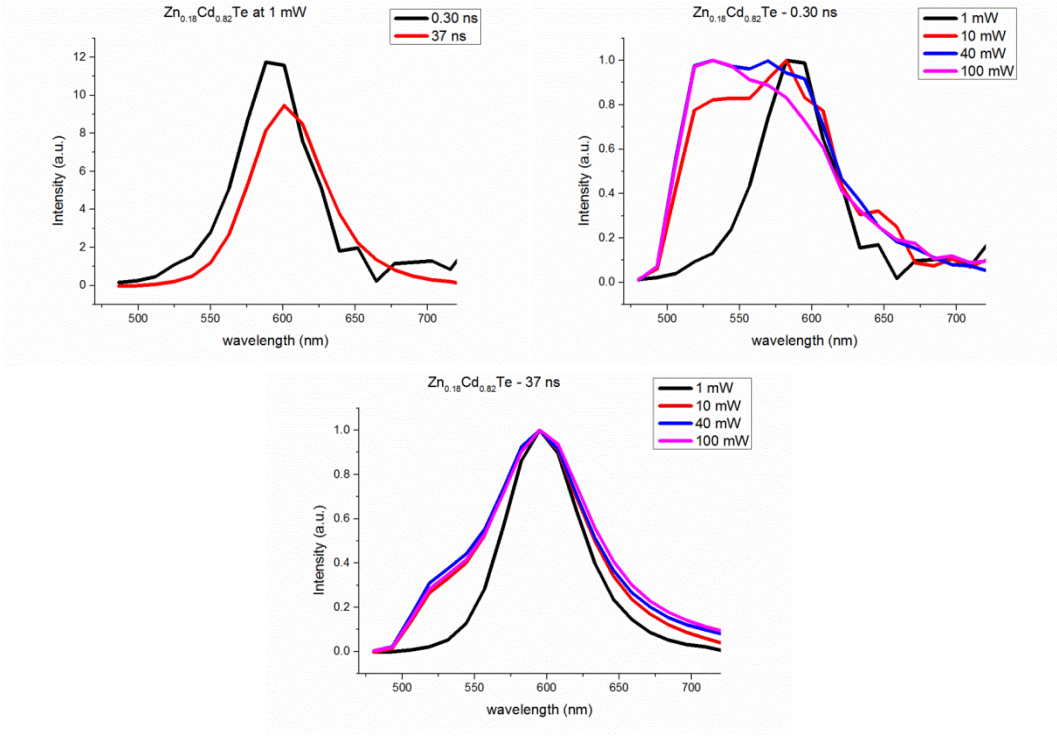

Figure 3. DAS with corresponding lifetimes for $Zn_{0.18}Cd_{0.82}Te$ at different excitation powers

which leads to photon densities varying between 10^{15} to 10^{17} photons/cm^2 per second, to induce multi-exciton dynamics. The photon density should be higher than 10^{12} photon/cm^2 per laser pulse to create multiple excitons per quantum dot [25]. All samples show strong ZnCdTe alloy emission at their fluorescence emission maximum, which varies between 560 nm – 620 nm depending on size and structure of the quantum dot, but a new emission band appears at shorter wavelengths (around 520 nm) for excitation powers above 1 mW for each type of ZnCdTe, independent of its size and structure.

To identify the multi-exciton dynamics of the homogeneous quantum dots, global analysis was performed on the recorded data at different excitation intensities. For ease of comparison, the fluorescence kinetics of ZnCdTe quantum dots are described with 2 lifetimes in all cases. However, it should be noted that for a good fit of the fluorescence data at least 3 lifetimes were required. On the other hand, when 3 (or more) lifetimes are used for fitting, the resulting DAS with fast lifetimes (shorter than 1 ns) are very noisy and they are anticorrelated (See Supporting Information, Figure S2). Therefore, two lifetimes are used to describe all fluorescence processes; one slow component for the single exciton emission lifetime and one fast component for all the annihilation processes with one effective average annihilation time and one average spectrum .

The DAS of the fast component for $Zn_{0.21}Cd_{0.79}Te$ (0.31 ns lifetime, black spectrum) displays a broad spectrum ranging from 500 nm to 650 nm at the lowest excitation power (1 mW) (Figure 2). For $Zn_{0.18}Cd_{0.82}Te$, the short lifetime is 0.30 ns. The DAS of the shortest component (the black DAS) shows a peak around 578 nm at 1 mW (Figure 3). In both $Zn_{0.21}Cd_{0.79}Te$ and $Zn_{0.18}Cd_{0.82}Te$ quantum dots, a new peak around 520 nm appears above 10 mW which becomes more intense as the excitation intensity increases (Figures 2&3). For $Zn_{0.18}Cd_{0.82}Te$ the contribution of the shortest lifetime component to the overall kinetics is relatively higher than for $Zn_{0.21}Cd_{0.79}Te$ (Figure 2&3).

The possible contribution of different non-radiative recombination processes to the short lifetimes makes the interpretation of these lifetimes complicated. In principle, the increase in size results in a decrease of the surface to volume ratio and therefore the number of possible defect states, which can act as recombination centers for excited electrons [37-39], should decrease as well [8]. As the number of defect states decreases, also a concomitant decrease of the extent of non-radiative decay is expected, and the fluorescence quantum yield should increase [37, 38, 40]. However, it is interesting that the short lifetime of the homogeneous quantum dots is even slightly shorter and contributes more to the overall kinetics for the largest quantum dots (at 1 mW). Also, the fluorescence quantum yield is smaller for the largest quantum dot (Table 1). It should be noted that the fastest decay rate is due to a combination of several ultrafast processes, one of which is singlet-singlet annihilation and the quantum yields of the quantum dots are calculated by steady-state spectroscopy, which means that they are not affected by annihilation. The most likely scenario for the drop in quantum yield is an increase of the number of defect states. Another possible scenario is the possibility of appearance of more excitations per quantum dot when the size increases, which leads to more and faster annihilation

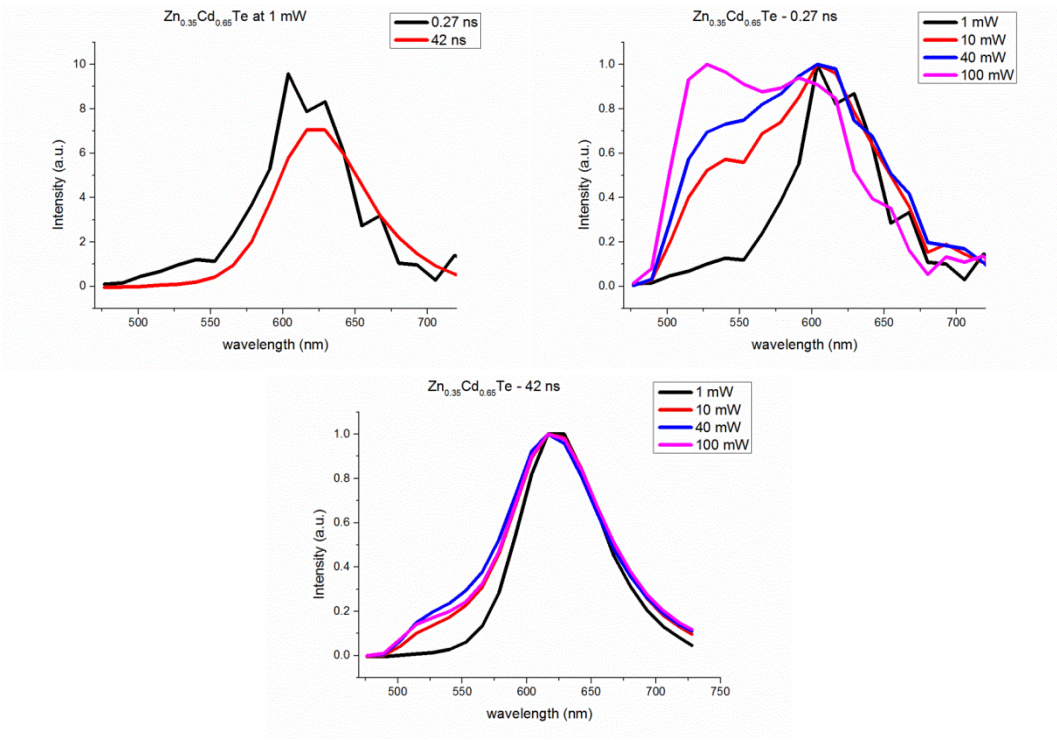

Figure 4. DAS with corresponding lifetimes for $Zn_{0.35}Cd_{0.65}Te$ at different excitation powers

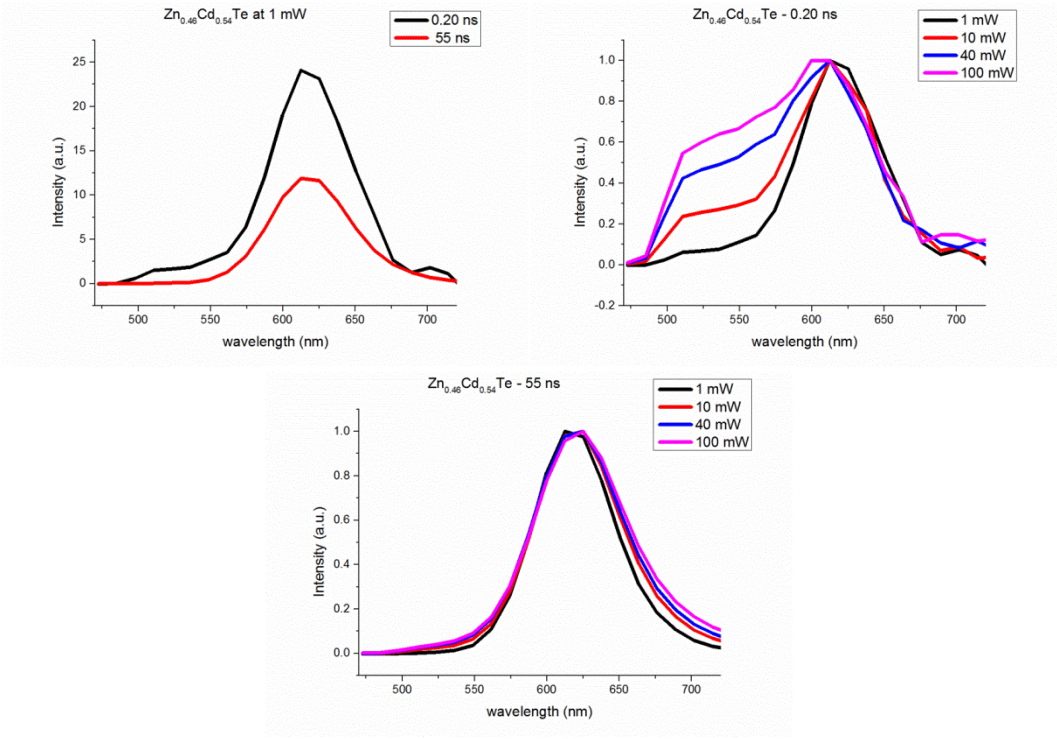

Figure 5. DAS with corresponding lifetimes for $Zn_{0.46}Cd_{0.54}Te$ at different excitation powers

processes. However, our current data are limited and these scenarios should be checked with further experiments and analysis.

The global analysis was also performed for streak camera images of heterogeneous quantum dots. The short component for $Zn_{0.35}Cd_{0.56}Te$ corresponds to a 0.27 ns lifetime (Figure 4). The DAS of this component (black DAS) displays a single positive peak around 605 nm at 1 mW. For $Zn_{0.46}Cd_{0.54}Te$, the shortest component corresponds to a 0.20 ns lifetime (Figure 5). The DAS of the short component (the black DAS) appears as a positive single peak around 610 nm at 1 mW excitation power. Another peak around 520 nm starts to develop and becomes more intense for both types of quantum dots as the excitation power increases (Figures 4&5). It should be noted that the relative contribution of the shortest lifetime component to the overall kinetics is higher for heterogeneous ZnCdTe quantum dots than for homogeneous ZnCdTe quantum dots (Figures 4&5).

For heterogeneous ZnCdTe quantum dots, the shortest component is even more pronounced and faster than for homogeneous ZnCdTe quantum dots, most probably because of a higher concentration of defect states in the crystal structure. Indeed, also the quantum yields of heterogeneous ZnCdTe quantum dots (around 20%) are significantly lower than those of homogeneous ZnCdTe quantum dots (around 40%) which implies that the number of defect states indeed becomes higher in heterogeneous ZnCdTe quantum dots. It should be noted that also the short lifetimes become slightly shorter as the size increases for heterogeneous ZnCdTe quantum dots, which shows that, like for homogeneous ZnCdTe quantum dots, the number of defect states increases with increasing size.

In both homogeneous and heterogeneous ZnCdTe quantum dots, the appearance of a new peak when using high excitation intensities shows that the fast radiative processes that occur from higher energy states become more favoured as the excitation intensity increases. Also recent studies demonstrated that for quantum dots a new peak appears in the higher-energy region of the emission spectrum when high pump intensities are being used [37, 38, 40, 41]. The origin of this peak has been attributed to several processes such as 1P – 1S relaxation and relaxation from trap states [37, 38, 40, 41]. When the quantum dots are over-excited with high excitation powers, the electrons are excited to a higher energy state, called the 1P state. The relaxation of the electrons from the 1P state to the 1S state proceeds with very fast kinetics (varies from hundreds of femtoseconds to tens of picoseconds) and is observed in the higher energy region of the emission spectrum [37, 38, 40, 41]. In our study, both for homogeneous and heterogeneous ZnCdTe quantum dots, we consider 1P – 1S relaxation to be one of the processes responsible for the new peak around 520 nm observed in the shortest-lifetime component for pump intensities above 1 mW. Observation of 1P – 1S relaxation indicates that the electrons move to the 1P energy state above 1 mW, and 1P population becomes more pronounced leading to more 1P-1S relaxation when the pump intensity becomes higher.

It should be noted that trap states, which occur due to defects inside the quantum dot or on its surface, can also induce very fast relaxation processes that correspond to the higher-energy region of the emission spectrum [38, 40]. In addition, the surface capping agent used in the synthesis of the quantum dots, thioglycolic acid, might serve as a sulphur precursor [37] leading to sulphur gradient regions in the quantum dots, which can also contribute to the kinetics that appears in the higher-energy region of the emission spectrum [40].

There are several different fast recombination processes such as electron recombination from doubly excited states or trap states, which correspond to a slightly higher energy than the peak of the single exciton emission (red DAS). [37, 38, 40-44]. In our study, for each quantum dot the peak position of the fast component was shifted to slightly higher energies as compared to that of the peak of the single exciton emission, which shows that electron recombination from doubly excited states or trap states can also be a factor that contributes to the fast lifetimes. Moreover, the contribution of the fast component to the overall kinetics increases with increasing pump intensity in both homogeneous and heterogeneous quantum dots, which shows that non-linear optical processes also take place with high pump intensities [18-23].

The red DAS corresponds to a very long lifetime of tens of nanoseconds, which has a positive single peak for each type of quantum dot (Figures 2,3,4&5). The lifetime values should be considered as highly inaccurate due to the relatively short measuring time window of 2 ns. In addition, a small shoulder, peaking around 520 nm becomes more intense upon increasing the excitation power (Figures 2,3,4&5). The long lifetime for ZnCdTe quantum dots is attributed to radiative single exciton dynamics. The radiative single exciton dynamics in quantum dots is characterized by very long lifetimes (in the range of tens of nanoseconds to hundreds of a nanosecond) and this lifetime changes with the size and structure of the quantum dot[45]. It should be noted that, the shoulder around 520 nm shows that there must be different radiative processes other than single exciton emission that occur with long lifetimes in case of high pump intensities. One of the possibilities might be relaxation of electrons from the 1P state to the 1S state. If the 1S state is fully occupied by electrons, then as long as electrons in 1S did not relax to the ground state, also electrons in 1P cannot relax to 1S. Only when electrons in 1S relax (tens of ns) then also electrons in 1P can relax and the decay component should have a similar lifetime as the 1S excited state, which would only be observed at high pump intensities. Another possibility is the contribution of the sulphur-gradient part to the kinetics. As mentioned before, thioglycolic acid can act as a sulphur precursor and can cause formation of sulphur gradient parts [37]. The sulphur-gradient part can contribute to the overall dynamics at high laser powers[40]. As the emission of CdS appears around 520 nm [40], then one might expect to observe a shoulder around this wavelength in the emission spectrum.

5.5 REFERENCES:

[1] M.G. Bawendi, Synthesis and spectroscopy of II-VI quantum dots: An overview, in: E. Burstein, C. Weisbuch (Eds.) NATO Advanced Study Institute on Confined Electrons and Photons - New Physics and Applications, Erice, Italy, 1993, pp. 339-356.
[2] M.G. Bawendi, P.J. Carroll, W.L. Wilson, L.E. Brus, LUMINESCENCE PROPERTIES OF CDSE QUANTUM CRYSTALLITES - RESONANCE BETWEEN INTERIOR AND SURFACE LOCALIZED STATES, Journal of Chemical Physics, 96 (1992) 946-954.
[3] P.M. Allen, M.G. Bawendi, Ternary I-III-VI quantum dots luminescent in the red to near-infrared, Journal of the American Chemical Society, 130 (2008) 9240-+.
[4] T. Jamieson, R. Bakhshi, D. Petrova, R. Pocock, M. Imani, A.M. Seifalian, Biological applications of quantum dots, Biomaterials, 28 (2007) 4717-4732.
[5] T. Nann, W.M. Skinner, Quantum Dots for Electro-Optic Devices, Acs Nano, 5 (2011) 5291-5295.
[6] C. Unlu, G.U. Tosun, S. Sevim, S. Ozcelik, Developing a facile method for highly luminescent colloidal CdSxSe1-x ternary nanoalloys, Journal of Materials Chemistry C, 1 (2013) 3026-3034.
[7] N. Hildebrandt, Biofunctional Quantum Dots: Controlled Conjugation for Multiplexed Biosensors, Acs Nano, 5 (2011) 5286-5290.
[8] I. Nabiev, A. Sukhanova, M. Artemyev, V. Oleinikov, Fluorescent colloidal particles as a detection tools in biotechnology systems, Colloidal Nanoparticles in Biotechnology, (2008) 133-168.
[9] I. Nabiev, A. Rakovich, A. Sukhanova, E. Lukashev, V. Zagidullin, V. Pachenko, Y.P. Rakovich, J.F. Donegan, A.B. Rubin, A.O. Govorov, Fluorescent Quantum Dots as Artificial Antennas for Enhanced Light Harvesting and Energy Transfer to Photosynthetic Reaction Centers, Angewandte Chemie International Edition, 49 (2010) 7217-7221.
[10] H.M. Chen, C.K. Chen, Y.C. Chang, C.W. Tsai, R.S. Liu, S.F. Hu, W.S. Chang, K.H. Chen, Quantum Dot Monolayer Sensitized ZnO Nanowire-Array Photoelectrodes: True Efficiency for Water Splitting, Angewandte Chemie-International Edition, 49 (2010) 5966-5969.
[11] H.M. Chen, C.K. Chen, R.S. Liu, C.C. Wu, W.S. Chang, K.H. Chen, T.S. Chan, J.F. Lee, D.P. Tsai, A New Approach to Solar Hydrogen Production: a ZnO-ZnS Solid Solution Nanowire Array Photoanode, Advanced Energy Materials, 1 (2011) 742-747.
[12] A. Hoshino, K. Fujioka, T. Oku, M. Suga, Y.F. Sasaki, T. Ohta, M. Yasuhara, K. Suzuki, K. Yamamoto, Physicochemical properties and cellular toxicity of nanocrystal quantum dots depend on their surface modification, Nano Letters, 4 (2004) 2163-2169.
[13] D.V. Talapin, J.S. Lee, M.V. Kovalenko, E.V. Shevchenko, Prospects of Colloidal Nanocrystals for Electronic and Optoelectronic Applications, Chemical Reviews, 110 (2010) 389-458.
[14] S.E. Lohse, C.J. Murphy, Applications of Colloidal Inorganic Nanoparticles: From Medicine to Energy, Journal of the American Chemical Society, 134 (2012) 15607-15620.
[15] R.E. Bailey, S.M. Nie, Alloyed semiconductor quantum dots: Tuning the optical properties without changing the particle size, Journal of the American Chemical Society, 125 (2003) 7100-7106.
[16] X.H. Zhong, M.Y. Han, Z.L. Dong, T.J. White, W. Knoll, Composition-tunable ZnxCd1-xSe nanocrystals with high luminescence and stability, Journal of the American Chemical Society, 125 (2003) 8589-8594.
[17] E. Jang, S. Jun, L. Pu, High quality CdSeS nanocrystals synthesized by facile single injection process and their electroluminescence, Chemical Communications, (2003) 2964-2965.
[18] X.F. Wang, P.B. Xie, F.L. Zhao, H.Z. Wang, Time-Resolved Photoluminescence of Stimulated Emission from ZnO Nanoparticles, Spectroscopy and Spectral Analysis, 29 (2009) 1459-1462.
[19] P. Maly, F. Trojanek, T. Miyoshi, K. Yamanaka, K. Luterova, I. Pelant, P. Nemec, Ultrafast carrier dynamics in CdSe nanocrystalline films on crystalline silicon substrate, Thin Solid Films, 403 (2002) 462-466.
[20] F. Scotognella, K. Miszta, D. Dorfs, M. Zavelani-Rossi, R. Brescia, S. Marras, L. Manna, G. Lanzani, F. Tassone, Ultrafast Exciton Dynamics in Colloidal CdSe/CdS Octapod Shaped Nanocrystals, Journal of Physical Chemistry C, 115 (2011) 9005-9011.
[21] Y. Kobayashi, T. Nishimura, H. Yamaguchi, N. Tamai, Effect of Surface Defects on Auger Recombination in Colloidal CdS Quantum Dots, Journal of Physical Chemistry Letters, 2 (2011) 1051-1055.

[22] B.G. Liu, C.Y. He, M.X. Jin, D.J. Ding, C.X. Gao, Time-resolved ultrafast carrier dynamics in CdTe quantum dots under high pressure, Physica Status Solidi B-Basic Solid State Physics, 248 (2011) 1102-1105.
[23] R. Sarkar, A.K. Shaw, S.S. Narayanan, C. Rothe, S. Hintschich, A. Monkman, S.K. Pal, Size and shape-dependent electron-hole relaxation dynamics in US nanocrystals, Optical Materials, 29 (2007) 1310-1320.
[24] Z.L. Wang, Y. Liu, Z. Zhang, Dynamic Properties of Nanoparticles, in: Handbook of Nanophase and Nanostructured Materials, Springer US, 2003, pp. 562-594.
[25] B. Fisher, J.M. Caruge, D. Zehnder, M. Bawendi, Room-temperature ordered photon emission from multiexciton states in single CdSe core-shell nanocrystals, Physical Review Letters, 94 (2005).
[26] A. Rogach, A. Meijerink, Exciton dynamics and energy transfer processes in semiconductor nanocrystals, in: Semiconductor Nanocrystal Quantum Dots, Springer Vienna, 2008, pp. 277-310.
[27] V.I. Klimov, A.A. Mikhailovsky, S. Xu, A. Malko, J.A. Hollingsworth, C.A. Leatherdale, H.-J. Eisler, M.G. Bawendi, Optical Gain and Stimulated Emission in Nanocrystal Quantum Dots, Science, 290 (2000) 314-317.
[28] M.G. Bawendi, Excitons and multiexcitons in semiconductor nanocrystal quantum dots: Single dots, many dots, applications, in: 229th National Meeting of the American-Chemical-Society, San Diego, CA, 2005, pp. 162-COLL.
[29] L. Eral Doğan, Synthesis and control of exciton dynamics in CdTe, CdTe/CdS and ZnxCd1-xTe colloidal nanocrystals, (2012).
[30] B. van Oort, A. Amunts, J.W. Borst, A. van Hoek, N. Nelson, H. van Amerongen, R. Croce, Picosecond Fluorescence of Intact and Dissolved PSI-LHCI Crystals, Biophysical Journal, 95 (2008) 5851-5861.
[31] B. Van Oort, S. Murali, E. Wientjes, R.B.M. Koehorst, R.B. Spruijt, A. van Hoek, R. Croce, H. van Amerongen, Ultrafast resonance energy transfer from a site-specifically attached fluorescent chromophore reveals the folding of the N-terminal domain of CP29, Chemical Physics, 357 (2009) 113-119.
[32] I.H.M. Van Stokkum, B. Van Oort, F. Van Mourik, B. Gobets, H. Van Amerongen, (Sub)-picosecond spectral evolution of fluorescence studied with a synchroscan streak-camera system and target analysis, in: Biophysical techniques in photosynthesis, Springer, 2008, pp. 223-240.
[33] S.P. Laptenok, J.W. Borst, K.M. Mullen, I.H.M. van Stokkum, A.J.W.G. Visser, H. van Amerongen, Global analysis of Forster resonance energy transfer in live cells measured by fluorescence lifetime imaging microscopy exploiting the rise time of acceptor fluorescence, Physical Chemistry Chemical Physics, 12 (2010) 7593-7602.
[34] K.M. Mullen, I.H.M. van Stokkum, TIMP: An R package for modeling multi-way spectroscopic measurements, Journal of Statistical Software, 18 (2007).
[35] J.J. Snellenburg, S.P. Laptenok, R. Seger, K.M. Mullen, I.H.M. van Stokkum, Glotaran: A Java-Based Graphical User Interface for the R Package TIMP, Journal of Statistical Software, 49 (2012) 1-22.
[36] I.H.M. van Stokkum, D.S. Larsen, R. van Grondelle, Global and target analysis of time-resolved spectra (vol 1658, pg 82, 2004), Biochimica Et Biophysica Acta-Bioenergetics, 1658 (2004) 262-262.
[37] Y. Kobayashi, N. Tamai, Size-Dependent Multiexciton Spectroscopy and Moderate Temperature Dependence of Biexciton Auger Recombination in Colloidal CdTe Quantum Dots, Journal of Physical Chemistry C, 114 (2010) 17550-17556.
[38] Y. Kobayashi, L.Y. Pan, N. Tamai, Effects of Size and Capping Reagents on Biexciton Auger Recombination Dynamics of CdTe Quantum Dots, Journal of Physical Chemistry C, 113 (2009) 11783-11789.
[39] A. Meijerink, Exciton dynamics and energy transfer processes in semiconductor nanocrystals, Springer, 2008.
[40] W.K. Bae, L.A. Padilha, Y.S. Park, H. McDaniel, I. Robel, J.M. Pietryga, V.I. Klimov, Controlled Alloying of the Core-Shell Interface in CdSe/CdS Quantum Dots for Suppression of Auger Recombination, Acs Nano, 7 (2013) 3411-3419.
[41] M. Achermann, J.A. Hollingsworth, V.I. Klimov, Multiexcitons confined within a subexcitonic volume: Spectroscopic and dynamical signatures of neutral and charged biexcitons in ultrasmall semiconductor nanocrystals, Physical Review B, 68 (2003).

[42] W. Qin, R.A. Shah, P. Guyot-Sionnest, CdSeS/ZnS Alloyed Nanocrystal Lifetime and Blinking Studies under Electrochemical Control, Acs Nano, 6 (2012) 912-918.
[43] T.C. Kippeny, M.J. Bowers, A.D. Dukes, J.R. McBride, R.L. Orndorff, M.D. Garrett, S.J. Rosenthal, Effects of surface passivation on the exciton dynamics of CdSe nanocrystals as observed by ultrafast fluorescence upconversion spectroscopy, Journal of Chemical Physics, 128 (2008).
[44] P. Guyot-Sionnest, M. Shim, C. Matranga, M. Hines, Intraband relaxation in CdSe quantum dots, Physical Review B, 60 (1999) R2181-R2184.
[45] K. Gong, Y.H. Zeng, D.F. Kelley, Extinction Coefficients, Oscillator Strengths, and Radiative Lifetimes of CdSe, CdTe, and CdTe/CdSe Nanocrystals, Journal of Physical Chemistry C, 117 (2013) 20268-20279.

Supporting Information:

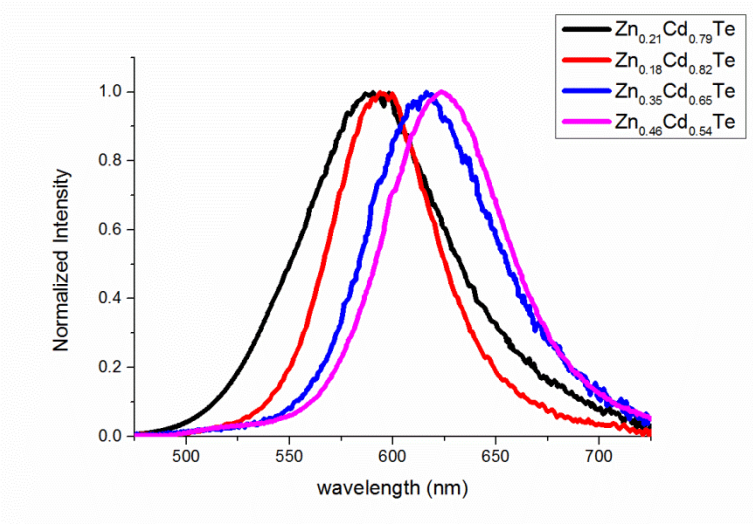

Figure S1 Steady-state Fluorescence spectra of ZnCdTe

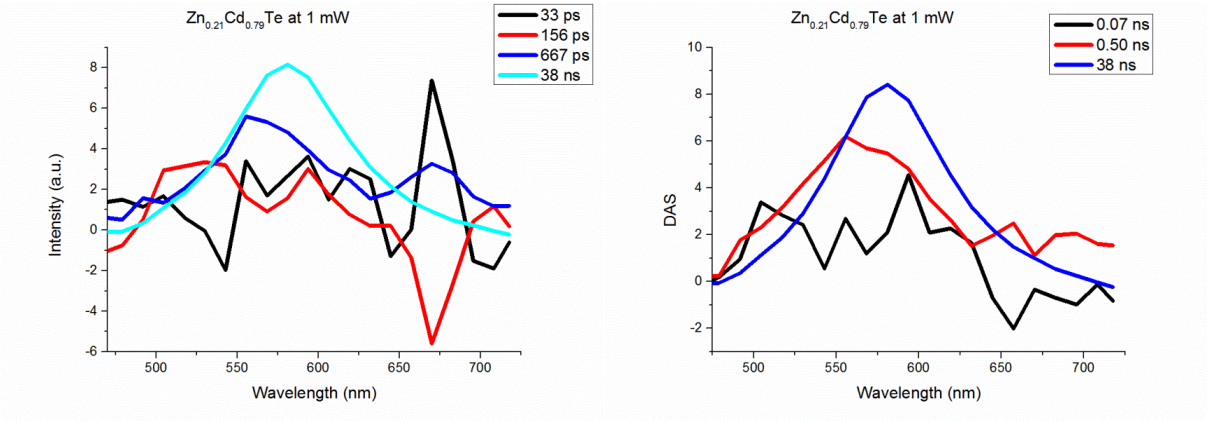

Figure S2. DAS and corresponding lifetimes for $Zn_{0.21}Cd_{0.79}Te$ fitted with 3 and 4 components

Chapter 6

General Discussion

CHAPTER 6

6.1 Introduction

Photosynthesis is the conversion of sunlight energy into chemical energy by many living organisms such as plants, green algae and cyanobacteria [1, 2]. In oxygenic photosynthesis, carbohydrates (glucose, fructose, starch…) and oxygen (as a by-product) are synthesized by using carbon dioxide and water [3]. Photosynthesis proceeds in two main steps, the light reactions and the dark reactions [1, 4, 5]. The process starts in the thylakoid membranes with the light reactions, and as a net result of the light reactions ATP, NADPH and oxygen are synthesized [1, 5]. ATP and NADPH are then used in the dark reactions to synthesize carbohydrates, which form one of the most important energy sources on Earth [4].

During the light reactions, the light absorbed by the photosystems induces electronic excitations, which lead to charge separation in the reaction centres of PSI and PSII located in the cores of the photosystems [6-12]. These photosystems are essential for photosynthetic electron transport, which operates in two different modes, cyclic electron flow and linear electron flow, to provide ATP and NADPH for the Calvin-Benson cycle in dark reactions. [13, 14].

For optimal linear electron transport from water to $NADP^+$ a balance is needed for the amount of light absorbed by the pigments in the two photosystems. Although both PSI and PSII contain chlorophylls (*chls*) and carotenoids (*cars*), their absorption spectra differ, with PSII being more effective in absorbing blue light and PSI in absorbing far-red light [15-17]. Because the intensity and spectral composition of light can vary, organisms need to rapidly adjust the relative absorption cross sections of both PSs. This regulation occurs via so-called state transitions, and it involves the relocation of Lhcs between PSII and PSI [18].

The foreseen "energy crisis" related to complete consumption of fossil-derived fuels on Earth is getting closer and to overcome the energy problem, alternative energy sources are set to be used, such as nuclear energy, wind energy, solar energy, etc… Nowadays "artificial photosynthesis", which is a photocatalytic water splitting process which splits water into hydrogen ions and oxygen by using sunlight [19-25], is becoming a more and more popular field of research. [19-26]. To design a system that performs artificial photosynthesis, it might for instance be possible to mimick the structural and functional organisation of natural photosynthesis [19-25]. In natural photosynthesis, *chls* and *cars* are used as light absorbing pigments [1, 2]. For artificial photosynthesis, *chls* and *cars* can be replaced with quantum dots, semiconductor nanocrystals comprised of groups II–VI or III–V elements, and recent studies showed that quantum dots can be a good alternative as a light harvesting molecules in artificial photosynthesis systems [27-29].

This thesis focuses on structural changes in photosynthetic systems upon state transitions in *Chlamydomonas reinhardtii*. Also, the role of minor harvesting complexes in excitation energy

transfer to reaction centers in photosystem II and multiexciton dynamics of the alloyed ZnCdTe quantum dots are studied in details.

6.2 State transitions in *Chlamydomonas reinhardtii*

Energy partitioning between PSI and PSII has already been the subject of intense research for many years [17, 30]. Genetic approaches have led to the discovery of key proteins involved, such as kinases and phosphatases, regulating the phosphorylation state of LHCII and its relocation between PSII and PSI [31-33]. Biochemical and physiological studies have provided information about the mechanism and importance of state transitions in plants [34, 35] and the green alga *C. reinhardtii* [36, 37]. Important differences seem to exist between state transitions in *C. reinhardtii* and plants, such as the participation of the monomeric antennae CP26 and CP29 only in *C. reinhardtii* [36, 37] and the percentage of LHCII that participates (80% for *C. reinhardtii* vs. 15% for higher plants) [18, 38].

In this thesis, we demonstrate with picosecond-fluorescence spectroscopy on *C. reinhardtii* cells that, although LHCs indeed detach from photosystem II in state 2 conditions, only a fraction attaches to photosystem I. The detached antenna complexes become protected against photodamage via shortening of the excited-state lifetime (**Chapter 2 & Chapter 3**). The main purpose of this study was to understand the functional/organizational differences for PSI, PSII, and dissociated LHCII in state 1 and 2. In **chapter 2**, to at least qualitatively distinguish between PSII and LHCII, the fluorescence decay kinetics was measured for state 1- and state 2-locked cells using different excitation wavelengths: 400 nm (excites relatively more the PSII core complexes) and 465 nm (excites relatively more the outer antenna complexes) at room temperature. In a previous study, it was shown that the amplitude of the fluorescence lifetime that is due to PSI increases significantly when LHCII becomes attached to it; even if on average only one LHCII trimer would move from PSII to PSI this should already lead to an increase of PSI amplitude by 6% [38]. However, we observed only relatively minor differences between the amplitude of the fluorescence lifetime of PSI for states 1 and 2, as well as between the lifetimes. Therefore, it should be concluded that the change in the average size of PSI is clearly smaller than one might have expected, based on the study of Delosme et al. [38]. On the other hand, there is a significant decrease of the average lifetime (not amplitude) of the slower decay components, which are usually thought to originate from PSII. The decrease of the average "PSII" lifetime is explained by a mechanism which suggests that a dynamic equilibrium exists between LHCII associated to PSII, LHCII associated to PSI, and LHCII dissociated from both PSs, being self-aggregated in a separate LHCII pool, where the fluorescence (excited state) of LHCII is quenched. Also, a substantial difference in the average lifetime is observed for the two excitation wavelengths in both states 1 and 2: It is much longer when relatively more outer antenna is excited at 465 nm as opposed to 400 nm. This means that a pool of LHCII is rather badly connected to the PSII cores (leading to long migration times and thus long fluorescence lifetimes) or even completely

disconnected. Concurrently, this badly connected pool of LHCII is substantially quenched, considering the relatively short excited-state lifetimes. Remarkably, a large difference in excited-state lifetime for the two excitation wavelengths is observed both for states 1 and 2, meaning that in both states part of the antenna is disconnected from PSII. In **chapter 3**, we have performed picosecond fluorescence measurements on state–locked WT *Chlamydomonas reinhardtii* cells at 77 K by using a streak-camera setup in order to investigate in detail the changes in fluorescence kinetics for different states which was necessary to resolve an apparent discrepancy between our room temperature time-resolved data and earlier 77K steady-state results. In **chapter 3**, it is observed that the fluorescence intensity around 680 nm (PSII-LHCII fluorescence region) decreases in state-2-locked cells. On the other hand, the fluorescence intensity around 720 nm (PSI region) remains rather similar. In order to understand the changes in fluorescence kinetics in more detail, global analysis has been performed of the streak-camera data and the analysis requires 5 lifetimes. The long lifetimes become shorter for state 2 whereas the short lifetimes are the same. Moreover, the DAS of each lifetime differs in structure for different states because of changes in the excitation energy transfer process. However, the changes in the DAS mostly occur in the PSII-LHCII fluorescence region whereas the change in the PSI fluorescence region is minor. Finally, it is concluded that a large part of the fluorescence of LHC/PSII becomes substantially quenched, probably because of LHC detachment from PSII, whereas the fluorescence of PSI hardly changes.

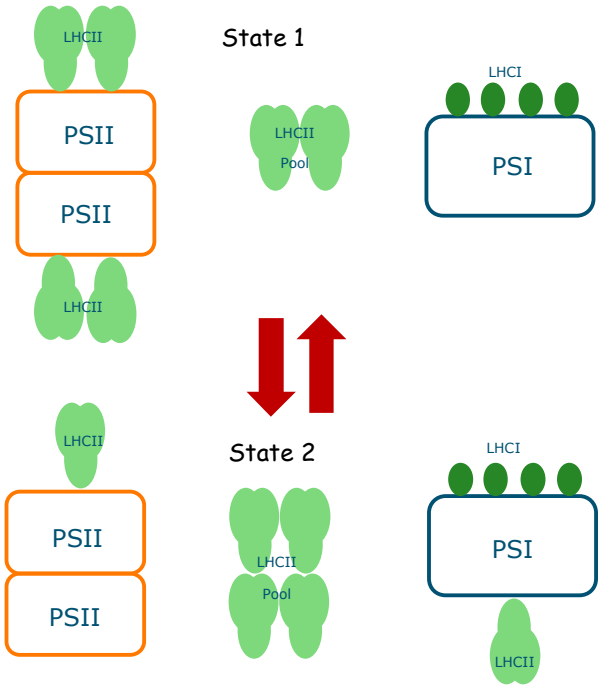

Figure 1. A simplified cartoon of the model for state transitions in C. reinhardtii as proposed in this thesis

6.3 The role of minor light-harvesting complexes in excitation energy transfer to reaction centers in PSII

Minor light-harvesting complexes (Lhcs) CP24, CP26 and CP29 occupy a position in photosystem II (PSII) of plants between the major light-harvesting complexes LHCII and the PSII core subunits. Lack of minor Lhcs *in vivo* causes impairment of PSII organization, and negatively affects electron transport rates and photoprotection capacity. In **chapter 4**, we used picosecond-fluorescence spectroscopy to study excitation-energy transfer (EET) in thylakoid membranes isolated from *Arabidopsis thaliana* wild-type plants and knockout lines depleted of either two (koCP26/24 and koCP29/24) or all minor Lhcs (NoM). The fluorescence decay curves of thylakoid preparations from WT, NoM, koCP29/24 and koCP26/24 mutants were strikingly different from each other. The decay of WT thylakoids was the fastest followed by those of koCP29/24, koCP26/24 and NoM, in that order. Amongst the mutants studied here, the most explicit slowdown of the fluorescence kinetics is observed for the NoM mutant as might have been expected since all minor antenna complexes are missing. For koCP26/24 the slowdown of the fluorescence kinetics is more pronounced than for koCP29/24. This observation is in good agreement with previous work [39], which indicates that both double mutants have disconnected LHCII, but the koCP26/24 mutant has more, although the mutant that was lacking CP26 showed faster fluorescence kinetics than the mutants lacking either CP24 or CP29 or both [40]. To get more quantitative information from the decay curves, they are fitted to a sum of exponential decay functions. The most significant changes concern the lifetimes of the PSII-LHCII components for all mutants, and this must originate from a reorganization or "disassembly" of PSII–LHCII. The increase in the lifetime of the PSII–LHCII components can be explained by the existence of badly connected or disconnected LHCII due to the absence of several minor antenna complexes. Also, we find that the average lifetime of PSII–LHCII for the NoM mutant is 2.3 times longer than the average lifetime of PSII–LHCII for WT. This huge difference is attributed to the disruption of PSII supercomplexes and the presence of detached LHCII. In conclusion, our results show that the missing minor complexes are not replaced by other Lhcs, implying that they are unique among the antenna subunits and crucial for the functioning and macro-organization of PSII. It has been suggested before that antenna size reduction is a valuable strategy for the optimisation of the light reactions: theoretical simulation of net CO_2 uptake suggested that a smaller antenna size would significantly improve photosynthetic efficiency on crop canopies[41]. However, strategies to improve light penetration must ensure that truncated antenna mutants are not photosynthetically impaired in ways other than reduced LHC content: indeed in higher plants, an extreme reduction in LHC complement lead to a lower photochemical yield and increases photoinhibition [42]. The present results in **chapter 4** show that depletion of even a sub-group of LHCs strongly affects the PSII light-harvesting efficiency and thus the photoautotrophic growth. To ensure that truncated-antenna strains will operate with improved light use efficiency, biotechnological approaches aimed at reducing antenna cross-section must focus on

trimeric LHCII, rather than monomeric Lhcb content: the latter leads to a strong impairment of PSII light-use efficiency, thus cancelling out benefits of optical density reduction, although only for the NoM mutant this leads to strongly reduced growth under continuous-light conditions.

6.4 The multi-exciton dynamics of the alloyed ZnCdTe quantum dots

In **chapter 5**, we have performed picosecond fluorescence measurements on ZnCdTe ternary quantum dots at room temperature by using a streak-camera setup in order to investigate in detail the fluorescence kinetics for ZnCdTe quantum dots with different size and structure by using different excitation laser intensities. The ZnCdTe quantum dots are classified into two groups (homogeneous and heterogeneous) according to their structural properties, and for both groups quantum dots have been synthesized with two different sizes (4.5 nm and 9.5 nm in diameter). To identify the multi-exciton dynamics of the homogeneous quantum dots, global analysis was performed on the recorded data at different excitation intensities. The fluorescence kinetics of ZnCdTe quantum dots are described with 2 lifetimes; one slow component for the normal lifetime and one fast component for all the annihilation processes with one effective average annihilation time and one average spectrum. The short lifetime of the homogeneous quantum dots becomes slightly shorter and contributes more to the overall kinetics for the largest quantum dots (at 1 mW) which shows that the number of defect states is the largest in the largest quantum dot. For heterogeneous ZnCdTe quantum dots, the shortest component is even more pronounced and faster than in homogeneous ZnCdTe quantum dots, most probably because of a higher concentration of defect states in the crystal structure. Also the short lifetimes become slightly shorter as the size increases for heterogeneous ZnCdTe quantum dots, which shows that the number of defect states increases with increasing size. In both homogeneous and heterogeneous ZnCdTe quantum dots, the appearance of a new peak when using high excitation intensities shows that the fast radiative processes that occur from higher energy states become more favoured as the excitation intensity increases. The long lifetime for ZnCdTe quantum dots is attributed to radiative single exciton dynamics. In addition, a small shoulder, peaking around 520 nm becomes more intense upon increasing the excitation power. In conclusion, in heterogeneous structured ZnCdTe quantum dots, the fluorescence kinetics becomes faster as compared to homogeneous structured ZnCdTe quantum dots. Also, in both homogeneous and heterogeneous ZnCdTe quantum dots, a new peak is observed in the high-energy region of the emission spectrum when using high excitation intensities, which shows that the radiative processes that occur from higher energy states become more favoured as the excitation intensity increases.

6.5 References:

[1] H. Van Amerongen, L. Valkunas, R. Van Grondelle, Photosynthetic Excitons, 2000, World Scientific, Singapore, 2000.
[2] R.E. Blankenship, Molecular mechanisms of photosynthesis, Blackwell Science Ltd, 2002.
[3] N. Nelson, A. Ben-Shem, The complex architecture of oxygenic photosynthesis, Nature Reviews Molecular Cell Biology, 5 (2004) 971-982.
[4] E.J. Badin, M. Calvin, The Path of Carbon in Photosynthesis .9. Photosynthesis, Photoreduction and the Hydrogen Oxygen Carbon Dioxide Dark Reaction, Journal of the American Chemical Society, 72 (1950) 5266-5270.
[5] D.I. Arnon, Light Reactions of Photosynthesis, Proceedings of the National Academy of Sciences of the United States of America, 68 (1971) 2883-&.
[6] G.H. Schatz, H. Brock, A.R. Holzwarth, Kinetic and Energetic Model for the Primary Processes in Photosystem-Ii, Biophysical Journal, 54 (1988) 397-405.
[7] A.N. Melkozernov, S. Lin, R.E. Blankenship, Excitation dynamics and heterogeneity of energy equilibration in the core antenna of photosystem I from the cyanobacterium Synechocystis sp. PCC 6803, Biochemistry, 39 (2000) 1489-1498.
[8] B. Gobets, R. van Grondelle, Energy transfer and trapping in photosystem I, Biochimica Et Biophysica Acta-Bioenergetics, 1507 (2001) 80-99.
[9] N. Nelson, C.F. Yocum, Structure and function of photosystems I and II, Annual Review of Plant Biology, 57 (2006) 521-565.
[10] A. Busch, M. Hippler, The structure and function of eukaryotic photosystem I, Biochimica Et Biophysica Acta-Bioenergetics, 1807 (2011) 864-877.
[11] R. Croce, H. van Amerongen, Light-harvesting in photosystem I, Photosynthesis Research, 116 (2013) 153-166.
[12] H. van Amerongen, R. Croce, Light harvesting in photosystem II, Photosynthesis Research, 116 (2013) 251-263.
[13] R. Croce, H. van Amerongen, Natural strategies for photosynthetic light harvesting, Nature Chemical Biology, 10 (2014) 492-501.
[14] H. Takahashi, S. Clowez, F.A. Wollman, O. Vallon, F. Rappaport, Cyclic electron flow is redox-controlled but independent of state transition, Nature Communications, 4 (2013).
[15] N. Murata, Control of Excitation Transfer in Photosynthesis .I. Light-Induced Change of Chlorophyll a Fluorescence in Porphyridium Cruentum, Biochimica Et Biophysica Acta, 172 (1969) 242-&.
[16] Bonavent.C, J. Myers, Fluorescence and Oxygen Evolution from Chlorella Pyrenoidosa, Biochimica Et Biophysica Acta, 189 (1969) 366-+.
[17] J.F. Allen, J. Bennett, K.E. Steinback, C.J. Arntzen, Chloroplast Protein-Phosphorylation Couples Plastoquinone Redox State to Distribution of Excitation-Energy between Photosystems, Nature, 291 (1981) 25-29.
[18] J.F. Allen, Protein-Phosphorylation in Regulation of Photosynthesis, Biochimica Et Biophysica Acta, 1098 (1992) 275-335.
[19] D. Gust, T.A. Moore, A.L. Moore, Solar Fuels via Artificial Photosynthesis, Accounts of Chemical Research, 42 (2009) 1890-1898.
[20] L. Hammarstrom, S. Hammes-Schiffer, Artificial Photosynthesis and Solar Fuels, Accounts of Chemical Research, 42 (2009) 1859-1860.
[21] W.J. Song, Z.F. Chen, M.K. Brennaman, J.J. Concepcion, A.O.T. Patrocinio, N.Y.M. Iha, T.J. Meyer, Making solar fuels by artificial photosynthesis, Pure and Applied Chemistry, 83 (2011) 749-768.
[22] S.W. Hogewoning, E. Wientjes, P. Douwstra, G. Trouwborst, W. van Ieperen, R. Croce, J. Harbinson, Photosynthetic Quantum Yield Dynamics: From Photosystems to Leaves, Plant Cell, 24 (2012) 1921-1935.
[23] S. Styring, Artificial photosynthesis for solar fuels, Faraday Discussions, 155 (2012) 357-376.
[24] S. Styring, Fuels from solar energy and water-from natural to artificial photosynthesis, Journal of Biological Inorganic Chemistry, 19 (2014) S721-S721.

[25] Y. Tachibana, L. Vayssieres, J.R. Durrant, Artificial photosynthesis for solar water-splitting, 6 (2012) 511-518.
[26] S.C. Warren, K. Voitchovsky, H. Dotan, C.M. Leroy, M. Cornuz, F. Stellacci, C. Hebert, A. Rothschild, M. Gratzel, Identifying champion nanostructures for solar water-splitting, Nature Materials, 12 (2013) 842-849.
[27] I. Nabiev, A. Rakovich, A. Sukhanova, E. Lukashev, V. Zagidullin, V. Pachenko, Y.P. Rakovich, J.F. Donegan, A.B. Rubin, A.O. Govorov, Fluorescent Quantum Dots as Artificial Antennas for Enhanced Light Harvesting and Energy Transfer to Photosynthetic Reaction Centers, Angewandte Chemie International Edition, 49 (2010) 7217-7221.
[28] H.M. Chen, C.K. Chen, Y.C. Chang, C.W. Tsai, R.S. Liu, S.F. Hu, W.S. Chang, K.H. Chen, Quantum Dot Monolayer Sensitized ZnO Nanowire-Array Photoelectrodes: True Efficiency for Water Splitting, Angewandte Chemie-International Edition, 49 (2010) 5966-5969.
[29] H.M. Chen, C.K. Chen, R.S. Liu, C.C. Wu, W.S. Chang, K.H. Chen, T.S. Chan, J.F. Lee, D.P. Tsai, A New Approach to Solar Hydrogen Production: a ZnO-ZnS Solid Solution Nanowire Array Photoanode, Advanced Energy Materials, 1 (2011) 742-747.
[30] J. Bennett, K.E. Steinback, C.J. Arntzen, Chloroplast phosphoproteins: Regulation of excitation energy transfer by phosphorylation of thylakoid membrane polypeptides, Proc.Natl.Acad.Sci.USA, 77 (1980) 5253-5257.
[31] S. Bellafiore, F. Barneche, G. Peltier, J.D. Rochaix, State transitions and light adaptation require chloroplast thylakoid protein kinase STN7, Nature, 433 (2005) 892-895.
[32] A. Shapiguzov, B. Ingelsson, I. Samol, C. Andres, F. Kessler, J.D. Rochaix, A.V. Vener, M. Goldschmidt-Clermont, The PPH1 phosphatase is specifically involved in LHCII dephosphorylation and state transitions in Arabidopsis, Proceedings of the National Academy of Sciences of the United States of America, 107 (2010) 4782-4787.
[33] M. Pribil, P. Pesaresi, A. Hertle, R. Barbato, D. Leister, Role of Plastid Protein Phosphatase TAP38 in LHCII Dephosphorylation and Thylakoid Electron Flow, Plos Biology, 8 (2010) -.
[34] M. Tikkanen, M. Grieco, S. Kangasjarvi, E.M. Aro, Thylakoid protein phosphorylation in higher plant chloroplasts optimizes electron transfer under fluctuating light, Plant physiology, 152 (2010) 723-735.
[35] M. Tikkanen, M. Piippo, M. Suorsa, S. Sirpio, P. Mulo, J. Vainonen, A.V. Vener, Y. Allahverdiyeva, E.M. Aro, State transitions revisited-a buffering system for dynamic low light acclimation of Arabidopsis, Plant molecular biology, 62 (2006) 779-793.
[36] M. Iwai, Y. Takahashi, J. Minagawa, Molecular remodeling of photosystem II during state transitions in Chlamydomonas reinhardtii, Plant Cell, 20 (2008) 2177-2189.
[37] H. Takahashi, M. Iwai, Y. Takahashi, J. Minagawa, Identification of the mobile light-harvesting complex II polypeptides for state transitions in Chlamydomonas reinhardtii, Proceedings of the National Academy of Sciences of the United States of America, 103 (2006) 477-482.
[38] R. Delosme, J. Olive, F.A. Wollman, Changes in light energy distribution upon state transitions: An in vivo photoacoustic study of the wild type and photosynthesis mutants from Chlamydomonas reinhardtii, Biochimica Et Biophysica Acta-Bioenergetics, 1273 (1996) 150-158.
[39] Y. Miloslavina, S. de Bianchi, L. Dall'Osto, R. Bassi, A.R. Holzwarth, Quenching in Arabidopsis thaliana Mutants Lacking Monomeric Antenna Proteins of Photosystem II, Journal of Biological Chemistry, 286 (2011) 36830-36840.
[40] B. van Oort, M. Alberts, S. de Bianchi, L. Dall'Osto, R. Bassi, G. Trinkunas, R. Croce, H. van Amerongen, Effect of Antenna-Depletion in Photosystern II on Excitation Energy Transfer in Arabidopsis thaliana, Biophysical Journal, 98 (2010) 922-931.
[41] D.R. Ort, X.G. Zhu, A. Melis, Optimizing Antenna Size to Maximize Photosynthetic Efficiency, Plant Physiology, 155 (2011) 79-85.
[42] C.E. Espineda, A.S. Linford, D. Devine, J.A. Brusslan, The AtCAO gene, encoding chlorophyll a oxygenase, is required for chlorophyll b synthesis in Arabidopsis thaliana, Proceedings of the National Academy of Sciences of the United States of America, 96 (1999) 10507-10511.
[43] F.A. Wollman, P. Delepelaire, Correlation between Changes in Light Energy-Distribution and Changes in Thylakoid Membrane Polypeptide Phosphorylation in Chlamydomonas-Reinhardtii, Journal of Cell Biology, 98 (1984) 1-7.

[44] W.P. Williams, J.F. Allen, State-1/State-2 Changes in Higher-Plants and Algae, Photosynthesis Research, 13 (1987) 19-45.
[45] M.M. Fleischmann, S. Ravanel, R. Delosme, J. Olive, F. Zito, F.A. Wollman, J.D. Rochaix, Isolation and characterization of photoautotrophic mutants of Chlamydomonas reinhardtii deficient in state transition, Journal of Biological Chemistry, 274 (1999) 30987-30994.
[46] G. Finazzi, R.P. Barbagallo, E. Bergo, R. Barbato, G. Forti, Photoinhibition of Chlamydomonas reinhardtii in State 1 and State 2 - Damages to the photosynthetic apparatus under linear and cyclic electron flow, Journal of Biological Chemistry, 276 (2001) 22251-22257.
[47] G. Forti, G. Caldiroli, State transitions in Chlamydomonas reinhardtii. The role of the Mehler reaction in state 2-to-state 1 transition, Plant Physiology, 137 (2005) 492-499.
[48] J. Kargul, M.V. Turkina, J. Nield, S. Benson, A.V. Vener, J. Barber, Light-harvesting complex II protein CP29 binds to photosystem I of Chlamydomonas reinhardtii under State 2 conditions, Febs Journal, 272 (2005) 4797-4806.
[49] H. Takahashi, M. Iwai, Y. Takahashi, J. Minagawa, Identification of the mobile light-harvesting complex II polypeptides for state transitions, Plant and Cell Physiology, 47 (2006) S105-S105.
[50] M. Iwai, M. Yokono, N. Inada, J. Minagawa, Live-cell imaging of photosystem II antenna dissociation during state transitions, Proceedings of the National Academy of Sciences of the United States of America, 107 (2010) 2337-2342.
[51] J. Minagawa, State transitions-The molecular remodeling of photosynthetic supercomplexes that controls energy flow in the chloroplast, Biochimica Et Biophysica Acta-Bioenergetics, 1807 (2011) 897-905.
[52] B. Drop, K.N.S. Yadav, E.J. Boekema, R. Croce, Consequences of state transitions on the structural and functional organization of Photosystem I in the green alga Chlamydomonas reinhardtii, Plant Journal, 78 (2014) 181-191.
[53] C. Unlu, B. Drop, R. Croce, H. van Amerongen, State transitions in Chlamydomonas reinhardtii strongly modulate the functional size of photosystem II but not of photosystem I, Proceedings of the National Academy of Sciences of the United States of America, 111 (2014) 3460-3465.
[54] G. Nagy, R. Unnep, O. Zsiros, R. Tokutsu, K. Takizawa, L. Porcar, L. Moyet, D. Petroutsos, G. Garab, G. Finazzi, J. Minagawa, Chloroplast remodeling during state transitions in Chlamydomonas reinhardtii as revealed by noninvasive techniques in vivo, Proceedings of the National Academy of Sciences of the United States of America, 111 (2014) 5042-5047.

Chapter 7

Summary

The possible mechanisms for reorganisation of outer LHCs of PSII (LHCII) upon state transitions in *Chlamydomonas reinhardtii* have been discussed for several decades [38, 43-54]. For a long time people adhered to the opinion that upon the transition from state 1 to state 2, 80% of LHCII detaches from PSII and attaches completely to PSI in *Chlamydomonas reinhardtii* [38, 45]. This thesis provides new insights for the mechanism of state transitions in *Chlamydomonas reinhardtii.* In the remainder of this thesis, the role of minor light-harvesting complexes in excitation energy transfer to reaction centers of photosystem II are discussed as well as multiexciton dynamics of the alloyed ZnCdTe quantum dots are studied in detail.

In **chapter 2**, we demonstrate with picosecond-fluorescence spectroscopy on *C. reinhardtii* cells that although LHCs indeed detach from Photosystem II in state-2 conditions only a fraction attaches to Photosystem I. The detached antenna complexes become protected against photodamage via shortening of the excited-state lifetime. It is discussed how the transition from state 1 to state 2 can protect *C. reinhardtii* in high-light conditions and how this differs from the situation in plants.

In **chapter 3**, we study the picosecond fluorescence properties of *Chlamydomonas reinhardtti* over a broad range of wavelengths at 77K. It is observed that upon going from state 1 (relatively high 680nm/720nm fluorescence ratio) to state 2 (low ratio), a large part of the fluorescence of LHC/PSII becomes substantially quenched, probably because of LHC detachment from PSII, whereas the fluorescence of PSI hardly changes. These results are in agreement with the proposal in chapter 2 that the amount of LHC moving from PSII to PSI upon going from state 1 to state 2 is very limited.

In **chapter 4**, we used picosecond-fluorescence spectroscopy to study excitation-energy transfer (EET) in thylakoids membranes isolated from *A. thaliana* wild-type plants and knockout lines depleted of either two (koCP26/24 and koCP29/24) or all minor Lhcs (NoM). In the absence of all minor Lhcs, the functional connection of LHCII to the PSII cores appears to be seriously impaired whereas the "disconnected" LHCII is substantially quenched. For both double knock-out mutants, excitation trapping in PSII is faster than in NoM thylakoids but slower than in WT thylakoids. In NoM thylakoids, the loss of all minor Lhcs is accompanied by an over-accumulation of LHCII, suggesting a compensating response to the reduced trapping efficiency in limiting light, which leads to a photosynthetic phenotype resembling that of low-light-acclimated plants. Finally, fluorescence kinetics and biochemical results show that the missing minor complexes are not replaced by other Lhcs, implying that they are unique among the antenna subunits and crucial for the functioning and macro-organization of PSII.

In **chapter 5**, we have performed picosecond fluorescence measurements on ZnCdTe ternary quantum dots at room temperature by using a streak-camera setup in order to investigate in detail the fluorescence kinetics for ZnCdTe quantum dots with different size and structure by using different excitation laser intensities. Our data show that the changes in fluorescence kinetics are mostly related

to the changes in structure and size. In heterogeneous structured ZnCdTe quantum dots, the fluorescence kinetics become faster as compared to homogeneous structured ZnCdTe quantum dots. Also, in both homogeneous and heterogeneous ZnCdTe quantum dots, a new peak is observed in the high-energy region of the emission spectrum when using high excitation intensities, which shows that the radiative processes that occur from higher energy states become more favoured as the excitation intensity increases. .

Hoofdstuk 8

Samenvatting

De mogelijke mechanismen voor de reorganisatie van de buitenste lichtopvangende complexen (LHCs) van fotosysteem II (PSII), LHCII, gedurende overgangen tussen verschillende toestanden ('state transitions') in *Chlamydomonas reinhardtii* zijn al enkele decennia lang onderwerp van discussie [38, 43-54]. Voor lange tijd hield men vast aan de mening dat in *C. reinhardtii* gedurende de overgang van 'state 1' naar 'state 2', 80% van LHCII loskomt van PSII en volledig bindt aan PSI [38, 45]. Dit proefschrift verschaft nieuwe inzichten omtrent het mechanisme van 'state transitions' in *C. reinhardtii.* In het overige deel van dit proefschrift wordt de rol besproken van de kleinere lichtopvangende complexen (Lhcs) in de overdracht van excitatie-energie naar reactiecentra van PSII, en wordt tevens multi-exciton dynamica van gemengde ZnCdTe kwantumdots in detail bestudeerd.

In **hoofdstuk 2** demonstreren we aan de hand van picoseconde-fluorescentiespectroscopie aan cellen van *C. reinhardtii* dat alhoewel LHCs inderdaad loskomen van PSII onder 'state 2'-condities, slechts een fractie bindt aan PSI. De ontkoppelde LHCs worden beschermd tegen fotoschade middels verkorting van de levensduur van de aangeslagen toestand. Besproken wordt hoe de overgang van 'state 1' naar 'state 2' *C. reinhardtii* kan beschermen onder hoge lichtcondities en hoe dit verschilt van de situatie in planten.

In **hoofdstuk 3** staan de picoseconde-fluorescentie-eigenschappen beschreven van *C. reinhardtti* over een breed golflengtegebied bij 77K. Het is waargenomen dat gaande van 'state 1' (relatief hoge 680nm/720nm fluorescentie-ratio) naar 'state 2' (lage ratio), een groot deel van de fluorescentie van LHC/PSII substantieel gedoofd wordt, waarschijnlijk ten gevolge van ontkoppeling van LHCII van PSII, terwijl de fluorescentie van PSI nauwelijks verandert. Deze resultaten zijn in overeenstemming met de bewering in hoofdstuk 2 dat de hoeveelheid LHC dat tijdens de overgang van 'state 1' naar 'state 2' van PSII naar PSI gaat, zeer beperkt is.

In **hoofdstuk 4** staat beschreven hoe picoseconde-fluorescentiespectroscopie is gebruikt om de overdracht van excitatie-energie (EET) te bestuderen in thylakoidmembranen geïsoleerd uit wild-type (WT) *Arabidopsis thaliana* planten en 'knock-out' lijnen waarin twee (koCP26/24 en koCP29/24) of álle kleinere Lhcs (NoM) uitgeschakeld zijn. In afwezigheid van alle kleinere Lhcs blijkt de functionele koppeling tussen LHCII en het 'core complex' van PSII ernstig afgezwakt te zijn, terwijl de fluorescentie van het 'ontkoppelde' LHCII substantieel gedoofd is. In beide dubbele 'knock-out'mutanten gaat het wegvangen van excitatie ('trapping') in PSII sneller dan in NoM-thylakoiden, maar langzamer dan in WT-thylakoiden. In NoM-thylakoiden gaat het ontbreken van alle kleinere Lhcs samen met een over-accumulatie van LHCII. Dit suggereert een compenserende respons op de gereduceerde efficiëntie van de 'trapping' onder limiterende lichtomstandigheden, wat leidt tot een fotosynthetisch fenotype dat lijkt op laag licht-geacclimatiseerde planten. Tot slot laten fluorescentiekinetiek en biochemische resultaten zien dat de ontbrekende kleinere complexen niet

vervangen worden door andere Lhcs, hetgeen impliceert dat deze uniek zijn onder de antenne-subeenheden en cruciaal voor het functioneren en de macro-organisatie van PSII.

In **hoofdstuk 5** staan picoseconde-fluorescentiemetingen beschreven aan ZnCdTe ternaire kwantumdots bij kamertemperatuur met een streak-camera opstelling waarmee ten einde in detail de fluorescentiekinetiek te onderzoeken van ZnCdTe kwantumdots van verschillende grootte en structuur, gebruik makend van verschillende intensiteiten van de excitatie-laser. Onze data laat zien dat de veranderingen in fluorescentiekinetiek vooral gerelateerd zijn aan veranderingen in structuur en grootte. In ZnCdTe kwantumdots met heterogene structuur is de fluorescentie-kinetiek sneller dan in ZnCdTe kwantumdots met homogene structuur. Daarnaast is bij gebruik van hoge excitatie-intensiteiten in zowel homogene als heterogene ZnCdTe kwantumdots een nieuwe piek waargenomen in het hoog-energetische deel van het emissiespectrum, hetgeen aantoont dat stralende processen vanuit toestanden met hoge energie meer plaatsvinden naarmate de excitatie-intensiteit toeneemt.

Acknowledgements

Although I put a lot of effort to finish this thesis, without massive help of my colleagues, my friends and my family; I would never be able to finish this thesis.

Herbert, you were an excellent supervisor to me. At the beginning of my Ph.D my knowledge on photosynthesis was limited with only this information; "sun + some green stuff = oxygen and food". You guided me very well and by the end of my Ph.D my knowledge on photosynthesis increased a lot. Thanks a lot for everything. I hope your future Ph.D students will be less troublesome than me.

Agah (hocam), you were a really great friend and a great mentor to me. You helped both me and Yelda a lot in the Netherlands. Now we are both in France, I just hope our friendship and collaboration will grow more and more in the future.

Rob, Arjen, Arie and Cor thanks a lot for all of your helps, ideas and technical support.

Netty, thank you very much for helping me out with all Dutch related stuff.

Shanthi, Evgenia and Shazia, thanks for being good friends with me. I really enjoyed every talk between us. I hope you will finish your thesis without any problems and continue in your careers with huge success.

Fugui, you were always there when I came to talk with you (even during weekends). I hope you will see benefits of your hard work soon.

Olga, Daan, Alena, Carel, Yashar and Helen thanks for your nice friendship.

Elena, Dane, Edo, Johannes, Folkert. John, Emilie, Frank and Pieter, thanks for your nice coffee-time talks.

Lijin, you are the one who helped me to settle down in my work area and helped me a lot in my study in the beginning. I wish you, your wife and your child(ren) the best.

I want to thank Roberta Croce, Bartlomiej Drop and Iryna Polukhina for their excellent collaboration. Together we performed a very nice work. I hope your success will continue.

I also want to thank Luca Dall'Osto for his nice collaboration and providing me with beautiful samples.

I specially want to thank Jacques Vervoort for helping me and my wife during our stay in the Netherlands.

Mehmet, Fatma, Mert, Eymen, Alper, Alev, Ali Mete... we were indeed one big family in Wageningen. Thanks to all of you, I and Yelda never became homesick. I never worried about any

emergency situation because I knew that one of you will help no matter what happens. I hope we will be together again in somewhere (perhaps in İzmir?)

The support of my family was like an endless river, they were always ready for any kind of help for me. My parents (Yılmaz – Nebile Ünlü), my parents-in-law (Tayfur-Ayşen Özkılınç), my brother (Mehmet Taner Ünlü) my sister-in-law, her husband and their daughter (Yeliz-Ahmet-Elif Kınsız) were always ready to talk to me, to help me. Thanks a lot for everything.

And finally, Yelda, my love, I do not know how I should describe your role in this thesis. Rather, I will describe your role in my life. Long story short, if it was not for you, I would never try to come in Netherlands, even try to be a scientist. Together we finished this thesis. This was an adventure for us, we lived this adventure together, and we will live next adventure together. Thank you for everything.

Education Statement of the Graduate School

Experimental Plant Sciences

Issued to: Caner Ünlü
Date: 20 May 2015
Group: Laboaratory of Biophysics
University: Wageningen University & Research Centre

1) Start-up phase	*date*
► **First presentation of your project**	
State transitions in *Chlamydomonas reinhardtii*	Feb 01, 2011
► **Writing or rewriting a project proposal**	
► **Writing a review or book chapter**	
► **MSc courses**	
Biophotonics and Photosynthesis (BIP - 32306)	Sep 2014
► **Laboratory use of isotopes**	
Subtotal Start-up Phase	*4.5 credits**

2) Scientific Exposure	*date*
► **EPS PhD student days**	
EPS PhD Student day, Wageningen University	May 20, 2011
EPS PhD Student day, Leiden University	Nov 29, 2013
► **EPS theme symposia**	
Annual EPS Theme 3 Meeting 'Metabolism and Adaptation', Wageningen University	Feb 10, 2011
Annual EPS Theme 3 Meeting 'Metabolism and Adaptation', University of Amsterdam	Mar 22, 2013
► **NWO Lunteren days and other National Platforms**	
Dutch Meeting on Molecular and Cellular Biophysics, Veldhoven	Oct 01-02, 2012
Dutch Meeting on Molecular and Cellular Biophysics, Veldhoven	Sep 30-Oct 01, 2013
Dutch Meeting on NWO-CW, Veldhoven	Feb 10-11, 2014
Dutch Meeting on Molecular and Cellular Biophysics, Veldhoven	Sep 29-30, 2014
► **Seminars (series), workshops and symposia**	
18th International Workshop on Single Molecule Spectroscopy , Berlin	Sep 05-07, 2012
WU/FAST workshop, Wageningen	Jan 22, 2014
Measuring the Photosynthetic phenome, Wageningen	Jun 07-09, 2014
State transitions symposium, Wageningen	Sep 02, 2014
Biophysica seminar series, WUR, Laboratory of Biophysics	2011 - 2014
► **Seminar plus**	
► **International symposia and congresses**	
Light Harvesting 2013 Satellite Meeting, St. Louis (USA)	Aug 08-11, 2013
The 15th international photosynthesis conference, St. Louis (USA)	Aug 11-16, 2013
Biophysics of Photosynthesis 2013, Rome	Oct 28-30, 2013
► **Presentations**	
Poster: 18th International Workshop on Single Molecule Spectroscopy, Berlin	Sep 05-07, 2012
Poster: The 15th international photosynthesis conference, St. Louis (USA)	Aug 11-16, ,2013
Oral: WU/FAST workshop, Wageningen	Jan 22, 2014
Oral: Dutch Meeting on NWO-CW, Veldhoven	Feb 10-11, 2014
Poster: Measuring the Photosynthetic phenome, Wageningen	Jun 07-09, 2014
Oral: State transitions symposium, Wageningen	Sep 02, 2014
Poster: Dutch Meeting on Molecular and Cellular Biophysics, Veldhoven	Sep 29-30, 2014
► **IAB interview**	
► **Excursions**	
Subtotal Scientific Exposure	*18.0 credits**

3) In-Depth Studies	*date*
► **EPS courses or other PhD courses**	
Microscopy and Spectroscopy in Food and Plant Science	May 06-09, 2014
► **Journal club**	
member of a literature discussion group at Biophysics	2011-2014
► **Individual research training**	
Subtotal In-Depth Studies	*4.2 credits**

4) Personal development	*date*
► **Skill training courses**	
Scientific Integrity	Oct 02, 2013
Scientific Publishing	Oct 03, 2013
Interpersonal Communication for PhD Students	Nov 13-14, 2013
Information Literacy including EndNote Introduction	Dec 03-04, 2013
Techniques for Writing and Presenting a Scientific paper	Apr 07-11, 2014
Voice Matters: Voice and Presentation Skills Training	Apr 01 & 15, 2014
Career Assessment	2014
► **Organisation of PhD students day, course or conference**	
► **Membership of Board, Committee or PhD council**	
Subtotal Personal Development	*3.6 credits**

TOTAL NUMBER OF CREDIT POINTS*	**30,3**

Herewith the Graduate School declares that the PhD candidate has complied with the educational requirements set by the Educational Committee of EPS which comprises of a minimum total of 30 ECTS credits

** A credit represents a normative study load of 28 hours of study.*